Available online at www.sciencedirect.com

ScienceDirect

Journal of Magnesium and Alloys 10 (2022) 2025–2061

www.elsevier.com/locate/jma

Review

Surface modification of magnesium alloys using thermal and solid-state cold spray processes: Challenges and latest progresses

Mohammadreza Daroonparvar[a,*], Hamid Reza Bakhsheshi-Rad[b,*], Abbas Saberi[b], Mahmood Razzaghi[b], Ashish K Kasar[a], Seeram Ramakrishna[c], Pradeep L. Menezes[a], Manoranjan Misra[d], Ahmad Fauzi Ismail[e], Safian Sharif[f], Filippo Berto[g]

[a] *Department of Mechanical Engineering, University of Nevada, Reno, NV, 89501, USA*
[b] *Advanced Materials Research Center, Department of Materials Engineering, Najafabad Branch, Islamic Azad University, Najafabad, Iran*
[c] *Department of Mechanical Engineering, National University of Singapore, 9 Engineering Drive 1, Singapore 117576, Singapore*
[d] *Department of Chemical and Materials Engineering, University of Nevada, Reno, NV, 89501, USA*
[e] *Advanced Membrane Technology Research Center (AMTEC), Universiti Teknologi Malaysia, Johor Bahru 81310, Johor, Malaysia*
[f] *Faculty of Engineering, Universiti Teknologi Malaysia, Johor Bahru 81310, Johor, Malaysia*
[g] *Department of Mechanical and Industrial Engineering, Norwegian University of Science and Technology, 7491 Trondheim, Norway*

Received 8 April 2022; received in revised form 30 June 2022; accepted 19 July 2022
Available online 7 September 2022

Abstract

Potential engineering applications of magnesium (Mg) and Mg-based alloys, as the lightest structural metal, have made them a popular subject of study. However, the inferior corrosion and wear characteristics significantly limit their application range. It is widely recognized that surface treatment is the most commonly utilized technique for remarkably improving a substrate's surface characteristics. Numerous methods have been introduced for the surface treatment of Mg and Mg-based alloys to improve their corrosion behavior and tribological performance. Among these, thermal spray (TS) technology provides several methods for deposition of various functional metallic, ceramic, cermet, or other coatings tailored to particular conditions. Recent researches have shown the tremendous potential for thermal spray coated Mg alloys for biomedical and industrial applications. In this context, the cold spray (CS) method, as a comparatively new TS coating technique, can generate the coating layer using kinetic energy rather than combined thermal and kinetic energies, like the high-velocity oxy-fuel (HVOF) spray method. Moreover, the CS process, as a revolutionary method, is able to repair and refurbish with a faster turnaround time; it also provides solutions that do not require dealing with the thermal stresses that are part of the other repair processes, such as welding or other TS processes using a high-temperature flame. In this review paper, the recently designed coatings that are specifically applied to Mg alloys (primarily for industrial applications) employing various coating processes are reviewed. Because of the increased utilization of CS technology for both 3D printed (additively manufactured) coatings and repair of structurally critical components, the most recent CS methods for the surface treatment, repair, and refurbishment of Mg alloys as well as their benefits and restrictions are then discussed and reviewed in detail. Lastly, the prospects of this field of study are briefly discussed, along with a summary of the presented work.

Keywords: Mg-based alloys; Surface modification; Thermal and cold spray processes; Corrosion behavior; Wear resistance.

1. Introduction

Mg and Mg alloys have recently attracted interest due to their possible applications in different industries, including aerospace, automotive, and electronics. They have unique properties like high specific strength, significant damping performance, good stiffness, and high capability for electro-

* Corresponding authors.
E-mail addresses: mr.daroonparvar@yahoo.com (M. Daroonparvar), rezabakhsheshi@pmt.iaun.ac.ir (H.R. Bakhsheshi-Rad).

https://doi.org/10.1016/j.jma.2022.07.012

magnetic shielding [1–3]. Nevertheless, the low wear and corrosion properties of Mg alloys can limit their applications [4]. It is extensively recognized that surface modification is the most common route to enhance a substrate's surface characteristics. As a barrier between the substrate and the environment, a coating layer can enhance the corrosion resistance of a metallic substrate [5]. Numerous methods based on conversion coating (CC) [6–8], sol-gel coatings [9–12], plasma electrolytic oxidation (PEO) [13–16], electroplating [17–19], anodization process [20–25], physical vapor deposition (PVD) [26–29], chemical vapor deposition (CVD) [30–33], ion implantation [34–38], superhydrophobic coatings [39], electrophoretic deposition [40], and thermal spray (TS) [41–48] have been introduced to modify the surface of Mg and Mg-based alloys to improve their corrosion behavior and tribology performance. Using toxic elements and compounds, including chromium, fluoride, and cyanide in the processes of pre-treatment and plating, is one of the main problems in the electroplating method. Moreover, the deposition of a dense, uniform, and pore-free coating on Mg-based alloys utilizing the electroplating method is challenging due to the narrow window for operating conditions and the variance in the surface chemistry of different Mg-based substrates [49].

On the other hand, CC often requires strict preparation processes such as alkaline treatment, water rinsing, acid pickling, and some post-treatments like water rinsing, neutralization, and drying. These preparations and post-treatments typically have risks for the environment and health [50]. Likewise, sufficient corrosion and wear protection against harsh service conditions cannot be attained by s (CCs) when they are used as a single layer [8,26,49].

The sol-gel method is other straightforward procedure that applies low-temperature curable coating for both decoration and protection purposes. The mechanism of protecting the surface may consist of a simple barrier coating (inorganic or hybrid organic-inorganic), an inhibitor coating, a sacrificial coating, or a coating with a self-healing characteristic [9]. However, operating this method at high temperatures, it is extremely challenging to deposit ceramic on magnesium-based materials.

PVD is an alternate method for addressing Mg's strong chemical reactivity and low electrode potential. PVD is a process that begins with the evaporation of a condensable substance and its subsequent condensation on the surface of the substrate. The coating substance, which is frequently denoted as condensable material, is vaporized from an external source (target or slug). The source material is located close to the substrate to be coated. The vapor is produced by very high temperatures/kinetic energy being applied to the source (solid or liquid). Condensable material transitions to the vapor state and travels in straight lines through the vacuum. Then the condensable vapor hits a cold surface, and the tiny agglomeration of atoms begins to hop on the surface, quickly losing their kinetic energy, a process referred to as lateral mobility or surface diffusion. These ultimately cool and condense to create a solid layer on the surface [26]. However, the coatings had random defects, which might cause the pre-failure of coatings. Similarly, the plasma immersion ion implantation (PIII) process modifies selected surface features and slows deterioration without introducing a foreign coating or changing the bulk characteristics, and is particularly advantageous for surgical implants with complicated geometry. PIII forms oxides or other corrosion-resistant compounds on the surface of Mg and Mg-based substrates [34]. Xu et al. [34] modified the surface of Mg substrate via Cr ion implantation at various voltages followed by oxygen ion implantation to enhance corrosion resistance and cytocompatibility. However, the presence of a Cr-rich layer with Cr in the metallic state underneath the protective oxide coating may jeopardize electrochemical stability by generating galvanic reactions, resulting in decreased corrosion resistance [34]. As other coating techniques, EPD electrophoretic deposition (EPD) is a colloidal process that uses electrophoresis to deposit a surface film with a high thickness on a working electrode with an oppositely charged charge on charged particles in suspension. However, the deposition process is often accompanied by the production of hydrogen bubbles, reducing the coating quality [40]. Protecting an active metal substrate with an inert metal layer is a common industrial operation. Technology for producing metal-based coatings is categorized into electroplating, electroless plating, plasma spraying, and cold spraying [51]. The electrochemical plating process is attractive due to its unique characteristics. The resulting metal coatings exhibit excellent solderability, electrical conductivity, and decorative appearance, as well as high corrosion and wear resistance, all while being simple to operate relatively inexpensive. They are classified into two types of electroplating and electroless plating. Electroplating (often called electrodeposition) is a plating technique that utilizes an electrical signal supplied by an external power source to decrease the cations of a chosen metal in the solution, resulting in a metallic coating. Currently, the main electroless plating process is a "self-reduction" technique that utilizes the autocatalytic reduction of metal ions in an aqueous solution containing a chemical reducer, usually sodium hypophosphite. As its name suggests, there is no need for an external power source for the process of electroless plating. Electroplating, as a contrast to electroless plating, may provide a thicker and more compact metal coating. These two plating techniques may be used alone or in combination with Mg alloys based on the service conditions and shapes of the components [17–19]. However, due to the high chemical activity of Mg alloys, for avoiding severe corrosion of Mg alloys in aqueous plating bath, pretreatment and an undercoating are needed before plating [51].

Anodizing as other coating process has lower sensitivity to the substrate's alloy type but has a more complicated process than CC and electroplating methods. The anodizing process can deposit a porous ceramic-like coating with good paint-adhesion properties and considerable wear and abrasion resistance. Nevertheless, the deposited coating cannot adequately protect the substrate from corrosive electrolyte without appropriately sealing the coating's pores. Moreover, this brittle ceramic coating is not applicable for load-bearing applications or applications needing electrical conductivity. Furthermore,

this coating does not offer satisfactory performance in many service conditions involving mechanical wear [49].

The PEO method is similar to anodizing, but it uses a higher potential, so discharges occur, and the resulting plasma modifies the oxide layer structure. This method makes an oxide layer with a good bonding strength to the substrate and acceptable average roughness of the surface. Anyway, the process can waste higher energy than anodizing and more pollute the environment. Furthermore, the structure of the deposited layer by PEO is porous, which could cause the permeation of aggressive solution and subsequently ruined the protection effectiveness of the coating [48–50,52,53] Another commercially used process is the thermal spray.

A wide variety of functional coatings (e.g., metallic, ceramic, cermet, etc.) designed for special environments can be sprayed utilizing various TS methods. Recent studies have shown the huge potential of TS methods to modify the surface of Mg-based alloys for biomedical and industrial applications. However, a complicated pre-treatment process of the substrate is usually required to ensure good bonding between the substrate and coating because of the high oxidizing nature of the Mg-based substrate. Nevertheless, the solutions suggested by these pre-treatments are often restricted. These factors drive the continuous evolution of new coating strategies for the surface protection of Mg-based alloys. In contrast to the TS techniques (e.g., twin wire arc spray, plasma spray, and HVOF) in which particles either partially or fully melt during the spraying process, the CS process as an emerging spraying technology can minimize the thermal defects, including phase transformation (formation of non-desirable phases), porosity, oxidation, grain growth, and tensile residual stresses [54,55].

The dense coatings with good bonding to the substrate can remarkably enhance the corrosion behavior of the substrate. However, the mentioned requirements may be provided by limited processes mentioned before [54,55]. As a comparatively new coating technique, the CS method utilizes kinetic energy to deposit the layer of coating rather than combined kinetic and thermal energies like the HVOF spray method. CS process consists of propelling fine powder particles, typically in the range of 5 to 50 μm, toward the surface of the substrate with a supersonic velocity in the range of 300 to 1200 m/s. The particles undergo adiabatic heating and plastic deformation (at solid-state) at extremely high shear rates as a result of the impact, resulting in flattening and strong bonding to the underlying surface (material jets formation) [54,55]. Moreover, The CS process could prevent microstructural damage to heat or oxidation-sensitive substrates like Mg alloys, which is frequently seen in alternative TS techniques, like the atmospheric plasma spray (APS) process [45,56–58].

Mg-based alloys are very susceptible to oxidation due to their highly active nature. They also are very vulnerable to creep deformation at elevated temperatures. It was reported that a heat-affected layer (HAL) or metamorphic layer of Mg alloy, which include some thermally grown oxides (TGOs) and creep deformation, can be formed at the interface of Ni-based coating and Mg-based substrate during the APS process when the spray jet impinged the Mg-based surface (with high substrate temperatures). In fact, MgO (as a TGO) was formed during APS, which was detected by elemental analysis (EDS) of the HAL. This issue adversely affected the coating's bonding strength [59]. In contrast to the APS method, a high bond adhesion strength of the coating was ensured by an oxide-free interface and strong mechanical anchoring at the CS Ni coating/Mg-based substrate interface. In fact, low processing temperature and high peening (tamping) influence of the powder particles in the CS process can lead to such high bond adhesion strength of the coating [60]. Many processes have been suggested for the fabrication of different coatings on Mg alloys, such as chemical conversion, sol-gel, PVD, PEO, EPD, and ion implantation [42–44]. With the use of these technologies, researchers are attempting to improve physical barrier coatings' compactness, durability, and thickness while maintaining their simple production techniques [51]. In this respect, the CS process coatings has also attracted tremendous attention recently, since it could also be used for dissimilar metal joining and structural repair of Mg-based alloys. CS process has a huge opportunity to raise manufacturing sustainability. This could be fulfilled by repairing Mg-based alloy components, which previously could only be replaced and recycled. The CS could be considered an environmentally friendly process [61]. In fact, toxic fumes or other harmful substances are not expected in the CS process. Repair and refurbishment with a faster turnaround time are expected from this revolutionary method. Moreover, the CS process could considerably mitigate thermal stresses that are part of the other repair processes (e.g., welding or TS processes). This review article reviews the recently designed coatings specifically applied to Mg alloys (mostly for industrial applications) employing various coating processes. Due to the increased utilization of CS technology both for 3D printed/additively manufactured coatings and repair of structurally critical components, the most recent CS methods for the surface modification, repair, and refurbishment of magnesium alloys are then critically discussed and reviewed in detail, as well as their benefits and restrictions. Lastly, the prospects of this field of study are briefly discussed, along with a summary of the presented work.

1.1. Thermal and cold spray processes

Thermal spray techniques are utilized to deposit coatings from feedstock (in the form of powder or wire). In these techniques (e.g., flame, arc, plasma, HVOF, and CS), molten, partially molten, or even solid particles are sprayed on the substrate surface to form the coat. Particles are propelled (directed) towards substrate surface using several ways based on the used energy in the process: It could be electrical (e.g., electric wire arc spray and plasma spray processes: [229/230]), chemical (e.g., flame spray process including combustion wire spray and combustion powder spray processes and HVOF spray process), or just kinetic energy (solid-state CS process) [62]. However, the solid-state CS process (as relatively new and immerging coating technol-

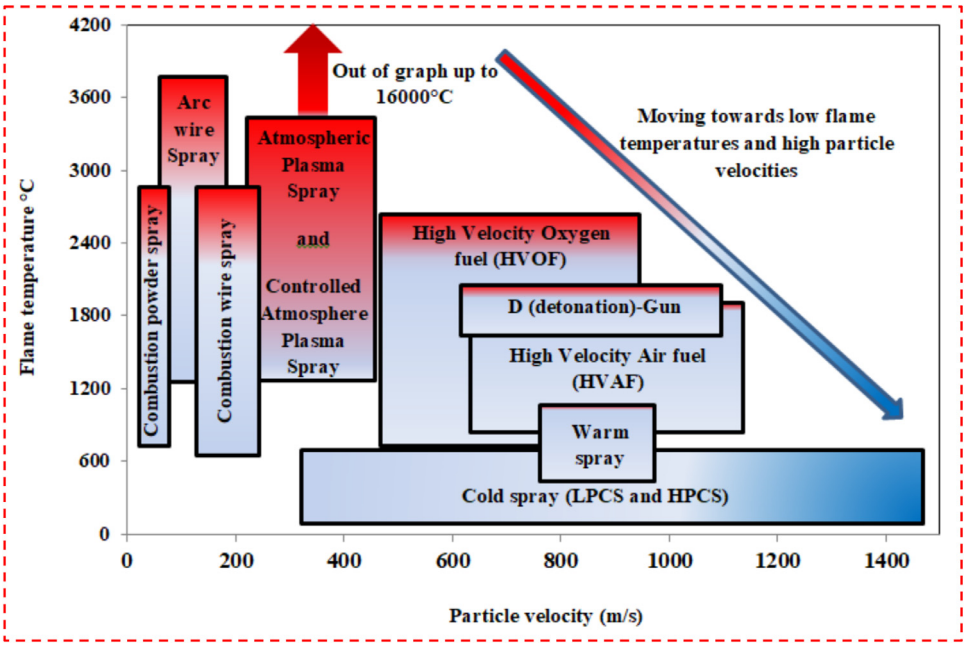

Fig. 1. TS processes (flame or spray stream temperature versus particle velocity) [62].

ogy) has many advantages compared to other types of TS methods. These advantages will be described in subdivision 4.1. Spray stream (gas) temperatures and particle velocities in different spray techniques are shown in Fig. 1 [62]. It is clearly seen that the thermal and kinetic energies impart to the spray particles by each spray technique differ in different spray processes. Flame (spray jet) temperature and gas velocity can directly determine the spray particles' thermal energy and kinetic energy, respectively. For instance, materials having high melting points (e.g., ceramics) are mostly sprayed using the plasma spraying process, which produces high-temperature spray jets. On the other hand, the HVOF process, which utilizes high kinetic energy and relatively low thermal energy, is able to affect the coating characteristics positively. This process is also suitable for spraying materials e.g. WC-based cermet coatings. Over the past decades, the trend has changed to using considerable amounts of kinetic energy compared to thermal energy in spray techniques. In this regard, pure and compact coatings can be achieved using the CS method as an economical and environmentally friendly method because of negligible or zero-level of oxidation during the spraying process [61]. In this method, the heat input is considerably low. This can substantially prevent the substrate from oxidation and also changing the substrate properties during the CS process [63,64]. CS process also eliminates the problems associated with the other TS processes, e.g., phase transformations caused by melting and formation of porosity caused by rapid cooling and solidification [65]. In the CS process, powder particles are not melted in the spray stream [66] due to the low temperature of the process gas, which is well below the powder particles' melting point. The tensile residual stresses, including tensile quenching stresses and also the stresses due to the differences in CTE between coating and substrate material (when sample cools off to room temperature), are generally observed in thermally sprayed coatings. These tensile stresses were lowered by using high-velocity TS processes, e.g., HVOF or high-velocity air-fuel (HVAF) processes, in which a compressive component (or peening stress) is introduced during spray. Moreover, these tensile stresses are considerably alleviated in the CS process. This process with low processing temperature ensures the powder particle deposition at solid state. Hence, compressive residual stresses are mostly anticipated in CS coatings due to high particle velocity impact [56]. So, this can make spraying dissimilar materials possible using the CS process [63,67].

From a microstructure point of view, it should be noted that the typical microstructure of the thermally sprayed coatings is mainly comprised of a lamellar build-up of melted, partially, and also un-melted particles, along with oxide inclusions and unavoidable pores (Fig. 2). On the contrary, mechanical and/ or metallurgical bonding is induced by the solid-state CS process, which utilizes kinetic energy. This can lead to the extremely low oxygen content and porosity level in the microstructure of the CS deposits [55,68].

It is interesting to note that the TS methods can spray almost all materials. Coatings for more minor demanding applications are mostly sprayed by methods such as flame and electric arc spray techniques. Higher oxygen contents and porosity levels are expected in the sprayed coatings produced by such methods. Ceramic coatings are usually sprayed by the plasma spraying method [62]. However, metallic and cermet (hard-metal) coatings are typically deposited by the HVOF method [65,69]. In fact, latitude in material selection (consisting of metals, metal-based alloys, ceramics, cermets, composites, and plastics) is smaller in the CS method compared to other TS processes [62]. Moreover, ceramic and non-ductile

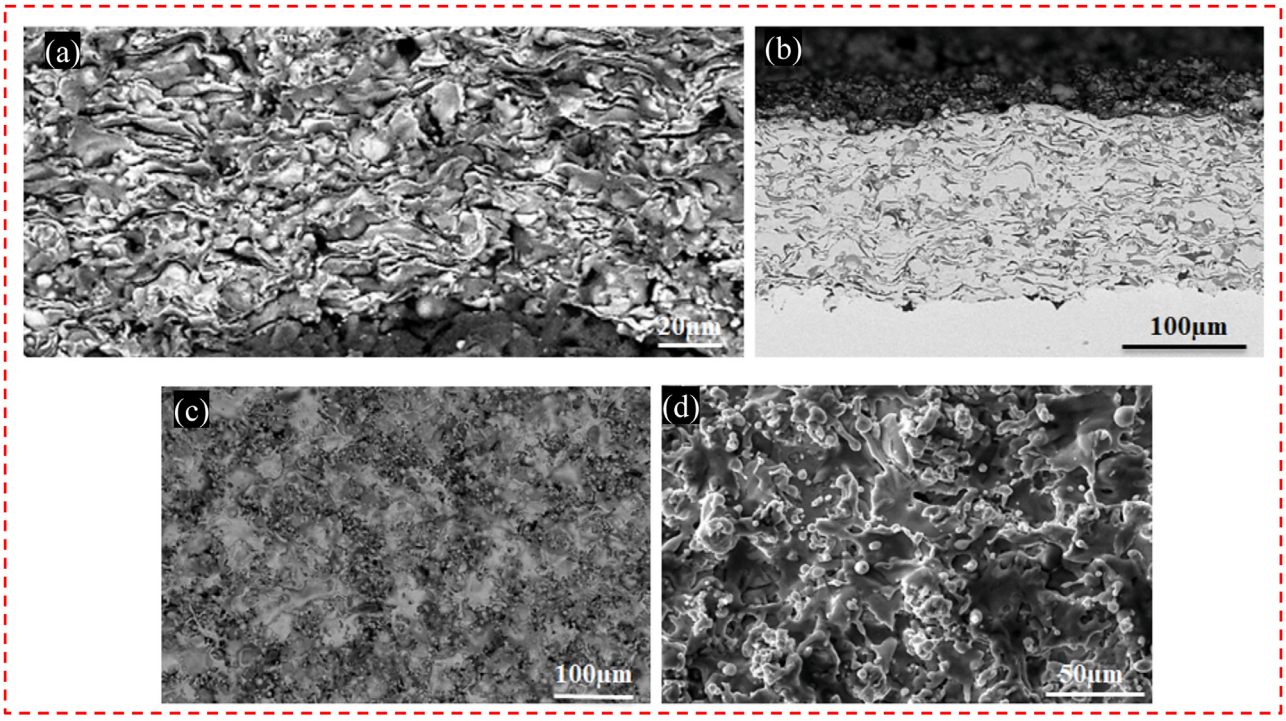

Fig. 2. A thermally sprayed layer (MCrAlYX, M: Ni, Co or both, X: Hf, Si, or Ta, etc.) (a) Fractured cross-section showing a lamellar coating build-up having pores, oxides, and un-melted, partially melted particles, (b) polished cross-section, (c) surface at low magnification, (d) surface at high magnification.

materials cannot be deposited alone by the CS process. A ductile component in the composite coatings is needed when the CS method is used. So, the ductility of the powder particles (i.e., the ability of plastic deformation) is one vital requirement for the sprayed material in the CS process [62,67,70]. Nevertheless, it has been reported that the CS process could be used to embed the ceramic particles on the substrate surface (as surface treatments) [55,71]. Likewise, the tamping effect (in the CS process) was used to easily deposit the cermet coatings (e.g., WC-based materials) on metallic substrates using porous powder particles [56]. Furthermore, a wide variety of materials including pure metals (e.g., Al, Zn, Cu, Ni, Ag, Ti, Fe, Ta, and Ni), metallic alloys (e.g., Ni-Cu, Ni-Cr, Ni-Al, Cu-Sn, Cu-Al, Cu-Zn, and MCrAlY) [72], stainless steels, and composites (e.g., Al-Al_2O_3, Cu-W-Zn, Al-Zn-Ti, Al+SiC, Cu+Al_2O, Ni+TiC) can be sprayed with CS method [62,67,73]. Metals, metallic alloys, polymers, ceramics, and even composites can be used as substrates in the CS process [67].

2. Thermal spray processes for surface modification of Mg alloys

2.1. Substrate pre-treatment

In general, it is crucial that a substrate surface be appropriately prepared and activated before TS processes. This ensures the appropriate bonding of the thermal sprayed coatings. Substrates surface should be roughened after cleaning and degreasing by grit blasting (e.g., aluminum oxide, chilled iron, etc.) or some other methods. This can also increase the surface area of the substrate surface. The grit blasting angle of about or less than 90° should be chosen, and also extreme grit blasting should be restrained to lower the grit inclusion in the substrate surface considerably. In order to remove residual dust, the substrate surface should be cleaned by clean, dry (compressed) air or nitrogen (after the grit blasting process). It has been recommended that the prepared surface of the substrate be coated quickly after surface preparation and final cleaning (with isopropyl alcohol and/or acetone and then (compressed) air or nitrogen) to avert the probability of contamination or substrate surface oxidation (or deactivation) [74].

It is worth mentioning that the oxidation and the mismatch of thermal expansion coefficient (TEC) mismatch between the coating and substrate Mg are the two main factors that can finally lead to the coating spallation in a coated Mg-based substrate. This might get even worse when the coating material is ceramic-based. The formation of a TGO layer on the Mg-based alloy (during the TS process) can significantly compromise the adhesion at the sprayed coating/Mg alloy substrate interface [75]. The Mg alloy surface can be directly affected and oxidized by the plasma flame (spray jet). This can be more pronounced when materials with high melting points (e.g., ceramics) are sprayed using the plasma spraying method. This can considerably debilitate the adhesion at the deposited ceramic layer/Mg alloy substrate interface. The swift detachment of the TS coating from the Mg-based alloy substrate (after the thermal spraying process and then cooling off to ambient temperature) resulted from the abovemen-

tioned problems. Hence, Mg substrate temperature reduction and/or a metallic bond coat were considered to mitigate the problems associated with Mg alloy substrate during the TS process. The TEC mismatch between a ceramic coating and the Mg alloy substrate [59,76] could be decreased utilizing a metallic bond coat (e.g., MCrAlY, M: Ni and/or Co). So, early detachment of the thermal TS processed coating from the Mg substrate (during the TS process and then cooling off to room temperature) could be prevented [58].

Xu et al. [77–79] investigated the plasma spraying ZrC-ZrB_2/Ni and Al_2O_3-TiB_2-TiC/Al cermet-based coatings on MB26 magnesium alloy substrate. The wear and corrosion resistances of Mg substrate considerably changed when cermet-based coatings were applied on MB26 Mg alloy substrate. However, the bond strength of coatings with Mg substrate was reduced. This was ascribed to the severe Mg substrate surface oxidation during the APS process. For preventing the thermal effect on the Mg substrate surface, Fan et al. applied Al interlayer or Ni-P interlayer or NiAl intermetallic compound (as bond coat) between the yttria-stabilized zirconia (YSZ) as thermal barrier coating (TBC) and Mg alloy [75,80,81]. Moreover, Yang et al. reported the complete prevention of Mg alloy from the thermal oxidation during plasma spraying YSZ due to the presence of sandwich Ni-P/Al/Ni-P interlayer on Mg alloy substrate [82]. Nevertheless, there is a significant standard reduction potential (SRP) difference between most metallic bond coats and Mg alloy substrates. There would be conspicuous electrochemical corrosion at the substrate surface when corrosive electrolyte infiltrates into the bonding interface over immersion time. Hence, the bonded areas between the coat and Mg substrate declined. Eventually, the coating came off and lost protection to the Mg alloy. So, an inert and well-bonded layer should be adopted to considerably reduce the unfavorable influences of galvanic corrosion on the bond stability of the thermal sprayed coatings. Therefore, MAO coating having an inert ceramic-like composition and high bond strength with Mg alloy substrate was investigated as a non-metallic bond coat on the Mg alloys. Moreover, no galvanic corrosion was observed at the MAO coating /Mg alloy substrate interface [83].

It was reported that MAO (as a non-metallic bond coat) could stand the molten droplets impact during the thermal spraying process and effectively preserve the Mg alloy substrate from the heat influence of the plasma jet [83]. The composite coating significantly delayed the corrosion electrolyte penetration into the sample (i.e., MAO bond coat/ceramic top layer). This coating also considerably lowered the corrosion rate of the Mg alloy [52,53,83]. This observation was also attributed to the existence of the MAO layer (as an inert bond coat) at the Mg alloy/thermally sprayed ceramic coating interface as well as lack of galvanic cell formation at the Mg alloy substrate/MAO coating interface in the course of long immersion time in chloride-containing solutions [52,83]. As mentioned earlier, the formation of a metamorphic Mg alloy layer consisting of some TGO and creep deformation at the interface between a sprayed bond coat and Mg-based alloy has been reported, when the Mg-based alloy substrate surface with high substrate temperatures is impacted by the plasma flame [5,59,75]. This metamorphic Mg alloy layer was also called HAL (heat-affected layer). The EDS analysis of the HAL layer disclosed that this layer had probably been mainly comprised of MgO compounds. Interestingly, the coatings whose substrates were cooled by cold water (WCS) and natural air (NCS) showed lower tensile bond strength values than that of coating whose substrate was cooled by compressed air (ACS) during the plasma spraying process [5,59]. The substrate temperatures (during the plasma spraying process) and hence the oxidation of samples were reported in the order of NCS > ACS > WCS. It was also reported that the controlled preheating of Mg alloy substrate might improve the bonding condition of the TS coating. This was because of the increment of creep deformation among HAL. A local ''toothed'' interface [84,85] can be formed by the deep penetration of some particles (upon impact) into the creep deformation layer of HAL. Hence, the mechanical interlocking contact (anchoring) at the Mg alloy substrates/splats interface could be increased by this phenomenon [86]. Therefore, the highest tensile bond strength of ACS coating could be ascribed to these observed phenomena [59,84–86].

2.2. Wear and corrosion properties of thermal spray coatings

Materials frequently experience corrosion and erosion as a result of their exposing environment. As a result of this issue, the lifetime of many parts is reduced, and maintenance expenses are increased [87]. Ceramic coatings, metallic and metallic alloy coatings, and cermet and composite coatings are all efficient routes to decrease wear and corrosion on metallic components [88–92].

2.2.1. Ceramics coatings

Ceramic and inorganic coatings are composed of oxides including TiO_2, WC, ZrO_2, SiO_2, CeO_2, Cr_2O, Al_2O_3, Cr_2O_3 and Al_2O_3-TiO_2, WC-TiO_2 phosphates (Ca-P salts), and silicates are used to protect the surface of Mg alloys from direct contact with the external environment by an inert surface. Preparing these coatings is a effective route to improve the hardness, wear, and corrosion resistance of Mg-based alloy substrates. Bolelli et al. [88] used pin-on-disk and dry sand/steel wheel experiments to evaluate the wear behavior of plasma-sprayed Al_2O_3, Al_2O_3-13%TiO_2, and Cr_2O_3 coatings and compared them to electroless Ni and Cr electroplating, as well as HVOF sprayed WC-17%TiO_2 and WC-10%Co-4%Cr cermets. Splats detaching caused dry particle abrasion on plasma-sprayed ceramics, which were brittle but hard. When few wheel revolutions are considered, Al_2O_3, as the most robust coating, showed the maximum wear resistance, overcoming HVOF sprayed and Cr electroplating coatings. No coating wears out in pin on disk testing against the 100Cr6 ball, which has an inferior hardness. Two alumina-based coatings have high friction coefficients and wear rates against the alumina ball because of their chemical affinity, whereas Cr_2O_3 coating was more resistant to wear, with a

lower friction coefficient, and caused less wear on the opposing object. Cr_2O_3 wear scars were made up of plastically deformed splats and particles that created a quite sticky tribofilm [88]. Zeng et al. [89] effectively deposited a TiO_2 coating on the surface of AM60 alloy specimens, employing a thermally sprayed approach, which was then sealed with sodium silicate. Due to galvanic corrosion between the substrate and the coating, the original coating unexpectedly enhanced the corrosion rate in Hank's solution. The TiO_2 coating was porous, according to the results of the experiments. The microhardness and layer thicknesses were 886 HV and 40 μm, respectively. The TiO_2 coating on Mg alloy increased the corrosion resistance of Hank's solution after further sealing with sodium silicate [89].

Rodríguez et al. [93] showed that WC-12Co dense coating with a high wear and corrosion resistance might be deposited on a highly flammable and low temperature melting ZE41 Mg alloy using HVOF. This was a promising novel application of a high-energy TS process on a low melting-point substrate. The spraying distance was 300 mm, which was approximately two to three times the distance suggested for HVOF spraying for the coating of WC-12Co on steels. Despite this, the deposited WC-12Co coatings were dense, uniform, and free of cracks. The coatings bonded to the substrate quite well, and the spraying distance allowed for no thermal effects on the substrate. To minimize a large mass increase in the specimens, the coating thickness was limited to 45 μm. The coatings decreased the substrate's wear rate by 104 times, making it more resistant to wear. Electrochemical corrosion tests were carried out to investigate the coatings' corrosion protection, revealing that the Mg-based substrate can be protected for 96 h in contact with a 3.5 wt.% NaCl aqueous solution [93].

Arrabal et al. [94] studied the corrosion behavior of Al/SiC TS coated AZ31, AZ80, and AZ91D alloys in neutral salt fog and high relative humidity settings. The as-sprayed Al/SiCp coatings had a low density, and there was poor interaction between the deposited aluminum splats and SiC particles. Cold-pressing decreased the amount of interconnected pores, resulting in more uniform and smoother coatings with better bonding at the substrate/coating interface. There was no evidence of the formation of diffusion layers or the degradation of SiC particles. In addition, samples with as-sprayed Al/SiCp coatings showed minimal surface degradation in high humidity environments, with the formation of bayerite in the coatings' outer regions and partial dissolution of the Mg substrates because of the galvanic corrosion. The through-coating pores and the different nobility of aluminum and Mg were the driving forces behind this. Because of the reduced number of interconnected pores, the Al/SiCp coatings were more effective against corrosion after the cold-pressing post-treatment. As a result, corrosion products containing β-$Al_2O_3{\cdot}3H_2O$ were only localized at the Al/SiCp interfaces in the coatings' surface [94].

2.2.2. Metallic and alloy coatings

In a corrosive environment, each metal has its own electrode potential/corrosion potential, which is a good indicator of corrosion resistance. In industrial applications, an inert metal coating is commonly used to protect an active metal substrate. Cold spraying, plasma spraying, electroplating, and electroless plating are the most common technological techniques for preparing metal-based coatings. Metal powder can be sprayed onto Mg alloy surfaces to provide a coating similar to Cu and Ni-based coatings [47]. Plasma spraying uses plasma as a heat source to melt or partially melt metal power, which is then sprayed onto the surface of Mg alloys to form a metal-based coating, such as an Al-based coating [48].

Arrabal et al. [90] research looked into the corrosion behavior of TS aluminum coatings applied to AZ31, AZ80, and AZ91D Mg alloys in various environments, including 3.5 wt.% sodium chloride solution, neutral salt fog, and high relative humidity with a 98% RH and 50 °C temperature. They also evaluated to determine the effects of a cold-press post-process on Al coatings' morphology and corrosion behavior. The existence of interconnecting pores in the as-sprayed Al coatings aided the galvanic corrosion of the Mg-based substrates in chloride-containing conditions. With a decreased amount of porosity, the cold-pressed aluminum coatings showed better corrosion behavior. Although the corrosion rates for all of the evaluated materials were lower in high-humidity environments than in a salt fog, similar corrosion properties were seen: formation of hydromagnesite on the surface of the materials that were not treated, galvanic corrosion in TS processed Al samples, and minimal corrosion attack of the Al coating with the formation of bayerite (β-Al_2O_3–$3H_2O$) for the cold-press treated samples [90].

García-Rodríguez et al. [95] used the HVOF deposition process to apply stainless steel coatings to the surface of the ZE41 Mg alloy for the improvement of corrosion resistance. The coatings with thicknesses ranging from 42 to 478 μm were found to be homogeneous, crack-free, and fully dense. Two coated samples had a corrosion resistance comparable with bulk stainless steel and protected the substrate for 7 days in a 3.5 wt.% sodium-chloride solution. One of the coated samples could protect the substrate after 48 days of immersion, with no signs of degradation [95]. Guo et al. [96] used HVOF thermally spraying to coat AZ61 Mg alloy with NiCrAl intermediate layer with outer of Fe-based amorphous coating. The typical mismatch of Fe-based materials and Mg-based substrate was overcome by the intermediate metallic coating, resulting in strong metallurgical bonding in the interface regions. In 3.5% NaCl solution, the protective Mg-based alloy with Fe-based amorphous coating had nearly ten times the hardness and two orders of magnitude lower corrosion rate than the Mg-based substrate, demonstrating nearly ten times the hardness and two orders of magnitude lower corrosion rate than the Mg-based substrate [96]. Pardo et al. [91] evaluated the corrosion behavior of Al and Al-11Si, TS coated AZ31, AZ80, and AZ91D Mg-based alloys in 3.5 wt.% sodium-chloride solution at a 22 °C temperature. Galvanic corrosion of Mg-based substrates was detected at the interface of the substrate and coating layer, while as-sprayed Al and Al-11Si coatings had a porous structure. A cold-press process was employed as post-treatment for smoothing and

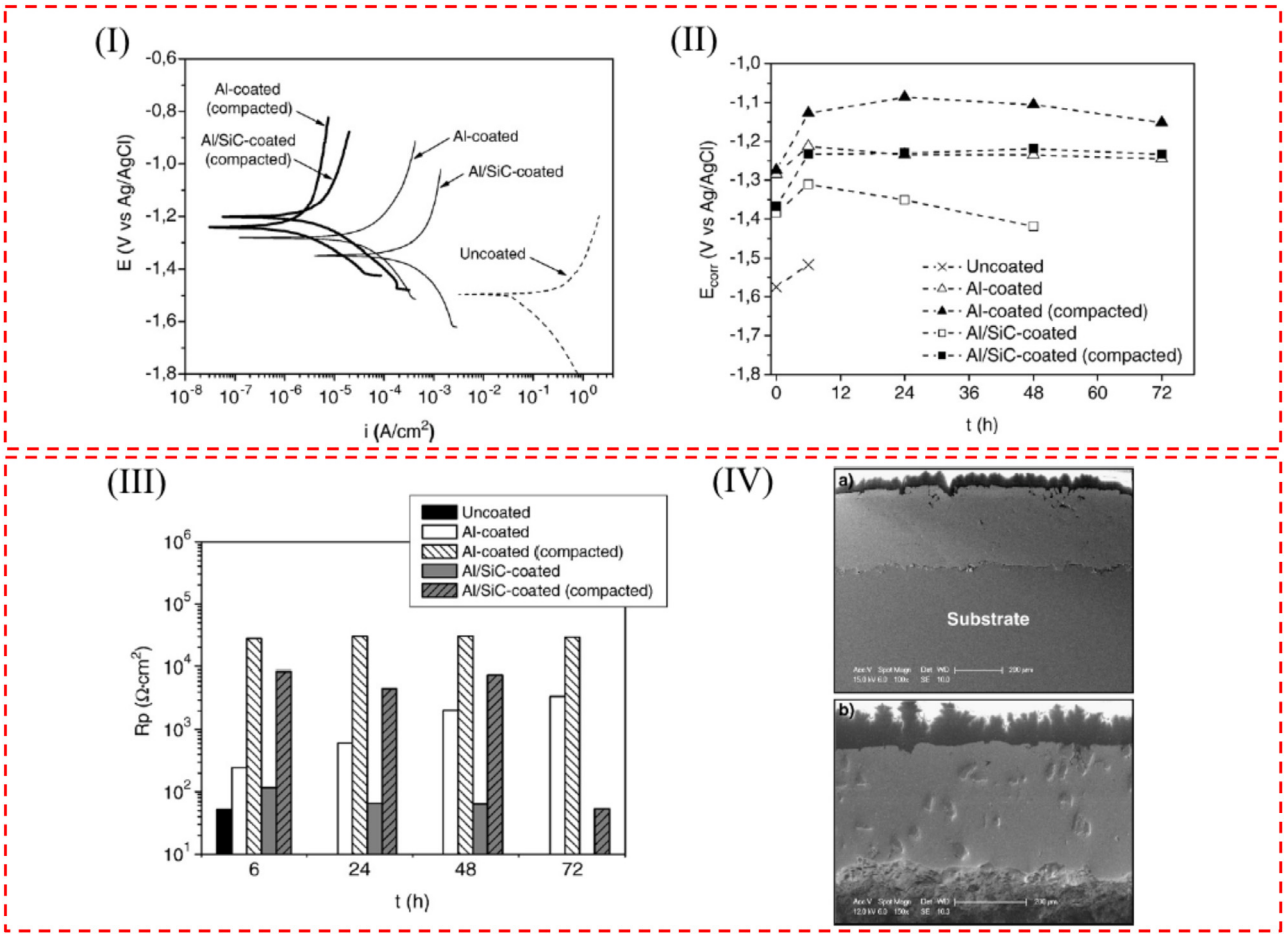

Fig. 3. Results of corrosion behavior evaluation of uncoated, Al-coated, compacted Al-coated, Al/SiC coated, and compacted Al/SiC coated pure Mg in 3.5 wt.% sodium-chloride solution. (I) PDP curves after 1 h of immersion (II) E_{corr} against immersion time. (III) Polarization resistance (Rp) against immersion time. (IV) Image of transversal-section of compacted coatings on pure Mg substrate after 24 h of immersion: a) monolithic Al coating and b) Al/SiC composite coating [92].

densification of the coatings, resulting in enhancement of contact between coating and substrate and significantly improving the corrosion resistance. In all cases, cold-pressed Al coatings performed admirably as a corrosion barrier, regardless of the composition of the Mg-based substrate, and showed the same corrosion performance. Nevertheless, the solution could penetrate to the cold-pressed Al-11Si coatings, and galvanic corrosion of Mg-based substrates was detected after some days of immersion [91].

2.2.3. Cermet and composite coatings

Campo et al. [92] studied the corrosion behavior of TS processed Al and Al/SiC composite coated monolithic Mg in a 3.5 wt.% NaCl solution. For the Al/SiC composite coating fabrication, 9 vol.% of reinforcement were used, and the porosity of the resultant coating was about 3.5%. As-sprayed monolithic Al coating porosity was between 2.4% and 4.4% based on the spraying distance and number of deposited layers. The Al and Al/SiC coatings were produced with almost porous coatings that were mechanically compacted at room temperature. In electrochemical measurements, all coatings had greater E_{corr} (approximately 200 mV) than untreated substrates (Fig. 3), whereas current densities were roughly two times less for the Al/SiC composite coatings and three times less for the monolithic aluminum coatings [92]. The compressed coatings provided considerably more protection, with current densities five to six times less than bare Mg [92]. Parco et al. [97] used the HVOF spray technique to coat AZ91 and AE42 Mg alloys. The HVOF spray technique could apply dense WC-Co coating on Mg-based alloy substrates. A "self-roughening" effect on the substrate was occurred because of the high kinetic energy of the WC-Co particles, allowing deposition on polished Mg alloy substrates. The coatings well adhered to the Mg-based substrates. Corrosion testing revealed that unsealed WC-Co coatings did not affect Mg alloy corrosion behavior. On the other hand, the duplex coating technique with an Al bond coat considerably enhanced the corrosion behavior of Mg alloys [97]. Kubatík et al. [98] used a high-enthalpy plasma spray process using a water-stabilized plasma torch to spray commercially pure (CP) Al and $AlCr_6Fe_2$ alloy. The deposited CP and $AlCr_6Fe_2$ coatings had a thickness of approximately 200 and 450 μm, respectively, and aluminum oxides existed on the coatings. Metallurgical bond layers with a thickness of roughly 100 μm

and a eutectic morphology were achieved for both coatings. Microstructure, elemental, and phase composition analyses showed that the bond layer with CP aluminum coating is primarily $Al_{12}Mg_{17}$, whereas the bond layer with $AlCr_6Fe_2$ alloy is a combination of $Al_{12}Mg_{17}$ and Al_3Mg_2. Despite porosity on the coatings, the resulted polarization resistances were higher than that of uncoated substrate. Adhesion tests did not show a decrease in adhesion strength because of the existence of intermetallic in the bond, and the phase composition and microstructure of the coatings were shown to be more important [98]. Yao et al. [99] employed a high-velocity suspension flame spray method to deposit biodegradable HAp/Mg composite coating on AZ91D Mg alloy substrates, using HA powder in nano size and Mg powder in micron size to enhance the corrosion behavior and bioactivity of Mg alloy. The composite coating's corrosion resistance was tested in Hanks' balanced salt solution (HBSS). The results revealed that the HAp/Mg composite coating mainly consisted of Mg and HA, with a small amount of MgO phases. The coating had a rough surface morphology, uniform element distribution, lamellar structure, and a well-bonded coating/substrate interface in cross-section. Mg particles exhibited improved deposition during spraying because of their better melting degree than HA particles. The HAp/Mg composite coating effectively improved the corrosion behavior of AZ91D Mg alloy substrate in HBSS, with Mg dissolving on the composite coating surfaces [99].

2.3. Post-thermal spray treatments

TS technology now includes several methods that apply a wide range of functional coatings with customized conditions. The major benefit of TS methods is the possibility of using a coating system with entirely distinct characteristics to the substrate material. New studies have revealed that these methods offer much potential for enhancing the wear and corrosion behavior of Mg alloys. In an air environment, the substrate surface oxidizes quickly because of Mg's strong oxygen affinity. A hydroxyl layer is typically generated on the surface within a few minutes. The adherence of TS coatings to the substrate can be considerably reduced due to the existence of this film [100]. Because of the inadequate adherence between TS coatings and Mg-based alloys substrate, some post-processes are required. One of these post-processes is high-energy beam treatment, in which a remelting of the coating and a thin layer of the top of the Mg-based substrate happens during this process. Different processes can be carried out in modified layers depending on the coating system used and the treatment method used [101]. Bobzin et al. [102] applied alloyed AlSi20 powder was onto the AZ31B Mg alloy by APS, laser cladding, and a combination of both processes. In a pin-on-disk arrangement, the thermally sprayed coating reduced the abrasion rate by 35% and the i_{corr} value by more than one order of magnitude. The abrasion was decreased by 57% after a laser remelting post-treatment, and the i_{corr} was lowered by another magnitude. In comparison to the laser remelted coating (total quantity of 61%), laser cladding did not substantially improve abrasive wear resistance, but it did show the best results in terms of corrosion protection because of a non-porous structure. All three coatings were tested for impact resistance at 50 Hz, 200–600 N, and up to 1 million cycles. All coatings were plastically deformed in the impact zone, with the laser cladding coating deforming the least and the laser remelted coating deforming the most. When a critical load/number of cycles was reached, a crack occurred at the interface between the thermally sprayed coating and the substrate. Wear and corrosion protection were provided by all coatings [102]. Pokhmurska et al. [101] presented several examples of laser and electron beam treatment of aluminum-based composite coatings and infrared irradiation of zinc-based coatings. They used arc spraying with Zn, $ZnAl_4$, and $ZnAl_{15}$ solid wires and cored wires in Al core with powder filling comprising various hard particles, like Si, B, and WC or TiO_2, for coating of AM20, AZ31, and AZ91 Mg alloy substrates as shown in Fig. 4 [101]. All procedures applied to treat the coatings resulted in the development of changed surface layers on the Mg-based substrate, enhancing wear and corrosion characteristics.

2.4. Mechanical properties of thermal sprayed coatings

APS is one of the most common TS technologies among other methods due to its adaptability, high deposition rates, and versatility. The plasma spray process is employed to deposit the coatings of almost all materials, including metallic alloys, ceramics, and cermet, with a similar melting point onto the substrate. It is well established that the characteristics of plasma spraying coatings depend on various plasma spraying process factors, including powder feed rate, spraying power, and spraying distance. These factors directly affect the heat and mass transfer between particles and the plasma jet, which in turn affects the degree of particle melting, the temperature, and the in-flight velocity of droplets before contact with the substrate [103]. Kumarasamy et al. [103] used the APS method to deposit alumina coatings at various power levels, powder feed rates, and stand-off distances. As hardness is the most critical attribute, it has a significant impact on the service life properties of coatings. The microhardness of plasma sprayed alumina coatings was predicted empirically using response surface methodology (RSM), including APS operating factors. At a 95% confidence level, the established relationship may be utilized to accurately estimate the microhardness of alumina coatings on AZ31B Mg alloy. The input power had a larger effect on the microhardness of plasma sprayed alumina coatings than process factors like powder feed rate and stand-off distance. Bakhsheshi-Rad and his co-workers [104] deposited NiCrAlY/nano-yttria stabilized zirconia (nano-YSZ) dual-layered coating on Mg-1.2Ca-3Zn alloy by plasma spray method and evaluated its microstructure, mechanical characteristics, and corrosion resistance. The results indicated that the nanostructured YSZ upper layer includes fewer porosities and microcracks than the NiCrAlY base layer. After NiCrAlY/nano-YSZ plasma spray coating, the microhardness of the untreated samples in-

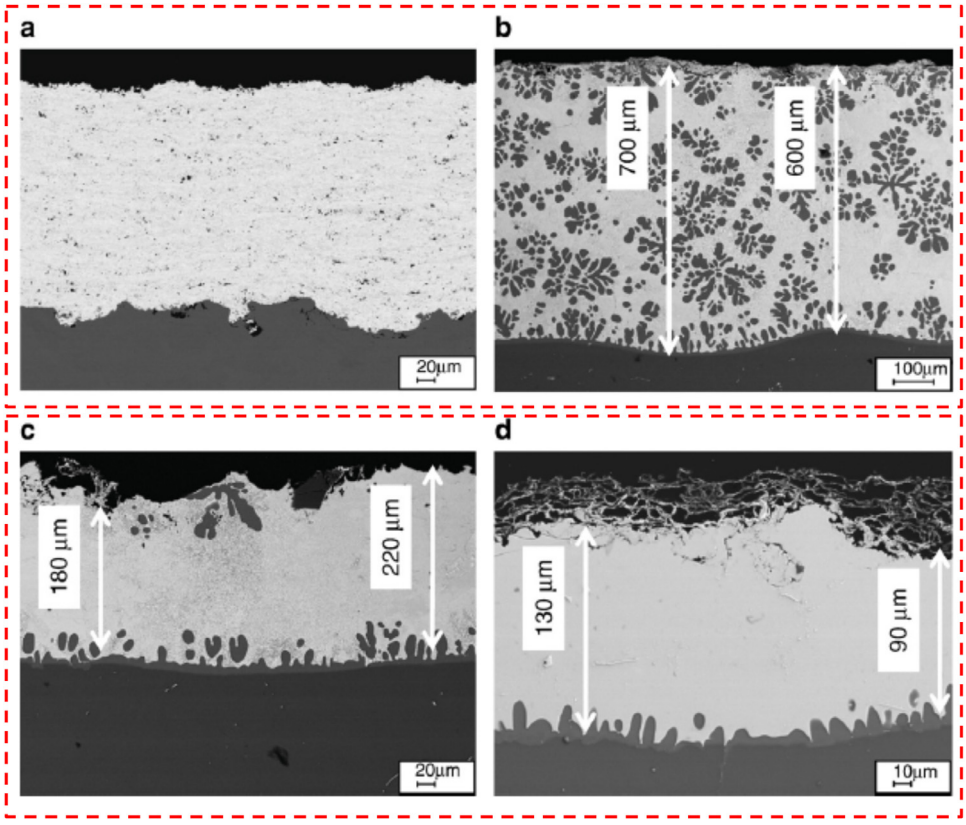

Fig. 4. (a) Cross-sections SEM images of the arc sprayed Zn coating on AM20 Mg alloy (b–d) the layer after infrared irradiation post-treatment modification with different distances from focus line (b) 0 mm, (c) 30 mm, and (d) 50 mm. Other process parameters: the power of 2.3 kW, power density in the focus of 3×10^6 W/m^2 [101].

creased considerably from 65.2 to 760.8 HV. However, as compared to the NiCrAlY/nano-YSZ coating, the NiCrAlY coating had a lower binding strength. The i_{corr} of the Mg-1.2Ca-3Zn alloy was reduced by single-layer NiCrAlY and dual-layer NiCrAlY/nano-YSZ plasma spray coatings [104]. In another study by Bakhsheshi-Rad et al. [105] novel combination of APS and dip coating methods was used to deposit a triple-layer nano-YSZ/polycaprolactone (PCL) coating on Mg-Ca alloy for the further improvement of mechanical and corrosion properties of the Mg alloy. After immersion in 3.5 wt.% NaCl solution, the compressive strength of the triple-layer plasma/polymer coating was greater than that of plasma-coated and untreated specimens. However, both single-layer and dual-layer plasma coatings exhibited greater bonding strength than the triple-layer plasma/polymer coating. The corrosion resistance of Mg alloy was remarkably enhanced by a triple-layer nano-YSZ/PCL coating, as evidenced by a lower corrosion current of 0.14 mA/cm^2 versus 285.3 mA/cm^2 for the bare Mg alloy, a higher E_{corr} of −1252.8 versus −1631.4 mVSCE, and a remarkably lower corrosion rate of 0.003 mm/year against 6.51 mm/year. A corrosion process was suggested for Mg alloy single, double, and triple-layer coating [105].

Gao et al. [106] used the plasma spraying technique to effectively coating an AZ91HP Mg alloy with Al_2O_3. As the transition layer, an Al-Si eutectic alloy was utilized to mitigate the difference in physical and chemical properties of Al_2O_3 and the Mg-based substrate. In this research, the coating's mechanical characteristics were investigated, and the findings indicated that the coating was mostly composed of stable and metastable γ-Al_2O_3 phases and had a lamellar microstructure. The peak loads of Mg-based substrate, the Al-Si layer, and the plasma-sprayed Al_2O_3 layer were 0.25, 0.6, and 2.2 mN, respectively, according to nano-indentation experiments results. The microhardness and modulus of elasticity of the deposited Al_2O_3 coating layer were 7.45–8.90 and 250 GPa, correspondingly, which were much higher than those of the Mg-based substrate (0.8 and 50 GPa). The plasma-sprayed Al_2O_3 coating had a wear volume of about two orders of magnitude lower than the Mg-based substrate. Kubatk et al. [107] deposited CP aluminum and $AlCr_6Fe_2$ aluminum alloy with the thicknesses of 450 and 490 µm on AZ91 Mg alloy, using plasma-spray process. The adhesion strength of plasma-sprayed aluminum was about 19 MPa, whereas the adhesion strength of the aluminum alloy was around 12 MPa. Plasma-sprayed coatings increased the AZ91 surface's wear resistance by up to fourfold [107].

Garcıá-Rodrıǵuez et al. [108] deposited stainless steel coatings by HVOF method on ZE41 Mg alloy substrates. For comparison, bulk 316 L stainless steel and ZE41 Mg alloys were also examined. The coatings provide up to 93% more wear resistance than uncoated ZE41 (at low loads and speeds)

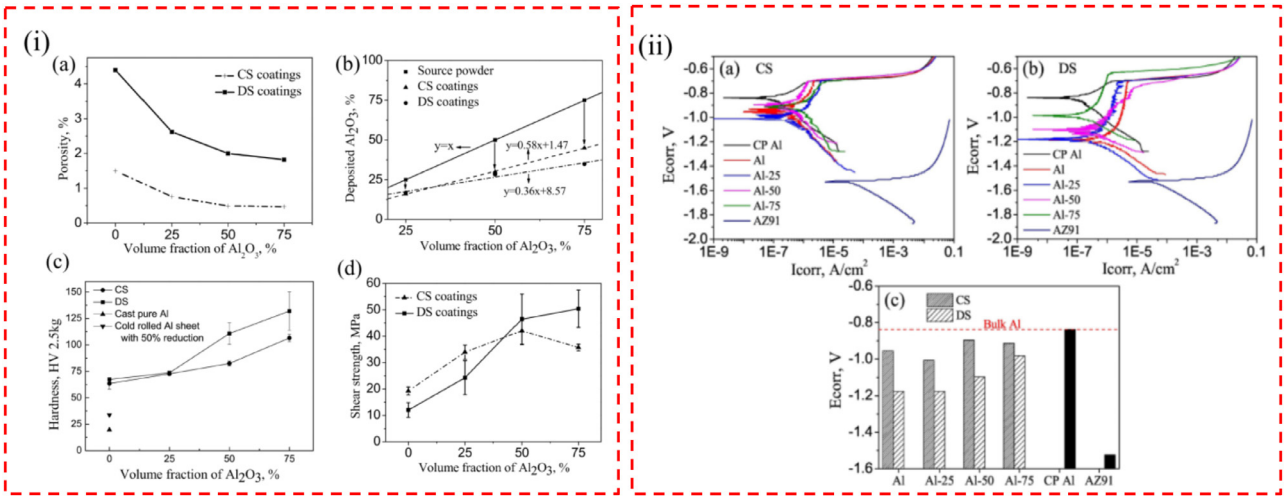

Fig. 5. i(a) The porosity changes of CS and DS coatings against the Al_2O_3 content; i(b) the deposited number of Al_2O_3 particles in CS and DS coatings compared to that in the source powder; i(c) The hardness of CS and DS coatings against Al_2O_3 content in the source powder; i(d) The shear bonding strength of CS and DS coatings against Al_2O_3 loading in the source powder. ii PDP curves of ii(a) CS coating and ii(b) DS coating against bulk CP aluminum and uncoated AZ91 alloy substrate, ii(c) the compare of corrosion potentials [109].

and only 11% less than bulk 316 L stainless steel under the optimum conditions (at high loads and speeds). The appearance of a mechanical mixing layer (MML), which considerably reduced the wear rate, changed the major wear mechanism due to the number of layers that produced the coatings [108].

Wang et al. [109] fabricated Al_2O_3 reinforced Al-based metal matrix composite coated AZ91 Mg alloy using two different coating methods, namely CS and thermal detonation spraying (DS). The findings indicated that the CS process, characterized by high kinetic and low thermal input energy, resulted in a dense structure due to particles colliding at high velocity with the solid-state. Because of melting and oxidation in the coating process, the DS treated coatings have rather high porosity. However, when the porosity of the ceramic reinforcement was decreased to a more significant volume percentage, the DS coating showed better bonding strength and hardness (Fig. 5-i) [109]. For both CS and DS treated composite coatings, raising the vol.% of Al_2O_3 particles in the source powder resulted in shifting from adhesive to cohesive mode. Both CS and DS composite coatings demonstrated increased corrosion resistance than the Mg-based substrate (Fig. 5-ii) [109].

3. Cold spray technology for designing 3D printed/additively manufactured coatings on Mg alloys

Thermal spraying on the surface of the Mg-based alloy is a fairly established process [110,111]; however, it unavoidably leads to substantial undesirable influences on the Mg-based alloy substrates (as discussed in 3.1). In recent years, an opportunity for the comprehensive improvement of the surface properties of Mg alloys has been provided by the development of CS technology [55]. The CS or cold gas dynamic spray (CGDS) method based on the aerodynamics principle is considered a relatively new kind of coating preparation process [112,113]. The improvement of surface properties for different applications, such as aerospace, automotive, power generation, medical, and electronics, could be potentially provided with the 3D printed/additively manufactured CS coatings. Moreover, the coatings of, e.g., nanostructured materials, composites, and multilayered functional gradient materials that are generally difficult to be produced by the other TS processes, can be sprayed by the CS process. The CS method can substantially prevent the thermal impact of the extreme spraying temperature on the Mg alloy substrate during the spraying process. This boils down to the temperature of the powder particles, which do not reach the melting temperature during the CS process. In the CS method, a good interface bonding between the coating and the Mg alloy substrate forms (i.e., mechanical interlocking and/or metallurgical bonding at the coating/substrate interface). This was mainly attributed to the high-speed impact of the powder particles, which densifies the coating and can remove the oxide film on the substrate surface (or underneath the deposited layer) [55,112]. Hence, CS technology can provide an effective method for surface protection/enhancement of Mg-based alloys.

3.1. Benefits and restrictions of the cold spray process

The followings are the advantages of the CS process [54,114–117]:

1. Nanocrystalline (NC) and non-crystalline materials that are sensitive to temperature, materials which are reactive to oxygen, e.g., Al, Cu, and Ti, and also the materials that are susceptible to the phase transformation, e.g., carbide composites can be deposited by the CS technology because of its low deposition temperature [118,119].
2. Generally, the CS process of metals can improve their fatigue resistance. This is mainly related to the micro shot-

Table 1
Different thermal spray methods (porosity percentage and oxygen contents range of coatings/deposits) provided from [55,68,69,117,118,121].

Method	Porosity%	Oxygen content (%)
Cold spray	Mostly less than 1	Similar to feedstock powder
HVOF	About 1	0.2
Plasma	1–7	0.5–1
Arc	10–20	0.5–3
Flame	10–20	4–6

peening effect (tamping effect), making compressive residual stresses in the CS coating layer.

3. The CS metals/alloys may be comparable to the wrought alloys/metals due to high degrees of consolidation in the microstructure of CS metals/alloys. This results from the inherent low-temperature and high-kinetic energy features in the CS process [120,121].
4. The CS deposits/coatings have higher electrical and thermal conductivity due to a denser microstructure and lower content of oxides [67,68]. In contrast to CS coatings, porosity and oxygen content are higher in the coatings produced by the other TS methods. In general, increment of particle velocity could lead to the reduction of porosity and oxygen content (Fig. 1 in 1.2 section and Table 1 [55,68,69,117,118,121]).
5. Higher deposition efficiency (D.E) has been reported for the CS method (e.g., up to 97% for CS Cu coating [122]); however, in contrast to the other TS processes [54,55] equal or abject deposition rate has been observed for the CS process [6].
6. In the CS process, smaller spray spot size (i.e., nozzle exit with a diameter of 5–7 mm) and shorter standoff distances (typically 25–30 mm) result in higher accuracy in controlling the deposition area on the substrate surface. This can also decline the requirement of covering (masking) of the as-sprayed part/coating during the CS process [55,123,124].
7. The CS technology fulfills the possibility of joining of different material types. This originates from the lower heat transfer into the substrate during the CS process, which reduces the importance of the material type of the substrate as shown in Fig. 6.
8. The microstructural damage of the heat-vulnerable substrates such as Mg alloys which are often observed in the alternative TS methods, is prevented by the CS process. In this process, the layers with higher thicknesses (up to 13 mm or even more) could be sprayed without de-bonding in the cold-spray additive manufacturing (CSAM) process. This stems from the presence of the higher compressively stresses in the CS layer [45,52,53,55,58,105,108].
9. Wide range of soft and hard metals or alloys, metal-matrix composites (MMCs), and some cermets could be CS processed [54,55].
10. Improving the corrosion behavior of Mg alloy is one of the main functions of the surface coatings. So, the effectiveness of different coatings should be investigated. Fig. 7 shows a graph of corrosion current density (i_{corr}) and E_{corr} of each coating as well as AZ31 and AZ91D Mg alloy substrates in 3.5 wt.% NaCl solution. Better general corrosion resistance is mainly attributed to the lower i_{corr} and higher (nobler) E_{corr}. Per Fig. 7, in general, CS coatings on Mg alloys showed better general corrosion resistance compared to the other types of coatings on Mg-based alloys [111,124–126].
11. The outcomes of the salt spray experiment on coated AZ31 and AZ91 Mg alloys showed that the conventional chromate CC on Mg alloys can last up to 120 h in the 5.0 wt.% NaCl spray solution, while non-chromate CCs can just withstand 24–48 h in this corrosive environment. In contrast to these coatings, anodized coatings can last up to hundreds of hours. Nevertheless, electro-plating and CS coated samples can withstand up to 1000 h (per ASTM B-117 salt fog spray test). However, top coatings can considerably improve the general corrosion resistance of all these coating systems [60,125,127]. Nevertheless, the followings are some restrictions of the CS process [54,55,117]:
12. In general, powder materials with adequate formability in the processing temperature window could be sprayed by the CS method (as a solid-state process). In contrast, powder materials which have a low capability to deform in low temperatures plastically are not appropriate to be deposited by the CS method. However, many attempts have been made to develop the CS systems spraying such powder materials (e.g., high strength metals and alloys) in recent years. In this regard, high-pressure cold spray (HPCS) systems as an alternative to low-pressure cold spray (LPCS) systems have allowed scientists to partly concur with the restrictions mentioned above on the type of powder materials for the CS process.
13. Powder particles generally experience a high plastic deformation rate during the CS process. This will result in a considerable decrease in the formability of the CS deposited materials. However, the temper of feedstock powder particles (i.e., heat-treating feedstock powder particles) might partially mitigate this mentioned problem. Nonetheless, post-CS heat treatments could considerably enhance the mechanical properties of the CS deposits/coatings.
14. The CS process, like the other types of TS processes, is a line-of-sight process. This restricts the CS process from being used for coating the internal surfaces (internal diameters or IDs). In recent years, some commercial manufacturers of CS equipment have presented special CS nozzles that can coat the IDs (with a minimum diameter of about 90 mm).
15. The working efficiency reduces when the CS nozzle is clogged up. This typical nozzle clogging mostly occurs during the spraying process when the powder particles with low melting point and density (e.g., Al, Zn, Mg, etc.) are cold sprayed. However, this problem can be alleviated by means of water-cooled nozzles along with specialized hardware. These nozzles get to decline the nozzle wall temperature considerably and can minimize the nozzle clogging during the CS process.

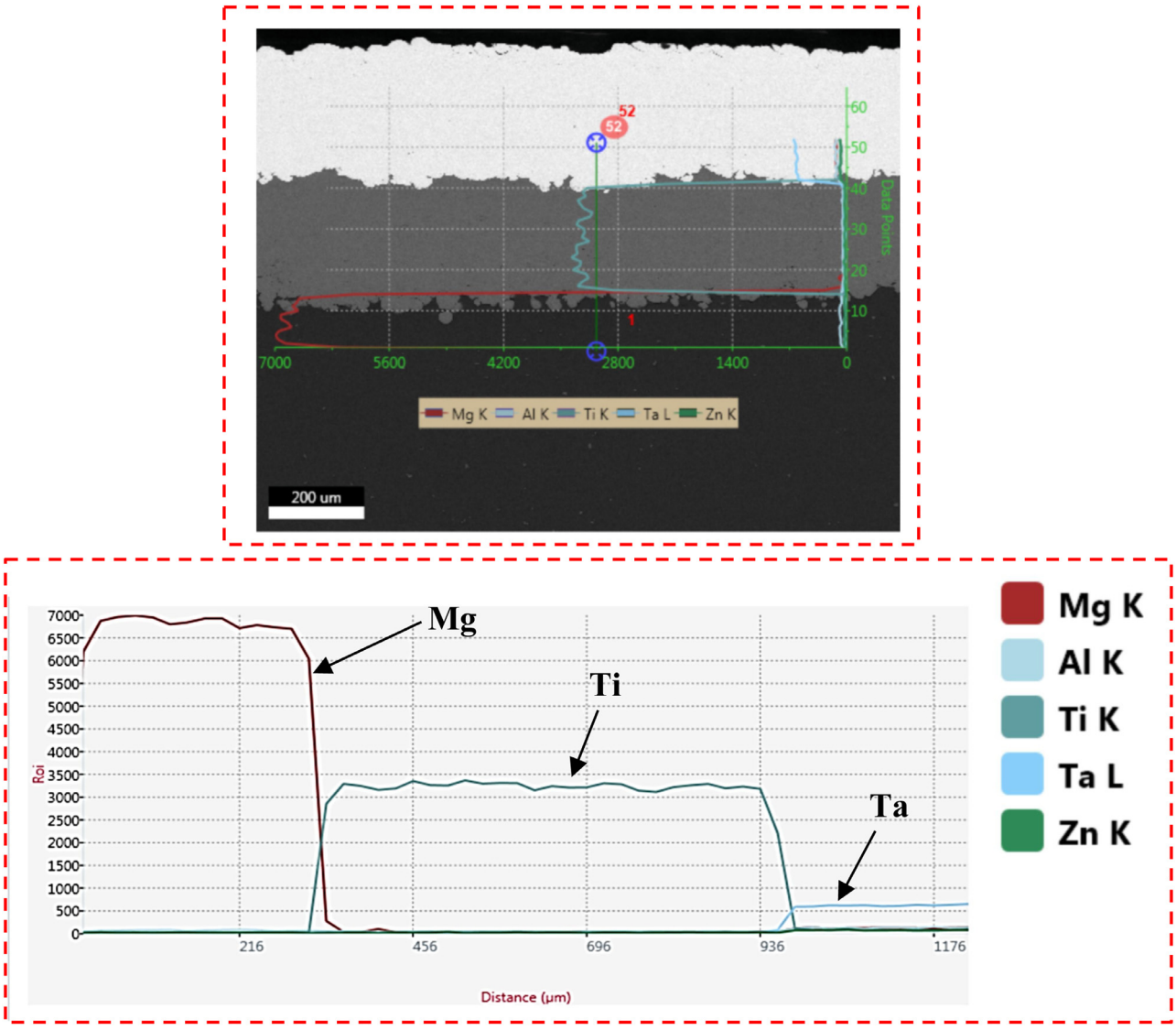

Fig. 6. CS bi-layered Ta/Ti coating on AZ31B Mg alloy.

16. Capital costs are significantly low in the flame spray and arc spray processes. On the other hand, these costs are higher in the HVOF process and even higher in low-pressure (LPPS) or vacuum plasma spray (VPS) processes. The main capital costs in the HPCS process are mainly related to the high-pressure powder feeder and gas heater as well [6]. Capital costs in the CS process are higher than those in the other processes (expect low-pressure and VPS processes). However, running costs in the CS process is at the same level as in the combustion powder (flame) spray and could be even lower than those in HVOF and plasma spray processes. In general, running costs would be lower in the methods which use wires rather than powders (from the feedstock price point of view). Likewise, processing (propellant) gas costs are high in the CS process and could be even higher when He is utilized as processing gas [55]. So, in recent years, the development of efficient CS systems which use cheaper processing gasses (e.g., N_2) has been given too much attention.

3.2. Surface preparation of Mg and its alloys before cold spray process

Two common methods are normally employed to prepare the substrate surface for the CS process: (1) substrate surface grinding using SiC abrasive papers. A roughness of around 0.5 μm could be obtained using this method. (2) Grit blasting, which is extensively used (as briefly explained in Section 3.1). In this method, a surface roughness of around 5 μm could be achieved [127,128]. However, apart from the substrate material type, type of used particle (grit), size and shape, gas pressure, blasting angle, and time are the characteristics that can affect the surface roughness average [55,129]. The substrate surface is normally grit blasted before the CS process until the surface gets a matte finish. The surface is then sprayed with isopropyl alcohol and brushed using a nylon brush to remove any large contaminants and residue. Extra cleaning of the surface using isopropyl alcohol and/or acetone and nitrogen blow-off are then recommended [123,124,126].

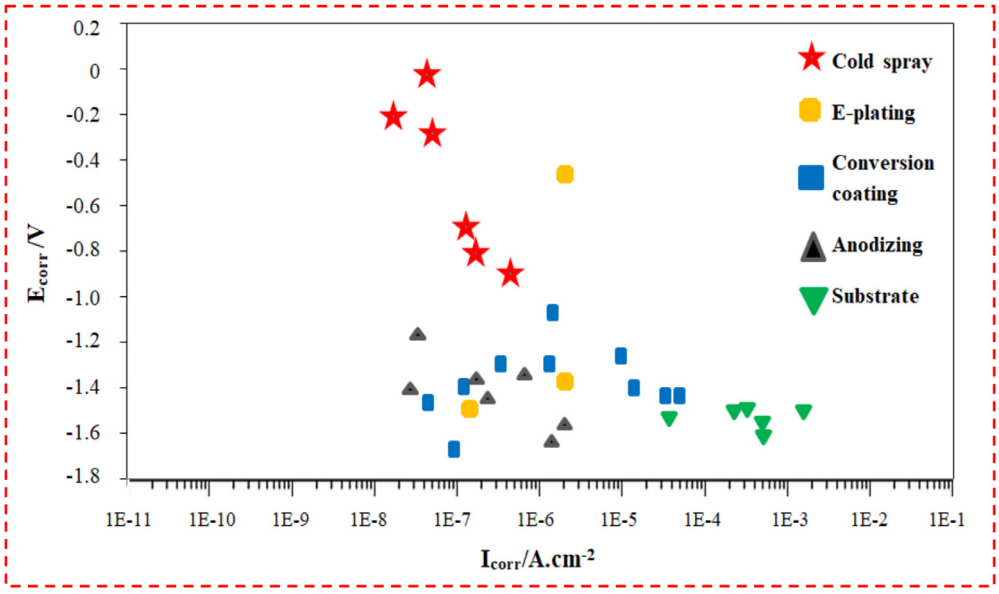

Fig. 7. The graph of Ecorr vs. i_{corr} for coated and uncoated AZ31 and AZ91 alloys in 3.5wt.% NaCl solution [111,124–126].

Interestingly, the grit blasting process quickly followed by the CS process may be performed using two spray powder feeders designed for the CS equipment. This could prevent the roughened surface from long exposure to the environment. Moreover, the oxides formation and/or dirt deposition on the roughened (or activated) surface are avoided using this method. It has been reported that the deposition efficiency of the powder material might increases when powder particles are cold sprayed on a rougher surface [128–131]. Powder particles get to severely deform on a rougher surface than a smooth surface with a smaller surface area than a roughened surface. Likewise, higher bond adhesion strengths were obtained for the coatings that are sprayed on the blasted surfaces [128–131].

3.3. Pre-cold spray treatments

In the CS method, the formation and properties of coatings are affected by many factors, e.g., powder compositions and morphology, CS process parameters (hereafter considered as pre-CS treatments), *in-situ* and post-CS treatments. On the other hand, the cold sprayed coating's corrosion resistance and mechanical properties are mainly influenced by the coating characteristics (e.g., porosity, microstructure, roughness, etc.). In this regard, Xie et al. [132] cold sprayed pure Zn coatings on AZ31B Mg alloy substrate using different CS process parameters. The Zn coating sprayed at 2.5 MPa, and 260 °C (related to N_2 process gas) showed nearly identical microhardness values in the entire coating. However, Zn coating produced at lower gas pressures indicated the gradient reduction in microhardness from the interface to the Zn coating surface. Work hardening due to deformation and the peening effect during the CS process caused the change in microhardness of the Zn coatings. A decrease in hardness of the Zn coating with raising process gas temperatures has been reported in the previous investigations. This was attributed to the improvement of thermal softening during the CS process [132,133]. After cold spraying pure Zn coating, i_{corr} and E_{corr} of Mg-based alloy were improved (Fig. 8a,b) [132]. Pure Zn coating could isolate the AZ31B Mg alloy substrate against 3.5 wt.% NaCl corrosive solution for at least 10 days (Fig. 8c,d) [132]. OCP of pure Zn coating remained stable even after immersion for 10 days. Moreover, according to fitted impedance spectra of samples, the electrical equivalent circuit model altered in the course of immersion time (Fig. 8e,h) [132]. This was related to the diffusion process (diffusion of reactants) and accumulation of electrolyte and corrosion products in the CS coating over time (Fig. 8e,f) [132]. Nevertheless, inter-particle boundaries having fine particles (as active sites) were reported to enhance the possibility of corrosion tunnels formation in the CS coating during immersion (Fig. 8i,l) [132]. Impact-induced melting could lead to the formation of a large number of fine particles (at inter-particle boundaries) that underwent severe plastic deformation during the CS process [132].

Spencer et al. [134] presented the anodic polarization behavior of 316 L stainless steel CS coatings with different coating thicknesses. The corrosion behavior of Mg alloy substrate (AZ91E T6 Mg) and wrought 316 L stainless steel was compared to that of CS coatings on Mg alloy in a neutral 5 wt.% NaCl solution. As coating thickness decreases, the curves of coated samples tend to follow a mostly dominated behavior by the Mg alloy substrate. In contrast, the curves of coated samples tend to accost the behavior of the wrought 316 L stainless steel, as coating thickness raises to 305 μm [134]. This shows that the corrosion resistance of the CS coatings enhances as their thickness increases. In fact, in a thicker coating, the formation of the interconnected path which can conduct the corrosive electrolyte towards the CS coating/substrate interface can occur after a longer immersion time than thin CS coatings. It should be noted that the poros-

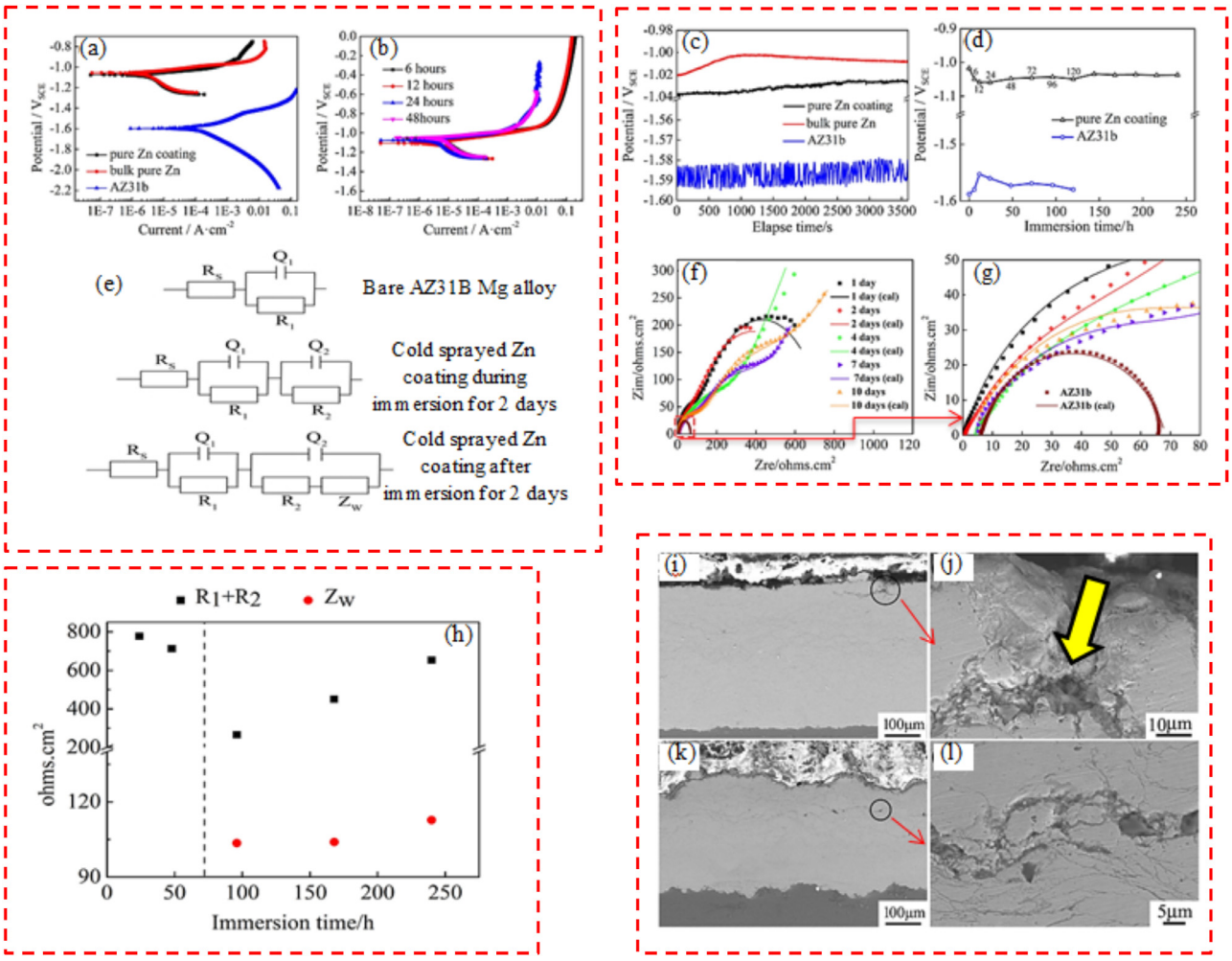

Fig. 8. (a, b) PDP curves of samples up to 48 h, (c, d) OCP curves of samples up to 240 h, (e) electrical equivalent circuits to fit the impedance spectra of samples in the course of immersion time, (f, g) Nyquist plots of samples up to 240 h, (h) fitted EIS test results of Zn coated sample, (i, j) cross-section of CS Zn coating after 7 days, (k, l) cross-section of CS Zn coating after 10 days [132].

ity level and coating thickness are the two important factors that can affect the corrosion resistance of the CS coatings. It has been reported that the CS coatings with a porosity level of less than 1% (considered as a compact coating) can keep the corrosion resistance during long-run immersion tests [128,135].

In addition to coating thickness and porosity level, the coating material is also a factor that can influence the coating system's corrosion behavior, including CS coating and substrate. There is a smaller SRP mismatch (galvanic potential) between CS Al coating and Mg alloy compared to CS 316 L stainless steel coating and Mg alloy. In the case of a larger SRP mismatch, an aggressive attack of the substrate is expected when a small substrate area is exposed to a corrosive environment [136]. This primarily occurs when the anode exposed to a corrosive electrolyte has a much smaller surface area than that of the cathode (as a protective or non-sacrificial CS coating). This shows that protective coatings (in the case of anodic protection) should be utilized with great care on the Mg-based alloys [134].

In general, the noble coatings (non-sacrificial anodic coatings) can obtain barrier protection for Mg-based alloys due to their SRP, which is higher than that of Mg-based alloy substrate. On the other hand, once corrosive solution infiltrates through the coating to the interface, the protection influence is immediately disrupted. This is when the coating is nobler than the substrate. Hence, the formation of galvanic cells between the coating and substrate is expected. So, the number of defects and porosity in a noble coating (non-sacrificial anodic coating) should be minimized [137]. Zhao et al. [111] applied NiCrAl coatings (with about 300 μm thickness) on AZ91D Mg alloy substrate using high-pressure CS and APS processes. In this research, the i_{corr} of the coated Mg alloys with thermally sprayed NiCrAl coatings was reported to be two orders of magnitude lower than that of uncoated Mg alloy. However, the i_{corr} of coated Mg alloys with CS NiCrAl coating was reported to be two orders of magnitude lower than that of coated samples with thermally sprayed NiCrAl coatings. Likewise, impedance modules at low frequency ($|Z|_{0.01\ Hz}$), charge transfer resistance (R_{ct}), and bode phase angle values were the highest for CS NiCrAl coated Mg alloy in com-

passion with those of other samples in 3.5 wt.% NaCl electrolyte. This could be mostly attributed to the higher porosity percentage of APS processed NiCrAl coatings (2.66–3.21%) compared to that of high-pressure cold sprayed NiCrAl coating in this research.

In contrast to CS Fe-based and Ni-based coatings, the aluminum-based coating is a potential candidate for corrosion protection coating of Mg-based alloys due to their (aluminum-based coatings) low density, considerable corrosion resistance, and minimum galvanic corrosion trend with Mg-based alloys [138]. In the past few years, CS Al-based coatings have been commonly sprayed on Mg-based alloys for anodic protection [139,140]. Apart from fine-tuning the CS process parameters (for getting compact CS Al-based coatings), another method to produce dense Al-based composite coatings with improved tribological performance is to add hard ceramic particles (e.g. Al_2O_3, SiC, B_4C, etc.) into the Al feedstock powder [136,141,142]. However, in some studies (Table 2), the CS MMC coatings did not provide long-term corrosion protection for Mg-based alloys, although a decrease in coating apparent density and short-term corrosion rate were reported [143,144]. Al matrix/ceramic particles interfaces behave as fast infiltrating channels for corrosive electrolyte over immersion time. This was noticed through the coating cross-sectional observation after the immersion test [142]. Meydanoglu et al. [145] reported higher corrosion current densities for CS Al-based composite coatings than T6 6061 Al substrate. This observed behavior was ascribed to the existence of more active sites for corrosion. In fact, a high degree of plastic deformation can lead to more active sites in the CS coating microstructure [146]. Moreover, lower i_{corr} of the unreinforced 7075 Al coating compared to that of composite coatings possibly comes down to that unreinforced 7075 Al coating has experienced lower plastic deformation than composite coatings during CS process [145]. Peak broadening in the XRD patterns of CS coatings could stem from a decrease in grain size and/or increment of internal stresses. Higher FWHM values were observed for composite coatings compared to unreinforced 7075 Al coating. This was attributed to the shot-peening (work hardening) influence of ceramic reinforcement particles on the 7075 Al matrix [145]. Li et al. [147] also reported the increment of corrosion current densities of the reinforced pure Al coatings that were related to the internal stresses caused by the Al_2O_3 reinforcement particles. This observed behavior was also attributed to the electrolyte attack on the main active sites (i.e., inter-particle boundaries between Al matrix and Al_2O_3 particles). Analogous observation for CS SiC reinforced Al 5056 composite coatings was reported by Wang et al. [148]. On the contrary, recent studies showed the higher protective performance (long-term corrosion protection) of Al-based MMC coatings than unreinforced Al-based coatings for Mg alloys [142,149,150]. This could be attributed to the type of Al alloy matrix and the amount of reinforcement used in MMCs. A summary of electrochemical corrosion test, micro-hardness test, and bond adhesion strength test results are listed with further relevant details in Table 2 where the variation in results between studies is clear.

Ti coating (from group 4B) is the next candidate for the corrosion protection of Mg-based alloys. This was mostly attributed to the low SRP mismatch between Ti coating and Mg substrate [151,152]. However, warm sprayed (WS) Ti coatings having through-thickness porosities showed poor corrosion protection performance and eventually led to the quick deterioration of Mg-based alloy in NaCl solution [151]. In contrast to WS Ti coating, developed CS Ti coating (using optimized CS parameters) improved the hardness and tribology performance of Mg alloy and considerably enhanced the general corrosion resistance of Mg alloy in 3.5 wt.% NaCl solution. Compared to Al-coated Mg alloy, Ti coating (with about 450 μm thickness) could substantially enhance the pitting corrosion resistance of Mg alloy in the chloride-containing electrolyte. Contrary to Al coated Mg alloy, CS Ti coating extraordinarily increased the repassivation capability of Mg alloy and showed excellent corrosion protection for Mg alloy even after 11 days of immersion in 3.5 wt.% NaCl solution as shown in Fig. 9 [126].

3.4. In-situ *treatments*

Recently, the use of *in-situ* micro-forging (MF) or shot peening-assisted CS process (Fig. 10) has been frequently reported for the production of compact CS coatings/deposits [60]. In the *in-situ* repassivation SP (shot peening)-assisted CS method, a blend of spray targeting powders and large-sized SP particles (typically between 150 and 300 μm) is cold sprayed. In fact, underneath substrate/sprayed layers are *in-situ* forged and more compacted by incoming large MF particles (with high impact energies). These MF particles then rebound from the surface during the CS process [60,140]. In this regard, a fully compact Ni coating with remarkable long-term corrosion protection for magnesium alloys was achieved using *in-situ* MF or shot peening assisted CS method and gas atomized Ni powders (Table 3). Nevertheless, there is a large SRP mismatch between Ni and Mg alloy [60,153]. This leads to the intense galvanic corrosion for Mg alloy when somehow corrosive electrolyte reaches Ni coating/Mg substrate interface. Moreover, Ni has a much higher density (8.9 g cm^{-3}) than that of Mg alloy. This reduces the lightweight competency of Mg alloy. Wei et al. [154] used the *In-situ* SP-assisted CS method to CS Al6061 alloy powder particles. In their research, large spherical stainless-steel powder particles were employed as shot peening particles. The plastic deformation and cohesion of sprayed Al606l powder were raised by the *in-situ* SP-assisted CS method caused by the enhanced cumulative tamping effect [60]. In this research, the porosity level of CS Al6061 coating decreased to 0.4% from 14.40% when the SP particles content increased to 60 vol.%. Nevertheless, the deposition efficiency of Al6061 powder particles was reported to reduce as the ratio of SP particles increased.

Interestingly, the fully dense Al6061 coating on AZ31B Mg alloy showed nearly the same electrochemical corrosion behavior (e.g., open circuit potential and dynamic polarization behavior) as bulk Al6061 (Table 3) [154]. In another research, an *in-situ* SP-assisted low-pressure CS method was employed

Table 2
Published researches pertained to pre-cold spray treatments.

Cold sprayed coating	Substrate	Corrosion characterization	Thickness (μm)	Environment for corrosion test	Porosity (%)	Bond adhesion strength (MPa)	Hardness (HV)	Comparison of corrosion test results	Microstructure characterization	Refs.
CP-Al and MMC with 50 vol.% and 75 vol.% $Mg_{17}Al_{12}$	AZ91D Mg	PDP	CP-Al:815±52 MMC-50 vol.% $Mg_{17}Al_{12}$: 2407 ± 41 MMC-75 vol.% $Mg_{17}Al_{12}$: 1874 ± 47	3.5 wt.% NaCl	CP-Al:6.2 ± 1.3 MMC-50 vol.% $Mg_{17}Al_{12}$: 0.2 ± 0.1 MMC-75 vol.% $Mg_{17}Al_{12}$: 0.4 ± 0.2	CP-Al: 7.2 ± 0.4, MMC-50 vol.% $Mg_{17}Al_{12}$: 32.9 ± 0.6, MMC-75 vol.% $Mg_{17}Al_{12}$: 19.7 ± 1.6	CP-Al ($HV_{0.1}$): 40–50 MMC-50 vol.% $Mg_{17}Al_{12}$: 54–60 MMC-75 vol.% $Mg_{17}Al_{12}$: 55–61	MMC coatings showed higher i_{corr} compared to CP-Al (bulk)	OM, SEM, XRD	[142]
Al-7075 and MMCs with 20 vol.%SiC and MMC with 20 vol.% B_4C	T6 6061 Al alloy	OCP, PDP	Al-7075:650 and MMCs with SiC: 450 and B_4C: 350	3.5 wt.% NaCl solution	Al-7075: 0.5 ± 0.1 vol.%, MMCs: dense microstructure	_____	Al-7075($HV_{0.3}$): 120–140, MMC with B_4C: 170–190, MMC with SiC: 180–195	CS coatings showed more noble E_{corr} but higher i_{corr} than those of T6 6061 Al substrate, MMC coatings showed higher i_{corr} than that of CS 7075 coating.	SEM, EDS, XRD, OM	[145]
CP-Al and MMC with 20vol% Al_2O_3	AA2024-T3	OCP, PDP, EIS	MMC: 800	3.5 wt.% NaCl solution	_____	_____	_____	MMC coating showed lower EIS values than CP-Al coating and substrate; MMC coating indicated higher i_{corr} compared to CP-Al coating and substrate.	SEM, EDS, OM, 3D topography	[147]
CP-Al and MMC with 1wt.% carbon nanotube	AZ91 Mg	PDP and OCP	_____	3.5 wt.% NaCl solution	_____	_____	CP-Al ($HV_{0.001}$) : 72.5 ± 2.9, MMC with 1wt.% carbon nanotube: 153.3 ± 22.1	MMC coating showed higher Ecorr and lower i_{corr} compared to CP-Al coating and substrate, after only short term PDP test.	XRD, SEM, EDS, Raman spectroscopy, OM, TEM,	[143]
AA5083, MMC-20 vol.%, 40, and 60% Al_2O_3	ZM Mg	OCP, immersion, PDP and EIS tests for 1h-24h	_____	3.5 wt.% NaCl solution	AA5083: 0.78 ± 0.09, MMC-20 vol.% Al_2O_3: 0.67 ± 0.12, MMC-40 vol.% Al_2O_3: 1.14 ± 0.18, MMC-60 vol.% Al_2O_3: 1.32 ± 0.21	_____	_____	i_{corr} increases as follows: MMC-20 vol.% Al_2O_3 < AA5083 < MMC-40 vol.% Al_2O_3 < MMC-60 vol.% Al_2O_3 over time (1h-24 h).	SEM, EDS	[144]

(*continued on next page*)

Table 2 (*continued*)

Cold sprayed coating	Substrate	Corrosion characterization	Thickness (μm)	Environment for corrosion test	Porosity (%)	Bond adhesion strength (MPa)	Hardness (HV)	Comparison of corrosion test results	Microstructure characterization	Refs.
AA5083, MMC-30vol.% SiC (15.6 μm) MMC-30vol.% SiC (72.8 μm)	Mg>99%	Extended immersion test, OCP, EIS, galvanic corrosion using ZRA technique,	_____	Aerated 0.1 M Na_2SO_4	AA5083: 2.5–3.2%, MMC-30vol.% SiC (15.6 μm):0.75–1% MMC-30vol.% SiC (72.8 μm): 0.75–1%	_____	AA5083 ($HV_{0.3}$): 100–120, MMC-30vol.% SiC (15.6 μm):130–160 MMC-30vol.% SiC (72.8 μm): 160–190	Long term OCP (91 days) confirmed highest and nearly stable OCP for MMC-30vol.% SiC (15.6 μm) compared to other CS coatings. Impedance values were highest for MMC-30vol.% SiC (15.6 μm) compared to other CS coatings after 91 days of EIS.	SEM, EDS, OM	[150]
CP-Al, MMC with 5wt.% Al_2O_3 and MMC with 5 wt.%Al_2O_3–1 wt.% CNT	Mg-LA43M alloy	OCP, PDP, EIS, and Long term immersion test (40 days).	_____	3.5% NaCl aqueous solution	_____	_____	CP-Al ($HV_{0.25}$): 87.11 ± 2.12 MMC with 5wt.% Al_2O_3: 89.21 ± 1.41 and 5 wt.%Al_2O_3–1 wt.% CNT: 91.11 ± 1.71	MMC with 5 wt.%Al_2O_3–1 wt.% CNT showed lowest i_{corr} and highest R_{ct} compared to other CS samples. MMC coatings showed almost no weight loss even after 1000 h of immersion.	FESEM, EDS, XRD	[149]
CP-Al and CP-Ti	AZ31B	OCP, CPP, EIS, long immersion test for 11 days	_____	3.5% NaCl aqueous solution	CP-Al: 1.00 _ 0.20% CP-Ti: 0.40 _ 0.20%	_____	CP-Al ($HV_{0.025}$): 50–70 CP-Ti: 250–280	Ti coating showed lowest i_{corr} and highest R_{ct} compared to other CP-Al coating. Ti coating could provide long-term corrosion protection.	SEM, EDS, XRD, OM	[126]

Table 3
Published researches related to *in-situ* cold spray treatments for production of coatings on Mg-based alloys.

Cold sprayed coating	Substrate	Shot peening (SP) powder particles	Corrosion characterization	Thickness (μm)	Porosity (%)	Bond adhesion strength (MPa)	Hardness (HV)	Comparison of corrosion test results	Microstructure characterization	Refs.
Pure Ni coating using gas atomized Ni powder	AZ31B	410 stainless steel SP powder 150–200 μm	OCP, PDP, EIS, long term EIS and Neutral salt spray corrosion tests for 1000 h	100–150 μm	————	65.4	————	Ni coated Mg showed lower i_{corr} and high EIS values same as bulk Ni after 1 h OCP. R_{ct} and $\lvert Z \rvert_{f = 0.01\ Hz}$ values were nearly stable during 1000 h of immersion in 3.5wt.% NaCl solution. Also, weight loss of Ni coated Mg was trivial after 1000 h corrosion test.	SEM, EDS, 3D laser scanning microscopy,	[60]
Al-based coatings using gas atomized CP-Al, AA2219 and AA6061 powders	AZ31B	Spherical martensitic 410 stainless steel (SS): 200–300 μm	OCP, PDP, and long term immersion, hydrogen evolution and EIS tests for 1000 h.	400–500 μm	CP-Al: 0.34 ± 0.11% AA2219: 0.23 ± 0.09% AA6061: 0.24 ± 0.08%	CP-Al : 91.5 ± 2.3, AA2219: 83.6 ± 2.8 and AA6061: 87.5 ± 2.3	CP-Al (HV_{100}) : 64.2 ± 2.8, AA2219: 118.5 ± 3.6 and AA6061: 97.4 ± 3.8	Pure Al coating showed lowest i_{corr} compared to other samples. Al-based coating showed negligible and stable H_2 evolution during 1000 h. Pure Al coating showed lowest weight loss and highest R_{ct} after 1000 h immersion in 3.5wt.% NaCl.	SEM, EDS, XRD, 3D laser scanning microscope.	[140]
Al-based coatings using gas atomized CP-Al, Al2024, and Al5083 powders	AA 2024-T3	Spherical Al_2O_3 particles	OCP, CPP, SVET for 24 h, long term immersion and EIS tests for 720 h	CP-Al: 90–100 μm Al2024: 120–140 μm Al5083: 160–170 μm	CP-Al: 1.46 ± 0.06% Al2024: 1.66 ± 0.16% Al5083: 1.50 ± 0.17%	CP-Al: 46 ± 6 Al2024: 50 ± 7 Al5083: 51 ± 6	CP-Al ($HV_{0.1}$): 57 Al2024: 115 Al5083: 132	CP-Al coating showed highest repassivation ability. CP-Al coating indicated lowest R_{ct} at $t < 480$ h, but, after that CS Al5083 displayed the lowest R_{ct} up to 720 h.	SEM, EDS, OM	[155]
CP-Al coating	AZ31B and AZ91 Mg	Spherical Ni particles: 70 μm	Long term immersion, OCP and PDP tests up to 336 h	240 μm	————	————	CP-Al on AZ31B ($HV_{0.1}$): 78 ± 2 CP-Al on AZ91 Mg: 80 ± 2	Al coated AZ91 Mg showed a significant increase in the polarization resistance (or gradual reduction in i_{corr}) over long term immersion time up to 336 h.	FESEM, EDS, OM, XRD, 3D profilometry.	[160]
Gas-atomized spherical Ni, carbonyl irregular Ni, and electrolytic dendritic porous Ni powders	AZ31B	Spherical martensitic 410 stainless steel (SS): 150–200 μm	Long term OCP and EIS tests up to 3000 h	150–200 μm	Spherical Ni: 0.21 ± 0.07% Irregular Ni: 0.3 ± 0.1% Dendritic Ni: 0.25 ± 0.09%	Spherical Ni: 65 ± 4 Irregular Ni: 62 ± 4 Dendritic Ni: 66 ± 3	———-	Irregular-Ni and dendritic-Ni coatings fail after only 10 h of immersion. Spherical Ni coating showed stable OCP and Rct values in the course of immersion time up to 3000 h.	SEM/EDS, OM, XRD	[153]
Gas atomized Al6061 alloy powder	AZ31B	Spherical 1Cr18 stainless steel: 200–300 μm	Short term OCP, PDP	200–300 μm	14.4% (non-SP) to 0.4 (using 60 vol.% SP)	————	Al6061 coating (using 60 vol.% SP): $90HV_{50}$	Al6061 coating on Mg (using 60 vol.% SP) showed lowest i_{corr} close to that of bulk Al6061 in 3.5 wt.%NaCl solution	SEM, EDS.	[154]

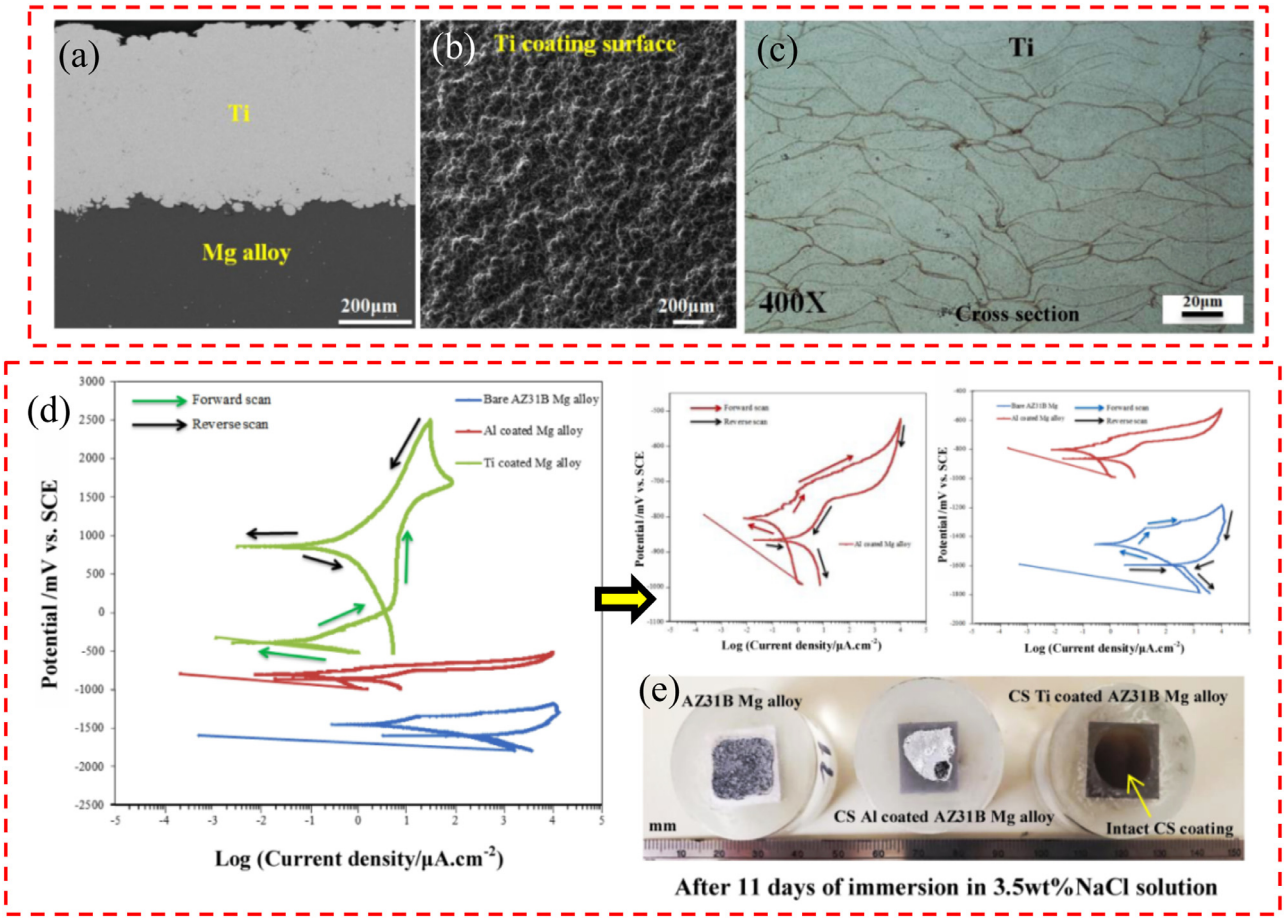

Fig. 9. (a) Polished cross-section of Ti coating on Mg alloy, (b) Ti coating surface, (c) polished cross-section of Ti coating after etching, (d) cyclic potentiodynamic polarization (CPP) curves of coated and uncoated Mg alloys, (e) surface of samples after immersion test in 3.5wt.% NaCl solution after 11 days [126].

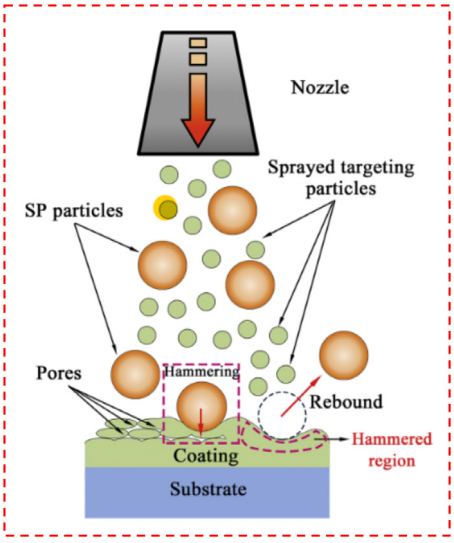

Fig. 10. *In-situ* shot-peening assisted CS process (schematic illustration) [60].

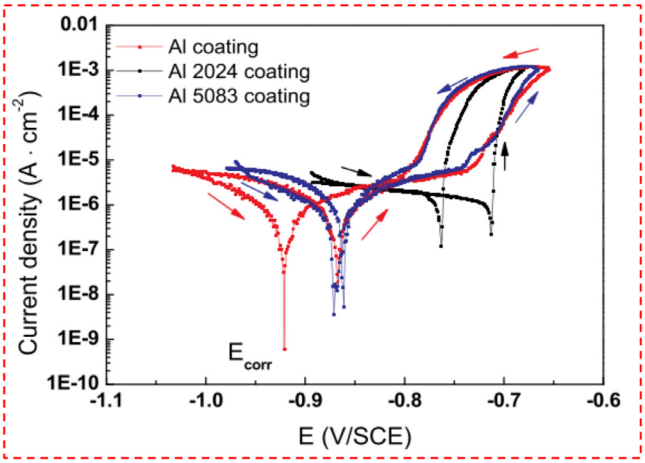

Fig. 11. Cyclic PDP curves of CS coated samples in 3.5 wt.% NaCl electrolyte (After 6 h immersion and at a scan rate of 1 mV/s) [155].

to produce protective dense Al-based coatings on AA2024-T3 alloy [155]. CS processed CP aluminum, and Al5083 coatings demonstrated lower i_{corr} than that of CS Al2024 coating. This implies less severe corrosion reactions on the surface of CP-Al and Al5083 coatings compared to the Al2024 coating surface (Table 3). From Fig. 11 and (E_{pit}–E_{corr}) values, it was found that CS Al2024 coating having the lowest (E_{pit}–E_{corr}) value is very vulnerable to pitting corrosion in comparison with CS CP-Al and Al5083 coatings, which showed higher (E_{pit}–E_{corr}) values [155]. As shown in Fig. 11, a positive hysteresis loop (on the reverse scan) was observed for

all coated samples [155]. So, further growth of pits is anticipated when the reverse scan moves to the higher anodic current densities compared to the forward scans [154–158]. In contrast to positive hysteresis loops, further development of pits is not expected when the reversed curve shifts to the lower anodic current densities (known as negative hysteresis loop) or reverse and forward scans overlap (known as neutral hysteresis loop). When the potential declines (in a positive hysteresis loop) and the forward scan at protection potential E_{rp} (or repassivation potential) is intersected by the reverse scan, pits could be repassivated. In fact, pit development stops when E_{rp} is higher than E_{corr}. Compared to CS Al5083 and Al2024 coatings, CS CP-Al coating showed the highest capability to re-passivation. This was attributed to the higher (E_{rp}-E_{corr}) value for CS CP-Al coating than that of other coatings (Fig. 11) [155].

According to the long-term EIS experiments (up to 720 h), the highest corrosion rate (lowest R_{ct}) was seen for CS Al 2024 coating in the course of immersion time. Interestingly, the lowest corrosion rate at $t < 480$ h was identified for CS CP-Al coating. However, the lowest corrosion rate was then observed for CS Al5083 coating until the end of the immersion test. The preferential dissolution of Mg-rich precipitates was responsible for the higher corrosion rate of CS Al5083 coating before 480 h. Nevertheless, the accumulation of a dense passivation film on the coating surface was accountable for the lower corrosion rate of CS Al5083 coating after 480 h.

This trend was also observed by Ezuber et al. [159], who studied the corrosion rate of bulk AA1100 and AA5083 samples in seawater at 23 °C. They noticed a higher corrosion rate for AA5083 than that of AA1100 during the early stages of immersion. However, AA1100 exhibited a higher corrosion rate than that of AA5083 after 28 days. In another research, a blend of Al powder (60 wt.%) with a particle size range of 1–8 μm and Ni powder (40 wt.%) with a particle size of about 70 μm was used as feedstock powder. The *in-situ* hammering effect caused by the relatively large Ni powder particles led to the CP-Al coating densification. Coating hardness also increased due to the shot-peening effect. In contrast to the XRD pattern of feedstock powder, no peaks of Ni were detected in the XRD patterns of CS Al coatings. It seems that Ni particles have most probably helped to densify Al coatings and then rebounded during the CS process. In this research, corrosion resistance of CP-Al coated AZ91Mg alloy increased over immersion time (up to 336 h) in 3.5 wt.% NaCl electrolyte (Table 3). This was attributed to the formation of a protective oxide layer (e.g., Al_2O_3) on the coating surface during immersion time. In fact, in this research work, the CS Al coating (as a noble barrier layer) prevented the penetration of chloride ions containing corrosive electrolyte) on the Mg alloy [160].

SP particles remained in the coating structure when Wei et al. [154] chose 350 °C and 3.5 MPa for N_2 process gas temperature and pressure, respectively. In this condition, SP particles' velocity (with PSD of 100–200 μm) was reported to be lower than their critical velocity for deposition. Actually, the adiabatic shear instability (ASI) phenomenon may not be a dominant mechanism of the SP particles inclusion. The inclusion of hard particles into the soft metallic-based coatings has been reported because of deep penetration. This was observed when ceramic and metallic particles were mechanically blended for the production of composite coatings/deposits [141,161–164]. This problem was overcome when the temperature and pressure of N_2 process gas declined to 300 °C and 2.5 MPa, respectively. Nevertheless, under this condition, a higher volume of SP particles should be employed for the production of compact CS coatings. This significantly declined the D.E of Al powder and raised the costs associated with SP particles and *in-situ* MF or shot peening assisted CS method. Zhang et al. also reported the detectable embedded SP spherical Al_2O_3 particles in the CS Al-based coatings after *in-situ* shot peening assisted the low-pressure CS process [155].

3.5. Post-treatments on the cold sprayed coatings on Mg-based alloys

As previously mentioned, extremely dense CS coatings with very low porosity levels can be obtained under appropriate spraying conditions. In this condition, the powder particles undergo severe plastic deformation during the CS process [165]. Nevertheless, the formation of some tensile residual stresses because of thermal effects can be expected under some spraying conditions and, contingent on the feedstock powder and substrate materials and their TEC, and powder particles temperature during the deposition [166,167]. Moreover, compressive residual stresses because of the kinetic effects can be extensively generated due to the severe impact of plastic deformation during the CS process. So, the mechanical, thermal, electrical, and corrosion resistance properties can be declined by the presence of residual stresses in the CS coatings. Heat treatment is one of the post-CS treatments that can improve the performance of CS coatings/deposits [165,168,169]. As for CS Al-based coatings on Mg alloys, Bu et al., cold sprayed dense and thick pure Al coatings on AZ91D-T4 Mg. Coated samples were then heat-treated for diverse holding times at 400 °C. The formation of Al_3Mg_2 (γ phase) and $Mg_{17}Al_{12}$(β phase) intermetallic phases at the interface of Al coating/Mg substrate were identified after heat treatment [170]. This was also observed by Spencer et al. [171]. These intermetallic layers with high hardness could improve the corrosion resistance of AZ91E Mg alloy to a level analogous to that of Al-based alloys [170,171]. Recently, the influence of low-temperature heat treatment (under vacuum at 300 °C for 1 h) on the CS Al coated AZ91D Mg alloy was studied by Siddique et al. They reported the formation of Mg-Al compound (only a few microns) around the interface because of the heat treatment. Heat-treated (HT) coatings showed better tribology performance than as-sprayed coatings on AZ91D. This was mainly because of the densification of the coating microstructure after heat treatment [172]. Nevertheless, the corrosion rate of Al coating slightly increased after HT compared to that of as-sprayed Al coating (Table 4).

Table 4
Published researches related to post-treatments on the cold sprayed (CS) coatings on Mg-based alloys.

Cold sprayed coating	Substrate	Type of post-cold spray treatment	Corrosion characterization	Thickness (μm)	Porosity (%)	Bond adhesion strength (MPa)	Hardness (HV)	Comparison of corrosion test results	Microstructure characterization	Refs.
CP-Al coating	AM50 Mg alloy	HCPEB irradiation	PDP, short term EIS in 3.5wt.% NaCl solution	———	———	———	Irradiated ($HV_{0.3}$): 68 Untreated: 55	Untreated i_{corr}: 19.16 μA/cm^2 Irradiated i_{corr}: 4.45 μA/cm^2 Untreated R_{ct}: 632 Ω cm^2 Irradiated R_{ct}: 5938 Ω cm^2	SEM, EDS, XRD	[174]
7075 Al free standing coating	7075 Al substrate was then removed after CS	PEO treatment	OCP, then PDP in 3.5wt.% NaCl solution	10,000 μm	———	———	$HV_{0.3:}$ 144 ± 3	Cold sprayed 7075+PEO, i_{corr}: 0.627 μA/cm^2 Cold sprayed 7075, i_{corr}: 1.16×10^{-4} A/cm^2	SEM, XRD, EDS	[186]
CP-Al coating	AA 7075-T6 alloy	Coating surface polishing using SiC abrasive papers	OCP up to 900 h, EIS up to 900 h in 3.5wt.% NaCl solution	As-sprayed: 309 ± 12 μm Polished: 204 ± 4 μm	Below 0.8	About 25	HV_{100}: 51±2 top –58± 1 bottom	As-sprayed coating, R_{ct}: 28 KΩ cm^2 Polished coating R_{ct}: 38 KΩ cm^2 after 850 h of immersion.	SEM, XRD, OM	[175]
CP-Al coating	AZ91E Mg alloy	Annealing at 400 °C	Immersion test up to 48 h and PDP test in 5% NaCl electrolyte	Intermetallic layers: 200 μm after coating surface polishing up to 0.05 μm surface finish.	———	———	Al_3Mg_2, HV_{200}: 275. $Al_{17}Mg_{12}$, HV_{200}: 250,	Al_3Mg_2 and $Al_{17}Mg_{12}$ layers showed better corrosion resistance than AZ91E and offered a similar level of corrosion resistance to Al-base alloys.	SEM, XRD	[171]
Al+Al_2O_3 and Al+Al_2O_3+PEO coatings	AZ31 Mg alloy	PEO process	OCP, then PDP in 3.5wt.% NaCl solution	Al+Al_2O_3: 500 μm, Al+Al_2O_3+ PEO: 520 μm	———	Al+Al_2O_3: 30, Al+Al_2O_3+ PEO: 27	Al+Al_2O_3 ($HV_{0.025}$): 100±7, Al+Al_2O_3+ PEO: 1100±88	Al+Al_2O_3, i_{corr}: 0.236 μA/cm^2, Al+Al_2O_3+ PEO i_{corr}: 0.518 μA/cm^2	SEM, XRD, EDS	[185]
CP-Al coating	AZ91D Mg alloy	Annealing at 300 °C	OCP, then PDP in 3.5wt.% NaCl solution	As-sprayed (AS) and heat treated (HT) coatings: about 900 μm	———	———	AS coating, ($HV_{0.\ 25}$): 60±5, HT coating: 56±3	AS coating, i_{corr}: 1.43 ± 0.03 μA/cm^2, AS coating, i_{corr}: 1.65 ± 0.02 μA/cm^2,	SEM, EDS, XRD	[172]

(*continued on next page*)

Table 4 (*continued*)

Cold sprayed coating	Substrate	Type of post-cold spray treatment	Corrosion characterization	Thickness (μm)	Porosity (%)	Bond adhesion strength (MPa)	Hardness (HV)	Comparison of corrosion test results	Microstructure characterization	Refs.
CP-Al coating	LA43M MgeLi alloy	Post-cold spray shot peening by 1Cr18 SS powder particles	OCP then PDP, long term immersion test including weight loss and EIS up to 1000 h	Shop-peened (SP) coating: and As-sprayed (AS) coating: about 300 μm	Shop-peened (SP) coating: 0.2%, As-sprayed (AS) coating: 12.4%	———————-	SP coating (HV_{50}): 50–60, AP coating (HV_{50}): about 40	AS coating, i_{corr}: 2.97 μA/cm^2, SP coating, i_{corr}: 0.215 ± 0.02 μA/cm^2, AS coating up to 1000 h R_{ct}: about 2 kΩ cm^2 SP coating up to 1000 h R_{ct}: about 75 kΩ cm^2	SEM, EDS, XRD	[173]
CP-Al coating	LA43M alloy	*In-situ* shot peening by stainless steel powder and then anodization of Al coating (AAO) and then sealing using silicon oxide (MAC)	Neutral salt spray cyclic corrosion, OCP then PDP, and EIS	————-	0.2	————	———————-	AAO coating, i_{corr}: 3.7 μA/cm^2, MAC coating, i_{corr}: 5.4 × 10^{-9} A/cm^2, AAO coating, up to 2 h, R_{ct}: 2.13×10^4 Ω cm^2 MAC coating up to 2 h R_{ct}: 4.81×10^5 Ω cm^2	SEM, EDS	[187]
CP-Al, Ti/Al and Ta/Ti/Al coatings	AZ31B Mg alloy	Applying passive top layers on CP-Al coating	OCP then PDP test, long term EIS test up to 48 h in 3.5.wt% NaCl solution	500–600 μm	Ta layer: 0.10 Ti layer: 0.50 ± 0.20 CP-Al layer: 1.10 ± 0.20%	————	Ta top coating ($HV_{0.025}$): 300–350 Ti top coating: 250–300 CP-Al coating: 50–60	CP-Al coating, i_{corr}: 0.402 μA/cm^2, Ti/Al coating, i_{corr}: 0.218 μA/cm^2, Ta/Ti/Al coating, i_{corr}: 0.019 μA/cm^2, CP-Al coating, up to 48 h, R_{ct}: 1.20×10^4 Ω cm^2 Ti/Al coating up to 48 h R_{ct}: 3.60×10^4 Ω cm^2, Ta/Ti/Al coating up to 48 h R_{ct}: 1.20×10^7 Ω cm^2,	SEM, EDS, EBSD, XRD, IFM, OM	[124]

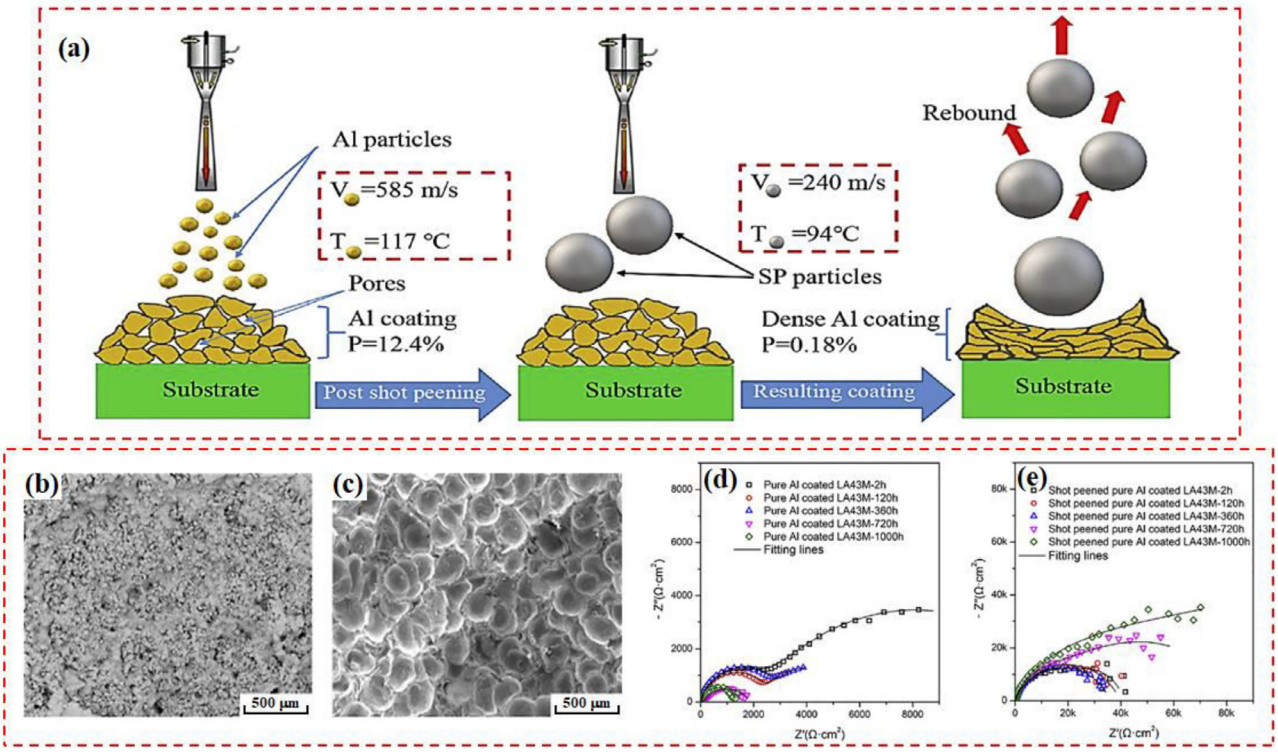

Fig. 12. (a) The production process of dense CS Al coatings on LA43M Mg alloy substrates by means of common CS and post-CS shot peening processes (schematic illustration), (b) surface morphology of as-cold sprayed pure Al coating on LA43M Mg alloy substrate, (c) surface morphology of CS pure Al coating on LA43M Mg alloy substrate after post-CS shot peening process, Nyquist plots of (d) as-cold sprayed pure Al coated LA43M Mg alloys and (e) shot-peened pure Al coated LA43M Mg alloys after different periods of immersion times (2, 120, 360, 720, and 1000 h) in 3.5 wt.% NaCl solution [173].

Although the corrosion behavior of Al coated, Mg alloy was improved by means of heat treatment [171], Table 4, it is essential to look over the effect of intermetallic compounds formation at coating/substrate interface (after heat-treatment) on the coating bond strength and whether the working temperature employed during the heat treatment is appropriate for the entire system, including coating material (e.g., low or high melting point coating materials, etc.) and Mg alloy substrate. In some cases, high temperature-heat treatment might lead to the mechanical properties degradation of Mg alloys [172]. Coating oxidation and increment of its oxide content (particularly between inter-particle boundaries and coating surface) might happen when high temperatures are used during heat treatment. High temperatures might also cause the coating deterioration and also lead to new crystalline phases or amorphous material formation in the coating. It should be noted that, in some cases, high temperatures, perhaps due to insufficiency, cannot close and eliminate large pores or microdefects (especially at inter-particle boundaries) [130]. In such cases, it is better to utilize the other post-CS treatments. It was noted that the influence of shot peening treatment (tamping effect) on the CS coatings is more important than bulk materials. Post-CS shot peening treatment was suitable for producing compact coatings with high corrosion resistance [173]. Lately, conventional CS process and post-CS shot peening treatment were utilized to produce dense Al coatings on LA43M Mg alloy substrate. Cold sprayed Al particles are able to absorb the kinetic energy of martensitic stainless-steel particles during post-CS shot peening treatment. The higher fraction of the sprayed Al particles was considerably densified by using this method. Moreover, the porosity level was substantially decreased to 0.2% (for the shot-peened Al coating) from 12.4% (for as-cold sprayed Al coating), Fig. 12a–c [173]. Likewise, contamination of soft metallic coatings like Al by hard SP particles was observed in this work [173].

The shot-peened Al-coated LA43M specimen displayed lower corrosion current density, higher open circuit potential, and better impedance than the as-CS Al-coated LA43M sample. Post-CS shot peening treatment could substantially enhance the compactness of CS monolithic Al coating and considerably increase the protective performance of the CS pure Al coatings on Mg LA43M alloy during corrosion. This was also proven by the surface morphology of samples (after fog salt spray test), EDS analysis of surface, and electrochemical impedance behavior of the specimens during long run immersion tests (Fig. 12d, e) [173]. Actually, in this research, the lower porosity level (0.2%) in the shot-peened CS pure Al costing is mainly accountable for its excellent corrosion behavior compared to as-cold sprayed pure Al coating with a 12.4% porosity level [173]. However, tribology performance and micro-hardness of shot-peened CS pure Al costings were not studied in this work. Guo et al. [174] employed high current pulsed electron beam (HCPEB) to irradiate the surface of CS Al coating on AM50 Mg alloy. The surface remelting and

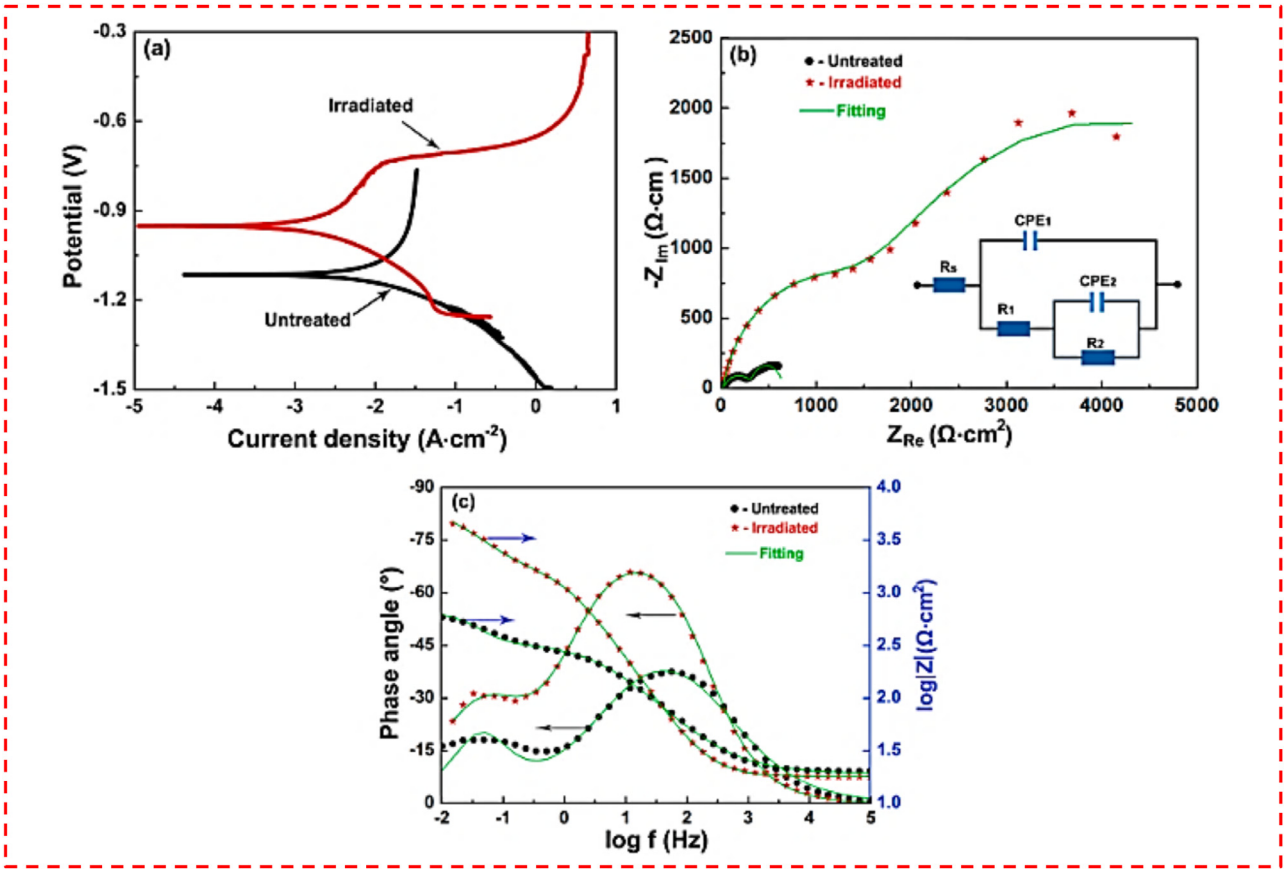

Fig. 13. (a) PDP curves of coated samples, (b) Nyquist curves of coated samples and used the electrical equivalent circuit to fit impedance spectra, (c) Bode plots of coated samples (including un-treated and HCPEB irradiated coatings) [174].

densification of the CS Al coating texture caused by HCPEB led to the higher polarization resistance, a lower i_{corr} of 4.45 μA/cm^2, and higher EIS values compared to as-sprayed (untreated) Al coating in 3.5 wt.% NaCl solution as shown in Fig. 13 [174].

Recently, high-pressure cold sprayed multi-layered coatings were developed on Mg-based alloys [123,124]. The compactness of the CS Al coating on Mg alloy was considerably enhanced by the SP effect of powder particles having high impact kinetic energy, micro-hardness, and density. High-pressure CS top coatings (mainly passive metals having low SRP mismatch with underneath coating/layer) can alleviate the disadvantages of regular CS CP-Al coatings. In fact, in order to reform the surface properties of the CS CP-Al based coatings on Mg alloys, a portion of CS Al coating thickness was replaced by high-pressure CS top coatings from highly passive metals (e.g., Ti, Zr, Ta, etc.). This innovative method substantially raised the micro-hardness and tribology performance of the CS CP-Al coated Mg alloy surface. This method can provide a balance between the cost reduction and greater surface properties of passive metals as shown in Fig. 14 [124]. da Silva et al. [175] reported that the rough and porous top layer of the as-CS Al coating could lower the corrosion resistance and be very harmful to the coating lifespan in a corrosive environment. The porous essence of the coating top layer and the presence of irregular and small micro-defects across the coating cross-section are responsible for this observed behavior. Primary accelerated corrosion through the pores of the top layer can boost chemical attacks. So, in this condition, the enlargement of minor defects and eventually appreciable attacks at the coating/substrate interface are anticipated. Nevertheless, removal of the top porous layer of the CS coating led to a decline in the initial corrosion rate of the coating surface. This suppressed the powerful attack on the small micro-defects (possibly at the inter-particle boundaries) and intercepted the corrosive solution penetration towards some regions at the CS Al coating/ 7075-T6 Al alloy interface. In the CS coatings, a porosity gradient (from coating surface to interface) includes a final rough surface finish having high true surface area, a more porous outer region (near coating surface), and a compact inner region (near interface) is regularly observed. This phenomenon is mainly attributed to the densifying (shot peening) of the previously deposited particles/layer by the incoming powder particles during the CS process [62]. A flattened coating surface with a low surface roughness average (R_a) can be obtained by removing the CS coating top layer [175]. Ti deposits with polished surfaces [175,176] showed higher corrosion resistance than that of as-cold sprayed Ti surfaces [176].

Wang et al. [177] also noticed the above-mentioned behavior. Compared to the TA2 (bulk Ti) sample, a higher corrosion rate was reported for the as-cold sprayed Ti coating.

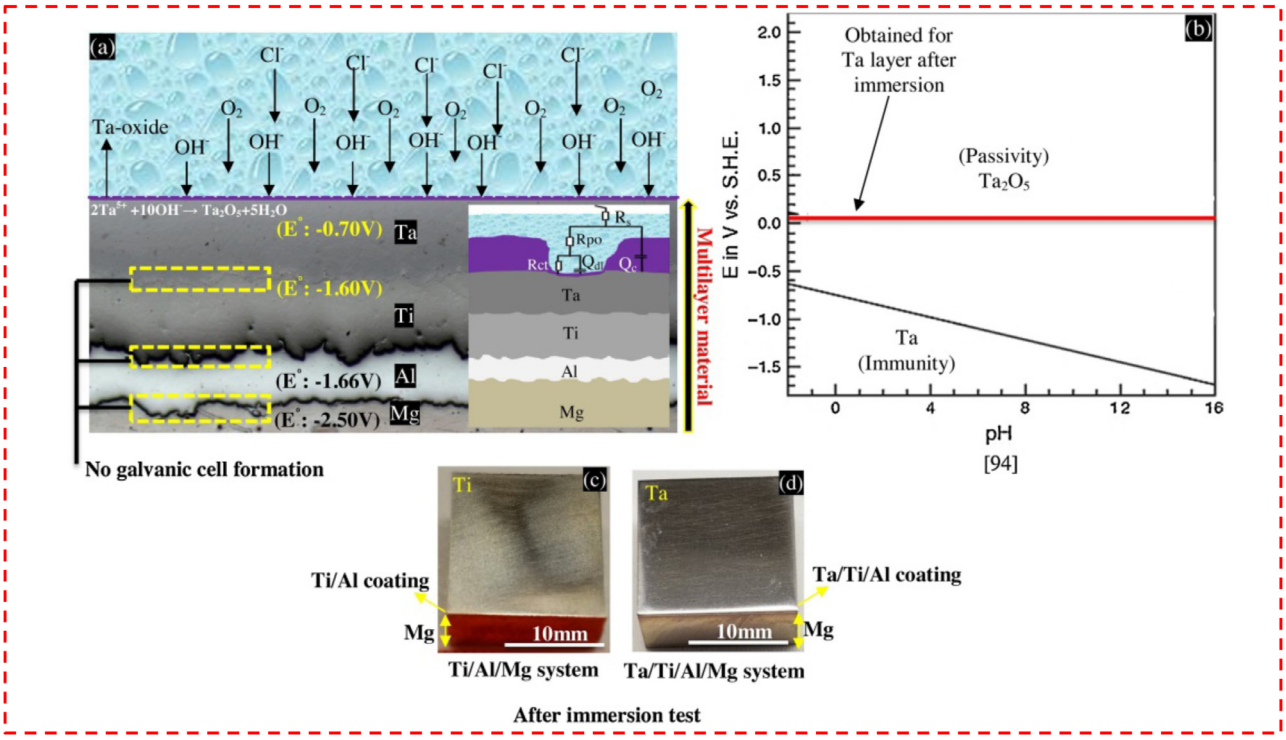

Fig. 14. (a) Depiction of Ta/Ti/Al coating on AZ31B alloy in 3.5 wt.% NaCl electrolyte and used EEC to fit impedance spectra (inset), (b) pourbaix diagram of Ta, (c) photo macrographs of Ti/Al coating on AZ31B Mg alloy, and (d) Ta/Ti/Al coating on AZ31B Mg alloy (after immersion test in 3.5 wt.% NaCl solution [124].

In contrast to as-cold sprayed Ti coating, ground and polished Ti coating also showed lower i_{corr} and higher E_{corr}. The elimination of the porous surface layer of the CS Ti coating improved its corrosion behavior in a corrosive environment. Among the other advantageous surface modification methods [178–180,231], the PEO method has been extensively employed to produce hard ceramic coatings on non-ferrous alloys (e.g., Al, Mg, Zr, Nb, Ti, etc.,) and lately on the CS coatings/deposits [52,53,181–185]. In this regard, the PEO method was used to apply an Al_2O_3-based coating on a CS 7075 Al alloy deposit (with about 10 mm thickness) [186]. Post-CS PEO treatment improved the electrochemical corrosion resistance of the CS 7075 Al alloy as presented in Table 4.

Interestingly, the growth kinetic of the PEO oxide layer is significantly increased on the CS Al coating compared to the growth kinetic of the PEO oxide layer on the bulk Al-based substrates. In contrast to single-step PEO treatment on the bulk Al substrates, the growth kinetic of the duplex cold sprayed-PEO oxide layer (as thick, dense, and crystalline Al_2O_3 top coating) was increased by a factor of 3. Although the presence of porosities in the CS coatings is normally unavoidable and undesirable, however, positive effect of the porosities in the CS coatings on the PEO growth kinetics was reported in this research (Fig. 15) [181].

A summary of electrochemical corrosion test, microhardness test, and bond adhesion strength test results are tabulated with details in Table 4, where the result differences between different post-CS treatments is conspicuous.

3.6. Bonding mechanism investigation at the Mg alloy/cold sprayed coatings interface

Two main bonding mechanisms in the CS process are metallurgical bonding and mechanical interlocking. Nano-scale chemical reactions at inter-particle boundaries or at the interface between coating and substrate can lead to metallurgical bonding [55,56,188–191]. The high-velocity impact encourages localized plastic deformation of the powder particles or substrate (at the contact interface). This will results in materials jetting [192] and ASI as well [193]. Moreover, the high-velocity impact can easily break the existent native oxide films on the metallic surfaces. Hence, the intimate metal-to-metal contact occurs when the outward metal jet extrudes the oxide debris from the contact interface. So, the chemical reaction as a result of the localized high pressure (at the contact interface) finally leads to metallurgical bonding (atomic bonding) [55,56,189,193]. The interfacial amorphous phase formation [56,189,190], interfacial intermetallic layer formation [56,188,189,194,195], localized melting [194], and also dimple-like morphology on the fracture surfaces of CS deposits [196,197] are recognized to be proof of interfacial metallurgical bonding. In contrast to metallurgical bonding (as a chemical bonding phenomenon), mechanical interlocking will occur when powder particles are mechanically embedded or trapped into the deposited coatings or substrate materials during the CS process [198].

A strong mechanical interlocking (anchoring) at the coating/Mg alloy substrate interface could guarantee the high

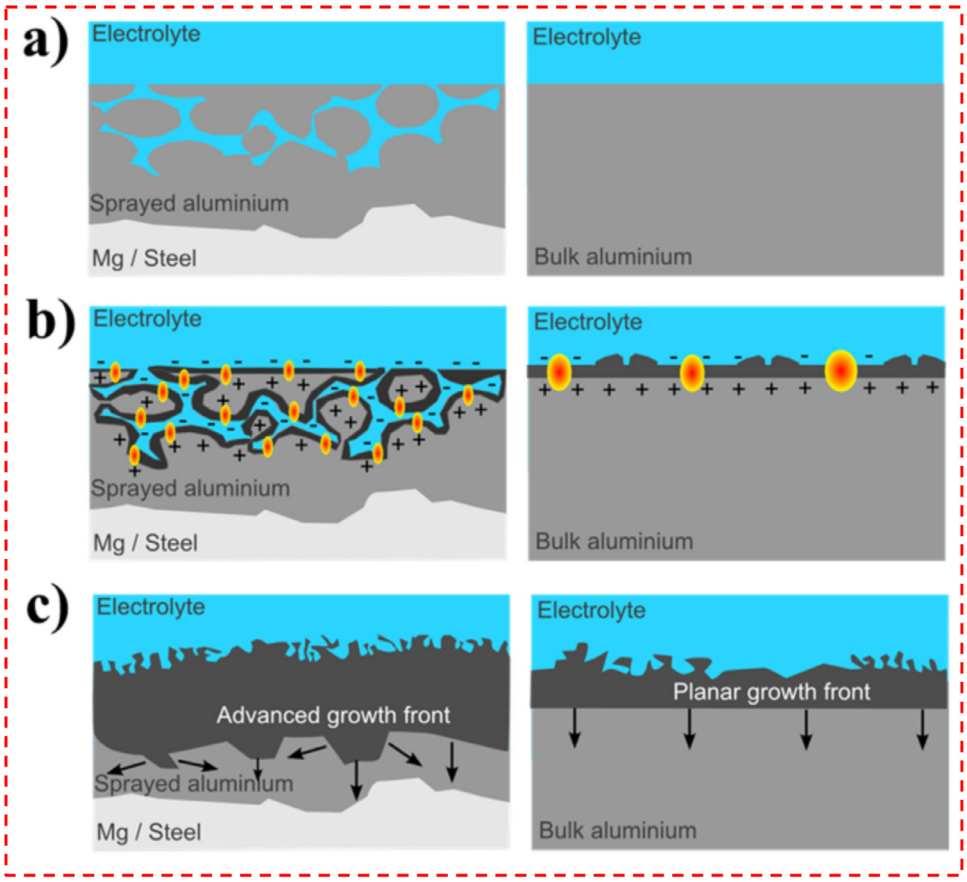

Fig. 15. Schematic illustration of the porosities in a CS Al coating and their effect on the PEO oxide layer growth, (a) before applying the current to the coated and bulk samples, (b) during the PEO process (the first minutes),(c) during the PEO process (after longer process time) [181].

bond adhesion strength of the coating. Extruded lips of Mg substrate and deposited Ti layer are seen in Fig. 16 [123]. Actually, a stronger peening effect on the underneath deposited layer or substrate can be achieved with incoming powder particles having relatively high hardness, density, and high-velocity impact during the HPCS process [199,200]. In a research work, the bond strength of HPCS CoCrMo and Ti6Al4V coatings on 6061-T651 Al alloy was reported to be about 66.17 MPa and 50.38 MPa, respectively [201].

These reported high shear bond strength values were attributed to the profound penetration of the CS powder particles into the substrate and/or the underneath deposited layer/particles [201]. In addition to the mechanisms of mechanical interlocking bonding and metallurgical bonding, another imperative bonding mechanism called microscale intermixing has been recently reported. In certain cases, when hard coatings are cold sprayed on the soft substrates, intense material plastic deformation, fracture, and then microscale vortex-like material mixing (generally between 10 and 50 μm) may occur at the interface between CS coating and the substrate [198,202]. It should be noted that intermixing mechanism at the interface (observed in this research) differs from nanoscale intermixing or interlocking phenomena (typically observed at scales of less than 100 nm) [56,189,203]. Wang et al. [189] used high-resolution transmission electron microscopy (HR-TEM) to validate the intimate metallurgical (atomic) bonding at the CS CP-Al coating/AZ91 Mg alloy substrate, using process gas of helium. They detected an intimate (atomic) interfacial bonding between the Al particle and the Mg alloy substrate within the central region of the Al particle/Mg substrate interface, where compressive strain dominated the plastic deformation, as can be seen in Fig. 17 [189,198]. They also observed an intermixing zone having amorphous features (with about 20 nm width) at the peripheral region of the Al particle/ Mg alloy substrate interface, as shown in Fig. 17a–c. Lattice interruption and elevation of temperature by ASI (actuated by shear plastic deformation at high strain rates) may have caused this nanoscale intermixing zone [189].

Recently, Yin et al. [198] observed the intermixing (microscale) phenomenon between Cu coating and Mg substrate when the temperature and pressure of N_2 propellant gas were chosen 100 °C and 2.5 MPa, respectively. Actually, after spraying the first-layer particles of the coating (Fig. 18a) [198], the majority of the incoming powder particles did not deposit; however, they rebounded after impact, instead. This behavior was related to the D.E of particles which were very low in this method. These rebounding particles repeatedly shot-peened the coating first layer. Hence, this layer ex-

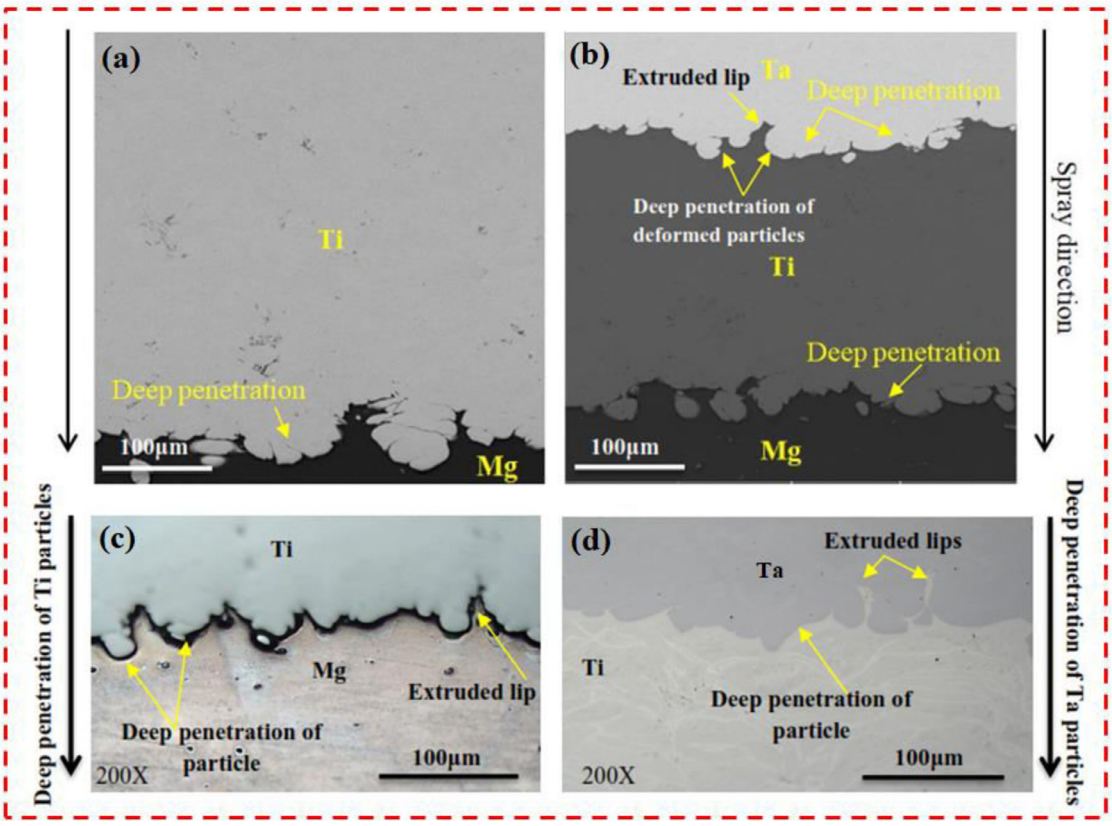

Fig. 16. Extruded lips of Mg alloy (a, b) and Ti layer (c, d) [123].

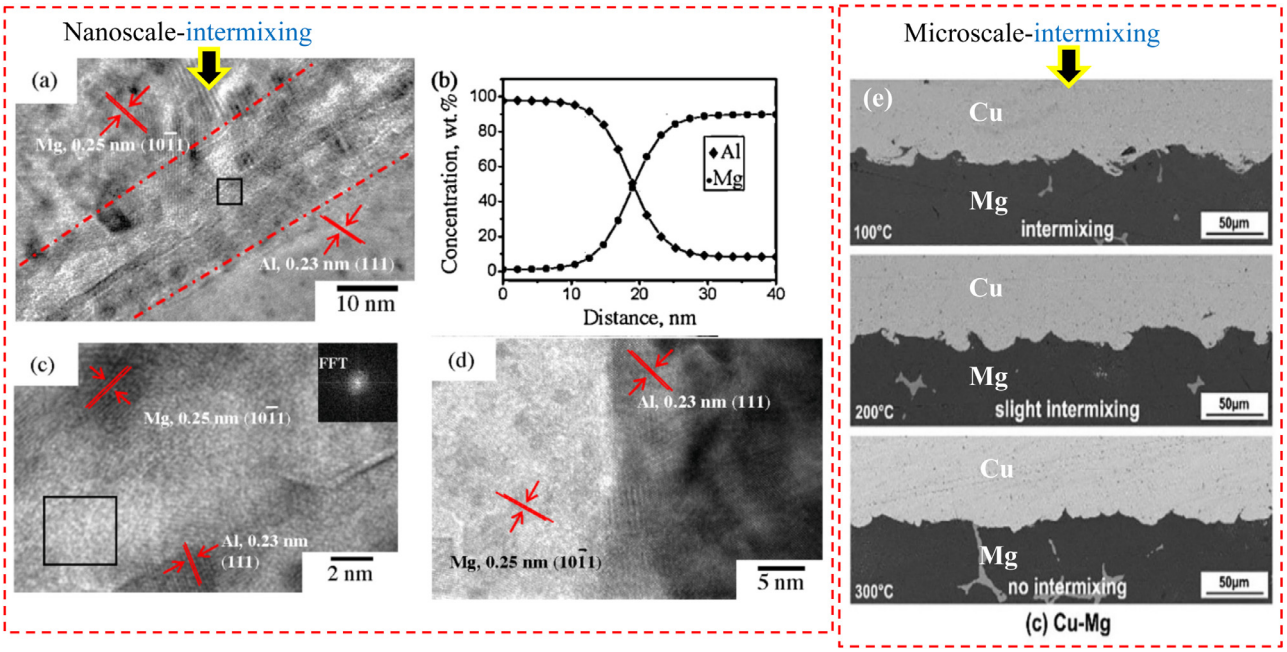

Fig. 17. (a) The periphery region of interface between deposited particle and substrate (typical HRTEM image), (b) the elemental distribution (EDS results) across the interface. (c) Magnified HRTEM image of the black-boxed area , the inset is selected area FFT pattern (with halation feature), (d) a region at the central region of interface between deposited particle and substrate (HRTEM image), and (e) polished cross-section of coating/substrate interfaces (sprayed under different propellant gas temperatures [189,198].

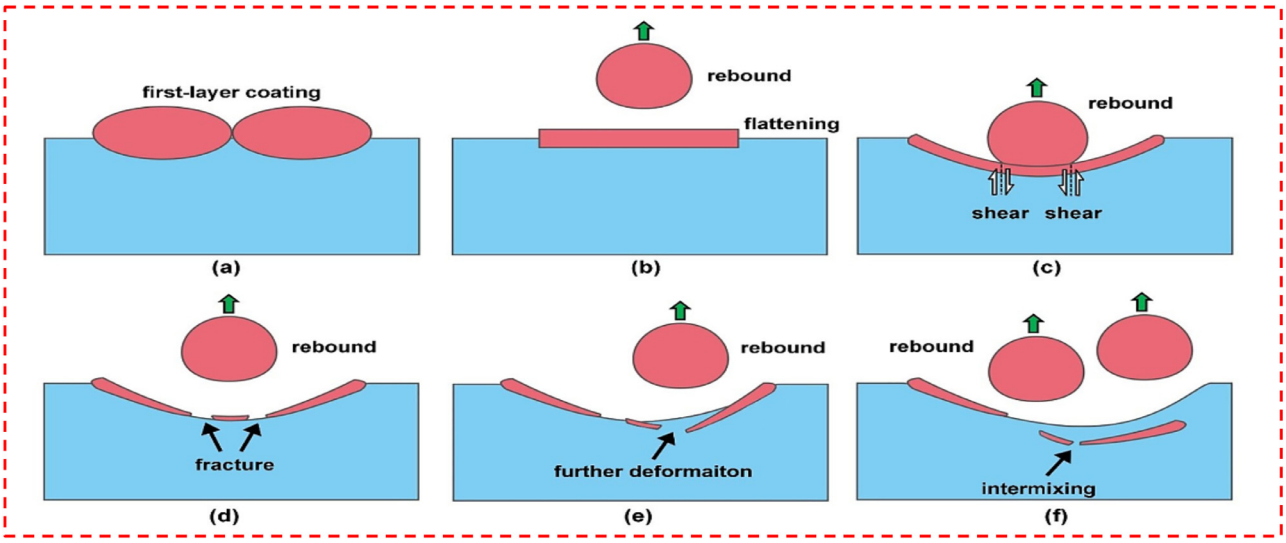

Fig. 18. Schematic illustration of the formation mechanism of the micro-scale intermixing interface [198].

perienced intense plastic deformation along with flattening (Fig. 18b) [198]. The brittleness of the first-layer coating was speculated due to the accumulation of plastic deformation, which resulted in a work-hardening effect during the process. As shown in Fig. 18c, the formation of internal shear stresses was also postulated because of the further plastic deformation of the first-layer coating into the substrate material. This was when more and more powder particles rebounded during the CS process [204]. The fracture of the weakest regions of the first-layer coating along with material movement due to accumulated shear stresses caused by the impact was also reported in this method as shown in Fig. 18d [198]. The subsequent impacts through shear were able to deform more and mix the coating fragments and substrate material (Fig. 18e) and eventually caused the intermixing structure formation at the interface (Fig. 18f) [198].

3.7. Mechanical and tribological properties of the cold sprayed coatings on Mg alloys

The improvement in the tribological properties of the lightweight Mg alloys can be carried out by forming protective coatings. There are various methods for the formation of coatings, such as electrodeposition, spraying, etc. However, Mg and its alloy can suffer from poor bonding with the coating material due to non-similar metal bonding or formation of brittle intermetallic at the interface. One potential method is CS deposition which does not require melting; instead, it is a solid-state process as defined earlier. The selection of the coatings materials on the Mg alloy is very critical for tribological applications. The most common cold spray coating materials on Mg alloys are Al and its alloy. The Al alloy CS coating on the Mg alloys has consistently improved mechanical and tribological properties [127,139,205]. The most commonly studied mechanical property on the CS coating is microhardness. At the same time, the wear resistance of the coating is an important tribological property.

In addition to pure Al CS coating on the Mg alloy substrate, the Al composite CS coatings have also been investigated. For example, the addition of 5 wt.% Al_2O_3 + 1 wt.% carbon nanotubes (CNTs) have shown improvement in the mechanical and tribological performance [149]. Before cold spray, the required amount of Al_2O_3 and CNTs were ball milled with the Al powders. The mixed Al-CNT powders were used for CS. The cross-section microstructures of the CS coatings shown in Fig. 19 suggest that adding Al_2O_3 and CNTs reduced the pores and resulted in denser coatings [149]. The effect of lesser pores and cracks was observed on the hardness values. The Al+Al_2O_3+CNTs coating showed a hardness value of 91 HV that is higher than 87 HV that of pure Al coating. The wear rate of the coatings followed the same trend as the hardness values. The Al+Al_2O_3 + CNTs coating yielded the least wear rate of 4.43×10^{-4} mm^3/m. The wear rate of the Mg alloy substrate, pure Al coating, and Al+Al_2O_3 were 4.35×10^{-2}, 6.78×10^{-3}, 1.21×10^{-3} mm^3/m, respectively.

Al coating on the Mg alloy significantly improves the mechanical and tribological properties. However, the presence of pores and cracks can restrict the full potential of Al coating. The properties of the CS coatings can be further enhanced by post-processing treatments such as heat treatment, irradiation, or the second layer of coatings. The simple heat treatment can be annealing, during which deposited particles can densify and reduce the inter-particle boundaries and pores demonstrated by Siddique et al. [172]. The pure Al CS coating on the AZ91D Mg alloy was heat-treated at 300 °C for one h in a vacuum, followed by furnace cooling. The resulted microstructure is shown in Fig. 20 that exhibited lesser boundaries after heat treatment [172]. However, the microhardness was reduced to 56 HV after heat treatment than 60 HV (as coated sample). The hardness of the CS coatings depends on two major factors: (i) compressive residual stress and (ii) the

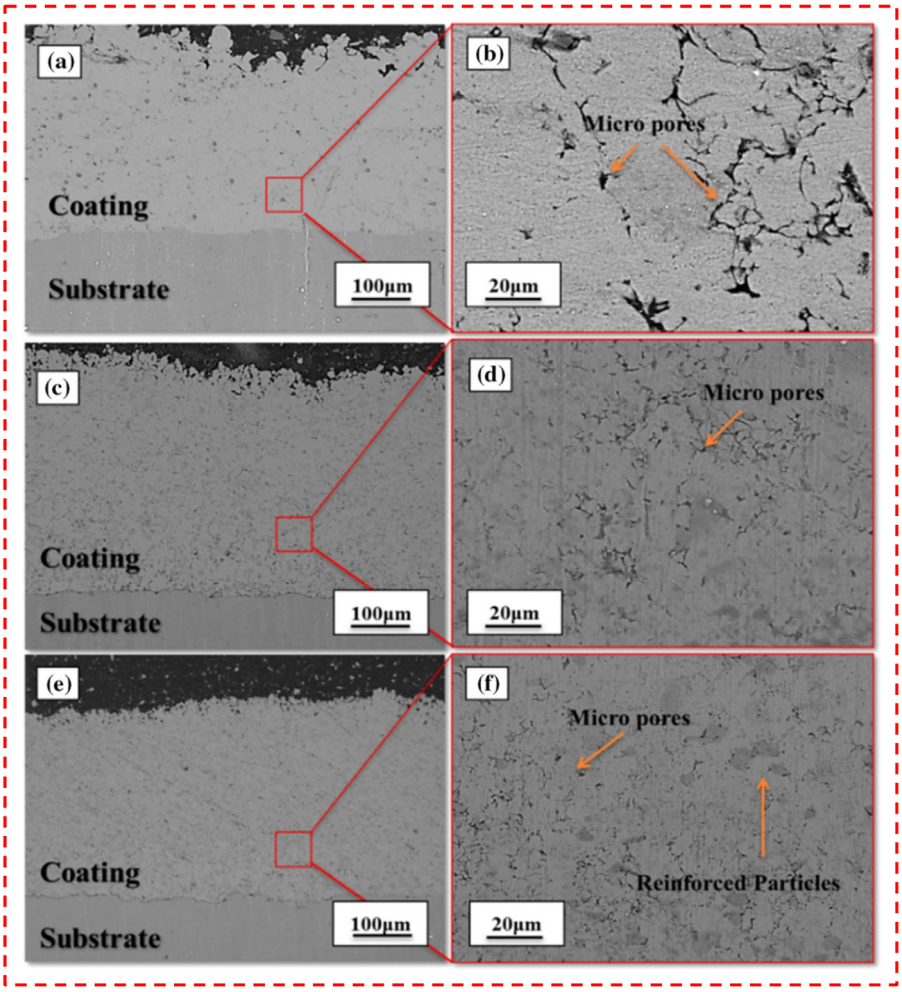

Fig. 19. SEM micrographs of (a, b) pure Al coating, (c, d) Al + Al_2O_3 coating and (e, f) Al + Al_2O_3 + CNTs coating [149].

presence of pores and cracks. In general, higher compressive residual stress and lesser pores yield higher hardness values. In this paper, the heat treatment reduced the pores and residual stress, resulting in a comparatively lesser hardness value. The tribological tests against a steel ball at 3 N normal load at a linear velocity of 150 mm/s showed that the heat treatment was beneficial that reduced the wear rate by ∼ 66 and 75% compared to the as coated sample and Mg substrate, respectively. However, the COF of the heat-treated and as-coated sample was ∼0.7 and 1, higher than the COF of AZ91D Mg substrate (∼0.36).

Guo et al. [174] utilized the HCPEB process on the pure Al coating deposited on AM50 Mg alloy. The effect of HCPEB irradiation was prominent on the mechanical and tribological properties. The Vickers hardness was increased to 88 HV compared to 55 HV that of the non-treated surface. The increase in hardness is due to remelting on the coating that reduced the micropores and produced denser coating. The increase in hardness also improved the tribological properties– the wear rate decreased to 1.06×10^{-4} $mm^3\cdot N^{-1}\cdot m^{-1}$ from 1.55×10^{-3} $mm^3\cdot N^{-1}\cdot m^{-1}$ (untreated coating). The sliding tests were carried out against Si_3N_4 ball of diameter 5 mm at 3 N and 250 RPM for 400 s.

Similar to HCPEB, Rao et al. [185] demonstrated the post-treatment of Al+Al_2O_3 CS coating on AZ31 Mg alloy. The authors employed plasma electrolytic deposition (PEO) to produce a double-layered coating on the Mg alloy. The addition of PEO coating increased the hardness of CS Al+Al_2O_3 coating from 120 HV to 1400 HV. The increase in hardness is expected due to the formation of a PEO coating that consists of oxide particles. The tribological tests against 180 mesh SiC wheel at 3 N normal load yielded the wear rate of double-layered coating to be 5.14×10^{-5} $mm^3\cdot N^{-1}\cdot m^{-1}$ which was one order of magnitude lesser than the wear rate of CS coating. The significance of the oxidation of Al coating on Mg alloy (LA43M) was also studied by Lu et al. [187]. In this study, the authors used anodization of cold sprayed Al coating in 10 wt.% H_2SO_4 electrolytic solution using Ag foil as a cathode in a two-electrode setup. In addition to oxidation, the sealing of resulted Al_2O_3 coating was performed by a chemical route where the polysilazane-xylene mixture was applied on the coating then cured at 200 °C for 2 h. This led to the formation of the SiO_2 sealing layer. The wear performance the resulted composite coating (CS Al/Al_2O_3/SiO_2) on LA43M alloy was evaluated by ball-on-disk sliding test against GCr15 bearing steel ball at 2 N normal load. The

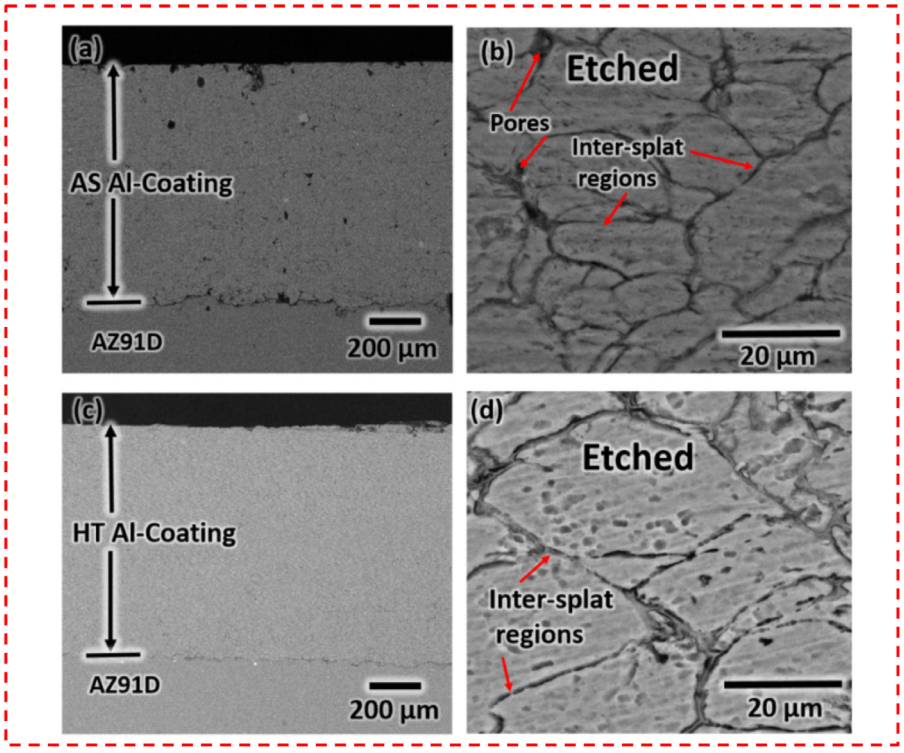

Fig. 20. SEM micrographs of (a)-(b) as coated Al coating and (c)-(d) heat-treated CS Al coating on AZ91D Mg alloy [172].

composite coating showed lesser wear width and depth compared to the Mg substrate. The wear volume of the composite was 0.05 mm^3 which is significantly lesser than the wear volume of substrate (0.61 mm^3) [187].

Besides CS Al coating on the Mg alloys, NiCrAl alloy CS coating has also been studied to achieve superior properties while protecting the Mg substrate [111]. The CS NiCrAl coating (CS-NCA) was performed using the powder composition (NCA powder) Cr-16 wt.%, Al-4.0 wt.%, Ni-balanced. The CS coating was also comparatively studied with the plasma sprayed coating of the same alloy using two different powders – (i) NCA powder and (ii) KF powder (Cr-14.6 wt.%, Al-4.4 wt.%, Ni-balanced) and the coatings are named APS-NCA and APS-KF, respectively. The mechanical property of the coating was measured in terms of Vickers hardness, as shown in Fig. 21a [111]. As expected, the CS-NCA coating yielded the highest hardness values due to residual stress two times the hardness value of ASP-NCA coating. The tribological test against the GCr15 steel ball showed the lowest COF (Fig. 21b) for Mg alloy substrate compared to the coatings due to the inherent material property of Mg [111]. Among the coatings, the CS-NCA yielded COF∼0.35, which is lesser than that of the APS-NCA and APS-KF coatings. The performance of the coatings in terms of wear volume was also evaluated – the CS-NCA showed the least wear volume of 3.026 mm^3 compared to the APS-KF (8.85 mm^3) and APS-NCA (4.698 mm^3), which aligns with the observed trend in hardness values. Moreover, Mg alloy yielded a wear volume of 498.4 mm^3. It suggests all the coatings outperform the Mg substrate in terms of wear volume.

Deposition of CS coatings on Mg and its alloy is advantageous in mechanical and wear resistance properties. A schematic shows a general trend in Fig. 22 to highlight that CS coating on Mg alloy improves the hardness and decreases the wear rate compared to the Mg alloy substrate. The improvement in hardness is due to two main reasons: (i) the inherent higher hardness of the coating material and (ii) the presence of residual stress due to CS deposition. In some studies, the CS deposited Al coating showed lower hardness or higher wear than the Mg alloy substrate [124,127,206]. This can be overcome or further enhanced by utilizing the composite CS coatings with suitable reinforcement particles, multilayered coating, and post-treatment such as annealing, anodic oxidation, plasma electrolytic deposition, etc., as schematically shown in Fig. 22.

4. Application of cold spray technology for the surface modification, repair, and refurbishment of Mg alloys

In addition to the wear resistance CS coatings on Mg alloy, the CS technology has also been employed to repair and refurbish the components. Due to wear, corrosion, fatigue, thermal exposure, etc., damaged components are often replaced due to lack of restoration or repairing techniques. In this regard, the CS's unique ability to deposit the material layer by layer in the solid-state is advantageous and cost-effective to repair the components. In this section, the repairing of Mg alloy components is focused. In general, CS repairing requires the following steps: (i) machining of the damaged area, (ii) surface treatment by grinding or grit-blasting to achieve desired

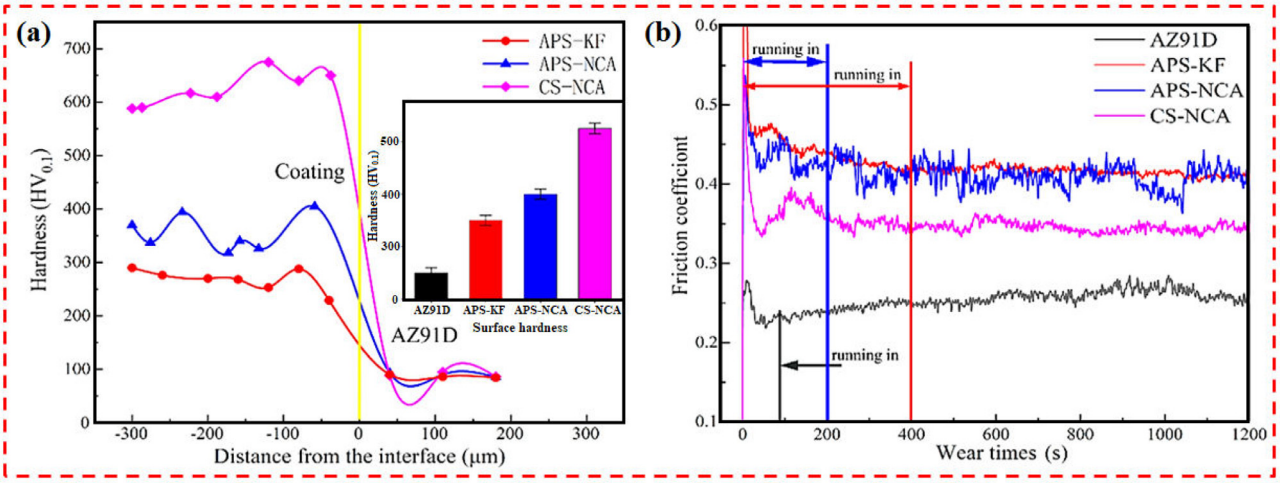

Fig. 21. (a) Vickers hardness and (b) COF variation of the AZ91D Mg substrate, NiCrAl plasma spray coating (APS-KF, APS-NCA), and NiCrAl-CS coating (CS-NCA) [111].

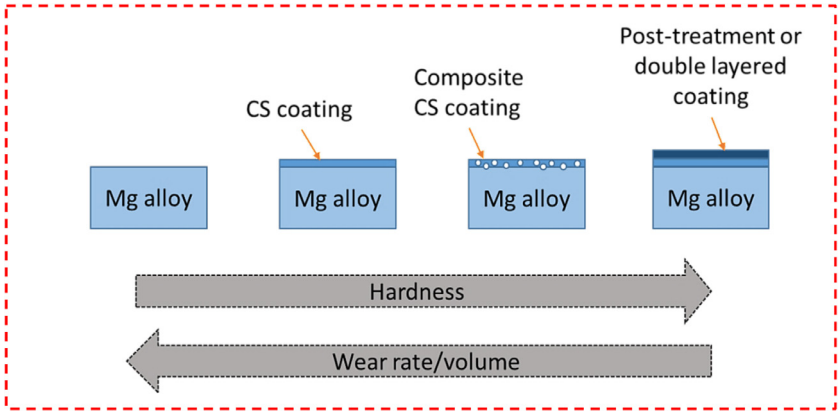

Fig. 22. The general trend of hardness and wear rate/volume on CS coatings and post-treatment of the coatings on Mg alloys.

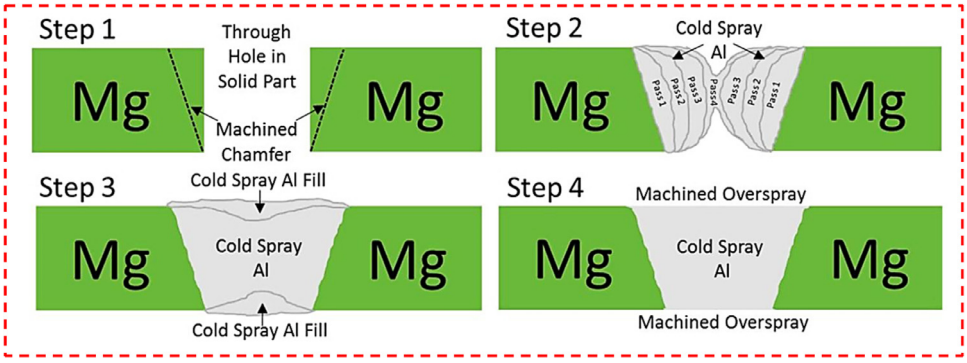

Fig. 23. Repairing of a through-hole in Mg alloy using CS technique [207].

surface roughness before CS, (iii) CS deposition, and (iv) post-machining to achieve original dimension [134]. Champagne et al. [207] demonstrated repairing a through-hole in ZE41A-T5 cast Mg alloy using Al6061 alloy by CS technique. The schematic shown in Fig. 23 depict the steps involved in repairing an Mg alloy hole using CS [207]. It is important to machine the sides to create a chamber that allows a suitable angle for CS deposition. After various passes of CS deposition, the excel fill was machined out to match the original dimension. The measured shear strength of the joint was 160.6 MPa which is similar to the shear strength of the original cast Al alloy (160 MPa). The similar strength of the CS repaired area creates components with uniform material property [207]. Thus, the advantage of CS, i.e., the ability to join dissimilar material without forming brittle intermetallic, helps to retain suitable mechanical strength at the joint.

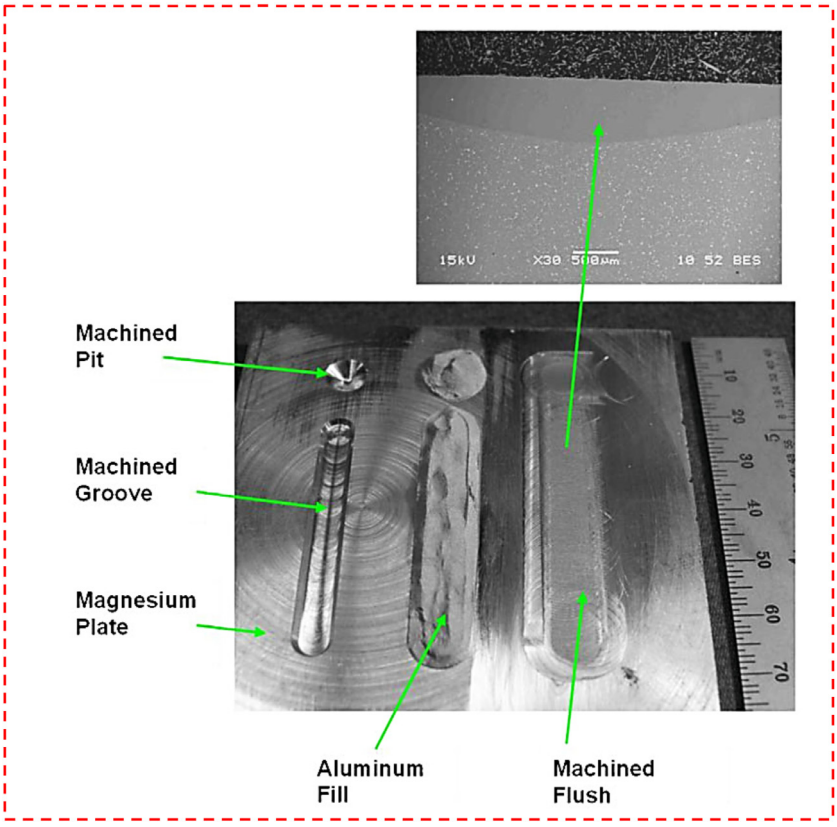

Fig. 24. CS repair of a gouged Mg plate [208].

Another example of CS repair on Mg alloy is shown in Fig. 24 [208]. The damaged area, such as cracks or deep grooves, needed machining to achieve a shallow depression (machined pit or groove) [208]. Then, the machined area was shot pinned with tool steel before CS. It is also important to note that the CS nozzle cannot position less than 45° to the spray direction. Therefore, an engineer needs to consider the spray angle before machining the damaged area to repair the component successfully.

Mg alloys are extensively utilized in the aerospace industry. However, they are prone to electrochemical oxidation that can reduce the component's life [17,208–228]. The CS has been used to repair the corroded helicopter gearbox sump and oil tube bores in helicopter cover made of Mg alloy [206]. The repairing steps of the Mg gearbox included machining, CS deposition of Al6061 alloy, and post-machining as well [208]. The suitable repairing on Mg component is Al and its alloy because Al also helps maintain the lightweight property for aerospace applications. Previous sections show that the CS coated Al on Mg alloy has superior wear and corrosion resistance. Thus, it allows a cost-effective repairing of the Mg components to make it re-employed to flying.

5. Summary and outlook

Mg and it's alloys have recently attracted interest due to their possible applications in different industries. Despite having unique properties, their inferior wear and corrosion properties limit their applications. In this review paper, various surface technologies, including CCC, sol-gel coating, anodizing, PEO, PVD, CVD, ion implantation, electroplating methods, and TS processes, for surface modification of Mg alloys were reviewed. In general, cold sprayed coatings on Mg alloys showed better general corrosion resistance compared to the other types of coatings on Mg-based alloys. Compact cold sprayed coatings showed excellent corrosion protection for Mg alloys even after longer immersion times in corrosive solutions.

1. Cold sprayed passive metals (e.g., Ti) could substantially improve the pitting corrosion resistance of Mg alloy and extraordinarily increased the repassivation capability of the passive layer in chloride-containing electrolyte.
2. Deposition of cold spray (CS) coatings on Mg alloy is also advantageous in mechanical and wear resistance properties. In general, CS coating on Mg alloy improved the hardness and decreased the wear rate compared to the Mg alloy substrate.
3. Multi-layer coatings may have a reduced wear rate, a longer lifetime, better corrosion resistance, and other surface properties. Corrosion and wear rates increase when incorrect process parameters are used and stress concentration zones, such as porosity, form. The electrolyte can permeate the coating if damaged or cracked, leading to localized corrosion pits that act as stress risers and fracture initiation sites, reducing fatigue life.

4. Despite multiple attempts to develop multi-functional coatings for Mg-based alloys, the issue of disregarding localized corrosion while retaining acceptable mechanical integrity of Mg alloys for a reasonable period of time has remained unresolved, and the search for the ideal solution continues.
5. Cold spray coatings prepared using optimized conditions may present very high adhesion, low porosity, excellent mechanical properties, and increased long-term corrosion resistance in an aggressive medium. Therefore, optimizing all spraying parameters is mandatory to successfully prepare coatings with high corrosion resistance and high mechanical properties performance.
6. Cold spray coatings with robust adhesion to the substrate, such as those used to repair cracks in structural components, can transfer load and stress to the new surface of the coating/part, away from the repaired interface, increasing fatigue crack resistance.
7. Although various physical barrier coatings for Mg alloys have been developed, such as metal-based coatings, metal hydroxides and hydrotalcite coatings, metal oxide coatings, and silane sol-gel coatings, the differences in protective characteristics between those coatings are not well understood. As a result, future studies should include systematic and long-term comparisons and evaluations to determine the advantages and disadvantages of each coating.

Galvanic corrosion is the major challenge that limits the protection of Mg alloys by noble barrier coatings. So, more robust coatings with negligible porosity levels, developing coating materials having lower SRP mismatch with Mg alloy, low corrosion rate, and high pitting corrosion resistance are in demand. As a result, more work will be required to fortify Mg-based alloys for various applications using these combined strategies.

Declaration of interests

The authors declare that they have no known competing financial interests or personal relationships that could have appeared to influence the work reported in this paper.

References

[1] Y. Mizutani, S.J. Kim, R. Ichino, M. Okido, Surf. Coat. Technol. 169–170 (2003) 143–146.
[2] X. Li, X. Liu, S. Wu, K.W.K. Yeung, Y. Zheng, P.K. Chu, Acta Biomater 45 (2016) 2–30.
[3] Q. Tan, A. Atrens, N. Mo, M.X. Zhang, Corros. Sci. 112 (2016) 734–759.
[4] M. Esmaily, J.E. Svensson, S. Fajardo, N. Birbilis, G.S. Frankel, S. Virtanen, R. Arrabal, S. Thomas, L.G. Johansson, Prog. Mater. Sci. 89 (2017) 92–193.
[5] J.E. Gray, B. Luan, J. Alloys Compd. 336 (2002) 88–113.
[6] X.B. Chen, N. Birbilis, T.B. Abbott, Corrosion 67 (2011) 035005–1-035005–16.
[7] S. Pommiers-Belin, J. Frayret, A. Uhart, J. Ledeuil, J.C. Dupin, A. Castetbon, M. Potin-Gautier, Appl. Surf. Sci. 298 (2014) 199–207.
[8] V.S. Saji, T.S.N. Sankara Narayanan, X. Chen, Conversion Coatings for Magnesium and Its Alloys, Springer International Publishing, Cham, 2022, doi:10.1007/978-3-030-89976-9.
[9] N. Kumar, R. Subasri, Recent Patents Corros. Sci. 2 (2012) 148–163.
[10] S. Sakka, J. Sol-Gel Sci. Technol. 2 (1994) 451–455.
[11] J. Zhang, C. Gu, Y. Tong, W. Yan, J. Tu, Adv. Mater. Interfaces 3 (2016) 1500694.
[12] H. Ashassi-Sorkhabi, S. Moradi-Alavian, A. Kazempour, Prog. Org. Coat. 135 (2019) 475–482.
[13] G. Barati Darband, M. Aliofkhazraei, P. Hamghalam, N. Valizade, J. Magnes. Alloy. 5 (2017) 74–132.
[14] D. Zhang, L. Ren, Y. Zhang, N. Xue, K. Yang, M. Zhong, Colloids Surf. B Biointerfaces 105 (2013) 51–57.
[15] Z. Ur Rehman, D. Choi, J. Magnes. Alloy. 7 (2019) 555–565.
[16] M. Toorani, M. Aliofkhazraei, M. Mahdavian, R. Naderi, Corros. Sci. 169 (2020) 108608.
[17] X.B. Chen, H.Y. Yang, T.B. Abbott, M.A. Easton, N. Birbilis, Corrosion 68 (2012) 518–535.
[18] A. Thakur, S. Gharde, B. Kandasubramanian, Def. Technol. 15 (2019) 636–644.
[19] Z. Kang, W. Li, J. Ind. Eng. Chem. 50 (2017) 50–56.
[20] C. Blawert, W. Dietzel, E. Ghali, G. Song, Adv. Eng. Mater. 8 (2006) 511–533.
[21] S. K, B. S, S. Chatterjee, R. N, J. Magnes. Alloy. 10 (2022) 1109–1123.
[22] J.C. Caicedo, F. Franco, W. Aperador, Mater. Chem. Phys. 232 (2019) 414–421.
[23] Y. Zhang, T. Lin, Colloids Surf. A Physicochem. Eng. Asp. 568 (2019) 43–50.
[24] S.F. Zhang, R.F. Zhang, W.K. Li, M.S. Li, G.L. Yang, Surf. Coat. Technol. 207 (2012) 170–176.
[25] L. Wu, D. Yang, G. Zhang, Z. Zhang, S. Zhang, A. Tang, F. Pan, Appl. Surf. Sci. 431 (2018) 177–186.
[26] I.S. Abela, in: Surface Modification of Magnesium and its Alloys for Biomedical Applications, Elsevier, 2015, pp. 81–100.
[27] F. Hollstein, R. Wiedemann, J. Scholz, Surf. Coat. Technol. 162 (2003) 261–268.
[28] M. Sivapragash, P. Kumaradhas, S.C. Vettivel, B.S.J. Retnam, J. Magnes. Alloy. 6 (2018) 171–179.
[29] H.R. Bakhsheshi-Rad, A. Najafinezhad, E. Hamzah, A.F. Ismail, F. Berto, X. Chen, J. Funct. Biomater. 11 (2020) 26.
[30] D.W. Stollberg, W.B. Carter, J.M. Hampikian, Surf. Coat. Technol. 94–95 (1997) 137–143.
[31] H. Jeong, J. Cho, Surf. Coat. Technol. 330 (2017) 71–76.
[32] S. Arthanari, A. Ananth, J.H. Boo, K.S. Shin, J. Mater. Eng. Perform. 28 (2019) 1360–1372.
[33] A.R. Siddiqui, R. Maurya, P.K. Katiyar, K. Balani, Surf. Coat. Technol. 404 (2020) 126421.
[34] R. Xu, X. Yang, J. Jiang, P. Li, G. Wu, P.K. Chu, Surf. Coat. Technol. 235 (2013) 875–880.
[35] R. Xu, X. Yang, X. Zhang, M. Wang, P. Li, Y. Zhao, G. Wu, P.K. Chu, Appl. Surf. Sci. 286 (2013) 257–260.
[36] H. Wu, G. Wu, P.K. Chu, Surf. Coat. Technol. 306 (2016) 6–10.
[37] X. Wei, P. Liu, S. Ma, Z. Li, X. Peng, R. Deng, Q. Zhao, Corros. Sci. 173 (2020) 108729.
[38] H. Wu, K. Xi, S. Xiao, A.M. Qasim, R.K.Y. Fu, K. Shi, K. Ding, G. Chen, G. Wu, P.K. Chu, Surf. Coat. Technol. 401 (2020) 126251.
[39] V.S. Saji, J. Magnes. Alloy. 9 (2021) 748–778.
[40] V.S. Saji, J. Ind. Eng. Chem. 103 (2021) 358–372.
[41] K. Nakamura, Y. Shimada, T. Miyashita, A. Serizawa, T. Ishizaki, Materials 11 (2018) 1659 (Basel).
[42] M. Daroonparvar, M.A.M. Yajid, N.M. Yusof, H.R. Bakhsheshi-Rad, J. Alloys Compd. 688 (2016) 841–857.
[43] M. Daroonparvar, M.A.M. Yajid, N.M. Yusof, H.R. Bakhsheshi-Rad, E. Hamzah, H.A. Kamali, J. Alloys Compd. 615 (2014) 657–671.
[44] C. Singh, S.K. Tiwari, R. Singh, Corros. Sci. 151 (2019) 1–19.
[45] M. Daroonparvar, M.A.M. Yajid, N.M. Yusof, H.R. Bakhsheshi-Rad, J. Alloys Compd. 645 (2015) 450–466.

[46] M. Carboneras, M.D. López, P. Rodrigo, M. Campo, B. Torres, E. Otero, J. Rams, Corros. Sci. 52 (2010) 761–768.
[47] M. Daroonparvar, M.A.M. Yajid, H.R. Bakhsheshi-Rad, N.M. Yusof, S. Izman, E. Hamzah, M.R. Abdul Kadir, Vacuum 108 (2014) 61–65.
[48] H.R. Bakhsheshi-Rad, E. Hamzah, R. Ebrahimi-Kahrizsangi, M. Daroonparvar, M. Medraj, Vacuum 125 (2016) 185–188.
[49] T.S.N. Sakara Narayanan, Surface Modification and Its Alloys For Biomedical Applications, Woodland publishing, 2015.
[50] J. Villafuerte, Magnesium Alloys-Corrosion and Surface Treatments, InTech, 2011, doi:10.5772/13985.
[51] D. Zhang, F. Peng, X. Liu, J. Alloys Compd. 853 (2021) 157010.
[52] M. Daroonparvar, M.A.M. Yajid, N.M. Yusof, H.R. Bakhsheshi-Rad, E. Hamzah, T. Mardanikivi, J. Alloys Compd. 649 (2015) 591–605.
[53] M. Daroonparvar, M.A.M. Yajid, R.K. Gupta, N.M. Yusof, H.R. Bakhsheshi-Rad, H. Ghandvar, E. Ghasemi, Trans. Nonferrous Met. Soc. China. 28 (2018) 1571–1581.
[54] Z. Monette, A.K. Kasar, M. Daroonparvar, P.L. Menezes, Int. J. Adv. Manuf. Technol. 106 (2020) 2079–2099.
[55] J.K.C.M. Kay, High Pressure Cold Spray: Principles and Applications, ASM International, 2016.
[56] X.T. Luo, C.X. Li, F.L. Shang, G.J. Yang, Y.Y. Wang, C.J. Li, Surf. Coat. Technol. 254 (2014) 11–20.
[57] H. Assadi, H. Kreye, F. Gärtner, T. Klassen, Acta Mater. 116 (2016) 382–407.
[58] M. Daroonparvar, M.A.M. Yajid, N.M. Yusof, H.R. Bakhsheshi-Rad, E. Hamzah, Ceram. Int. 42 (2016) 357–371.
[59] X. Fan, Y. Liu, Z. Xu, Y. Wang, B. Zou, L. Gu, C. Wang, X. Chen, Z.S. Khan, D. Yang, X. Cao, J. Therm. Spray Technol. 20 (2011) 948–957.
[60] Y.K. Wei, Y.J. Li, Y. Zhang, X.T. Luo, C.J. Li, Corros. Sci. 138 (2018) 105–115.
[61] G. Prashar, H. Vasudev, J. Clean. Prod. 310 (2021) 127606.
[62] E.V. Champagne, The Cold Spray Materials Deposition Process: Fundamentals and Applications, Woodhead Publishing Ltd, Cambridge, 2007.
[63] M. Grujicic, C. Zhao, C. Tong, W. DeRosset, D. Helfritch, Mater. Sci. Eng. A 368 (2004) 222–230.
[64] T.H. Van Steenkiste, J.R. Smith, R.E. Teets, J.J. Moleski, D.W. Gorkiewicz, R.P. Tison, D.R. Marantz, K.A. Kowalsky, W.L. Riggs, P.H. Zajchowski, B. Pilsner, R.C. McCune, K.J. Barnett, Surf. Coat. Technol. 111 (1999) 62–71.
[65] J.N. Viktor Veniaminovich Sobolev, J.M. Guilemany, High Velocity Oxy-Fuel Spraying, illustrate, Maney, London, UK, 2004.
[66] T. Stoltenhoff, H. Kreye, H.J. Richter, J. Therm. Spray Technol. 11 (2002) 542–550.
[67] R.C. Dykhuizen, M.F. Smith, J. Therm. Spray Technol. 7 (1998) 205–212.
[68] J.R. Davis, Handbook of Thermal Spray Technology, 1st ed., ASM International, 2004.
[69] L. Pawlowski, The Science and Engineering of Thermal Spray Coatings, John Wiley & Sons Ltd., New York, USA, 1995.
[70] A. Papyrin, et al., Cold Spray Technology, 1 ed., Elsevier, the Netherlands, 2007 printed in.
[71] H.Y. Lee, Y.H. Yu, Y.C. Lee, Y.P. Hong, K.H. Ko, Appl. Surf. Sci. 227 (2004) 244–249.
[72] Y. Ichikawa, Deposition Mechanisms of Cold Gas Dynamic Sprayed MCrAlY Coatings, Global Coating Solutions, ASM International, 2007.
[73] V. L, Roman Gr. Maev, Physics and Technology, Wiley-VCH Verlag GmbH&Co, Germany, 2009.
[74] J. Robert, C. Tucker, Thermal Spray Coatings, ASM Handbook, 1994.
[75] X. Fan, L. Gu, S. Zeng, L. Zhu, C. Wang, Y. Wang, B. Zou, W. Huang, X. Chen, Z.S. Khan, X. Cao, Surf. Coat. Technol. 206 (2012) 4471–4480.
[76] X. Fan, B. Zou, L. Gu, C. Wang, Y. Wang, W. Huang, L. Zhu, X. Cao, Appl. Surf. Sci. 265 (2013) 264–273.
[77] J. Xu, B. Zou, X. Fan, S. Zhao, Y. Hui, Y. Wang, X. Zhou, X. Cai, S. Tao, H. Ma, X. Cao, J. Alloys Compd. 596 (2014) 10–18.
[78] J. Xu, B. Zou, S. Zhao, Y. Hui, W. Huang, X. Zhou, Y. Wang, X. Cai, X. Cao, Ceram. Int. 40 (2014) 15537–15544.
[79] J. Xu, B. Zou, S. Tao, M. Zhang, X. Cao, J. Alloys Compd. 672 (2016) 251–259.
[80] X. Fan, Y. Wang, B. Zou, L. Gu, W. Huang, X. Cao, J. Therm. Spray Technol. 23 (2014) 304–316.
[81] X. Fan, L. Zhu, W. Huang, J. Alloys Compd. 729 (2017) 617–626.
[82] S. Yang, B. Zou, J. Shen, X. Cai, Y. Wang, X. Cao, L. Zhu, Surf. Coat. Technol. 367 (2019) 278–287.
[83] X. Fan, J. Xu, Y. Wang, H. Ma, S. Zhao, X. Zhou, X. Cao, Surf. Coat. Technol. 240 (2014) 118–127.
[84] M. Parco, L. Zhao, J. Zwick, K. Bobzin, E. Lugscheider, Surf. Coat. Technol. 201 (2007) 6290–6296.
[85] H.Y. Lee, S.H. Jung, S.Y. Lee, Y.H. You, K.H. Ko, Appl. Surf. Sci. 252 (2005) 1891–1898.
[86] P.C. King, S.H. Zahiri, M. Jahedi, Acta Mater 56 (2008) 5617–5626.
[87] D. Toma, W. Brandl, G. Marginean, Surf. Coat. Technol. 138 (2001) 149–158.
[88] G. Bolelli, V. Cannillo, L. Lusvarghi, T. Manfredini, Wear 261 (2006) 1298–1315.
[89] R.C. Zeng, W. Dietzel, J. Chen, W.J. Huang, J. Wang, Key Eng. Mater. 373–374 (2008) 609–612.
[90] R. Arrabal, A. Pardo, M.C. Merino, S. Merino, P. Casajús, M. Mohedano, P. Rodrigo, Corrosion 65 (2009) 817–830.
[91] A. Pardo, M.C. Merino, R. Arrabal, P. Casajús, M. Mohedano, S. Feliú, S. Merino, Corrosion 67 (2011) 025003-1.
[92] M. Campo, M. Carboneras, M.D. López, B. Torres, P. Rodrigo, E. Otero, J. Rams, Surf. Coat. Technol. 203 (2009) 3224–3230.
[93] S. García-Rodríguez, A.J. López, V. Bonache, B. Torres, J. Rams, Coatings 10 (2020) 502.
[94] R. Arrabal, A. Pardo, M.C. Merino, M. Mohedano, P. Casajús, S. Merino, Surf. Coat. Technol. 204 (2010) 2767–2774.
[95] S. García-Rodríguez, A.J. López, B. Torres, J. Rams, Surf. Coat. Technol. 287 (2016) 9–19.
[96] S.F. Guo, F.S. Pan, H.J. Zhang, D.F. Zhang, J.F. Wang, J. Miao, C. Su, C. Zhang, Mater. Des. 108 (2016) 624–631.
[97] M. Parco, L. Zhao, J. Zwick, K. Bobzin, E. Lugscheider, Surf. Coat. Technol. 201 (2006) 3269–3274.
[98] T.F. Kubatík, Z. Pala, K. Neufuss, M. Vilémová, R. Mušálek, J. Stoulil, P. Slepička, T. Chráska, Surf. Coat. Technol. 282 (2015) 163–170.
[99] H.L. Yao, X.Z. Hu, H.T. Wang, Q.Y. Chen, X.B. Bai, M.X. Zhang, G.C. Ji, J. Therm. Spray Technol. 28 (2019) 495–503.
[100] E. Lugscheider, M. Parco, K.U. Kainer, N. Hort, in: Magnesium, Wiley-VCH Verlag GmbH & Co. KGaA, Weinheim, FRG, 2005, pp. 860–868.
[101] H. Pokhmurska, B. Wielage, T. Lampke, T. Grund, M. Student, N. Chervinska, Surf. Coat. Technol. 202 (2008) 4515–4524.
[102] K. Bobzin, N. Kopp, T. Warda, C. Schulz, G. Rolink, A. Weisheit, J. Therm. Spray Technol. 22 (2013) 207–212.
[103] D. Thirumalaikumarasamy, K.S. Kamalamoorthy, V.B. Visvalingam, J. Magnes. Alloy. 3 (2015) 237–246.
[104] H.R. Bakhsheshi-Rad, E. Hamzah, A.F. Ismail, M. Daroonparvar, M. Kasiri-Asgarani, S. Jabbarzare, M. Medraj, Ceram. Int. 41 (2015) 15272–15277.
[105] H.R. Bakhsheshi-Rad, E. Hamzah, A.F. Ismail, M. Daroonparvar, M.A.M. Yajid, M. Medraj, J. Alloys Compd. 658 (2016) 440–452.
[106] Y. Gao, M. Jie, Y. Liu, Surf. Coat. Technol. 315 (2017) 214–219.
[107] T.F. Kubatík, P. Ctibor, R. Mušálek, M. Janata, Mater. Tehnol. 51 (2017) 323–327.
[108] S. García-Rodríguez, B. Torres, A.J. Lopez, W.M. Rainforth, E. Otero, M. Muñoz, J. Rams, J. Therm. Spray Technol. 27 (2018) 1615–1631.
[109] Q. Wang, Q. Sun, M.X. Zhang, W.J. Niu, C.B. Tang, K.S. Wang, X. Rui, L. Zhai, L. Wang, Surf. Coat. Technol. 352 (2018) 627–633.
[110] A. Riquelme, P. Rodrigo, M.D. Escalera-Rodríguez, J. Rams, Results Phys. 13 (2019) 102160.
[111] X. Zhao, T. Dong, B. Fu, G. Li, Q. Liu, Y. Li, Coatings 11 (2021) 193.

[112] A.A. Tiamiyu, C.A. Schuh, Surf. Coat. Technol. 403 (2020) 126386.
[113] C.M. Sample, V.K. Champagne, A.T. Nardi, D.A. Lados, Addit. Manuf. 36 (2020) 101371.
[114] I.S.M. Zulkifli, M.A.M. Yajid, M.H. Idris, M.B. Uday, M. Daroonparvar, A. Emadzadeh, A. Arshad, Ceram. Int. 46 (2020) 22438–22451.
[115] M. Daroonparvar, M. Azizi Mat Yajid, N.M. Yusof, H.R. Bakhsheshi-Rad, M. Sakhawat Hussain, E. Hamzah, Adv. Mater. Sci. Eng. 2013 (2013) 1–13.
[116] J.K.M. Daroonparvar, Charles M Kay, Adv. Mater. Process. 176 (2018) 40–43.
[117] M.R. Rokni, S.R. Nutt, C.A. Widener, V.K. Champagne, R.H. Hrabe, J. Therm. Spray Technol. 26 (2017) 1308–1355.
[118] M.F. SMITH, in: Cold Spray Materials Deposition Process, Elsevier, 2007, pp. 43–61.
[119] J. Villafuerte, Modern Cold Spray: Materials, Process, and Applications, Springer International Publishing, Berlin, 2015.
[120] N.M. Chavan, B. Kiran, A. Jyothirmayi, P.S. Phani, G. Sundararajan, J. Therm. Spray Technol. 22 (2013) 463–470.
[121] L. Pawlowski, Science and Engineering of Thermal Spray Coatings, 2nd ed., John Wiley & Sons Ltd., New York, USA, 2008.
[122] J. L, A. Rezaeain, R. Chromik, S. Yue, E. Irissou, in: Proceedings of the Thermal Spray 2008 Thermal Spray Crossing Borders, 2008, pp. 2–4.
[123] M. Daroonparvar, M.U. Farooq Khan, Y. Saadeh, C.M. Kay, R.K. Gupta, A.K. Kasar, P. Kumar, M. Misra, P.L. Menezes, H.R. Bakhsheshi-Rad, Mater. Chem. Phys. 256 (2020) 123627.
[124] M. Daroonparvar, M.U.F. Khan, Y. Saadeh, C.M. Kay, A.K. Kasar, P. Kumar, L. Esteves, M. Misra, P. Menezes, P.R. Kalvala, H.R. Bakhsheshi-Rad, R.K. Gupta, Corros. Sci. 176 (2020) 109029.
[125] J. Wang, X. Pang, H. Jahed, AIMS Mater. Sci. 6 (2019) 567–600.
[126] M. Daroonparvar, A.K. Kasar, M.U. Farooq Khan, P.L. Menezes, C.M. Kay, M. Misra, R.K. Gupta, Coatings 11 (2021) 57.
[127] M. Diab, X. Pang, H. Jahed, Surf. Coat. Technol. 309 (2017) 423–435.
[128] F.S.d. Silva, J. Bedoya, S. Dosta, N. Cinca, I.G. Cano, J.M. Guilemany, A.V. Benedetti, Corros. Sci. 114 (2017) 57–71.
[129] P. Richer, B. Jodoin, L. Ajdelsztajn, E.J. Lavernia, J. Therm. Spray Technol. 15 (2006) 246–254.
[130] F.S. da Silva, N. Cinca, S. Dosta, I.G. Cano, J.M. Guilemany, A.V. Benedetti, Eclét. Quím. J 42 (2017) 09.
[131] T. Schmidt, H. Assadi, F. Gartner, H. Richter, T. Stoltenhoff, H. Kreye, T. Klassen, J. Therm. Spray Technol. 18 (2009) 1038 1038.
[132] C. Xie, H. Li, X. Zhou, C. Sun, Surf. Coat. Technol. 374 (2019) 797–806.
[133] J.G. Legoux, E. Irissou, C. Moreau, J. Therm. Spray Technol. 16 (2007) 619–626.
[134] K. Spencer, M.X. Zhang, Surf. Coat. Technol. 205 (2011) 5135–5140.
[135] S. Dosta, M. Couto, J.M. Guilemany, Acta Mater. 61 (2013) 643–652.
[136] K. Spencer, D.M. Fabijanic, M.X. Zhang, Surf. Coat. Technol. 204 (2009) 336–344.
[137] E. Lapushkina, 2020. (Doctoral dissertation, Université de Lyon; Tohoku gakuin university (Sendai, Japon)) https://tel.archives-ouvertes.fr/tel-03127323.
[138] Y. Tao, T. Xiong, C. Sun, L. Kong, X. Cui, T. Li, G.L. Song, Corros. Sci. 52 (2010) 3191–3197.
[139] B.S. DeForce, T.J. Eden, J.K. Potter, J. Therm. Spray Technol. 20 (2011) 1352–1358.
[140] Y.K. Wei, X.T. Luo, Y. Ge, X. Chu, G.S. Huang, C.J. Li, J. Alloys Compd. 806 (2019) 1116–1126.
[141] Y. Tao, T. Xiong, C. Sun, H. Jin, H. Du, T. Li, Appl. Surf. Sci. 256 (2009) 261–266.
[142] H. Bu, M. Yandouzi, C. Lu, D. MacDonald, B. Jodoin, Surf. Coat. Technol. 207 (2012) 155–162.
[143] Y. Zhang, Q. Wang, G. Chen, C.S. Ramachandran, Surf. Coat. Technol. 403 (2020) 126380.
[144] X. Yang, W. Li, S. Yu, Y. Xu, K. Hu, Y. Zhao, J. Mater. Sci. Technol. 59 (2020) 117–128.
[145] O. Meydanoglu, B. Jodoin, E.S. Kayali, Surf. Coat. Technol. 235 (2013) 108–116.
[146] K. Balani, T. Laha, A. Agarwal, J. Karthikeyan, N. Munroe, Surf. Coat. Technol. 195 (2005) 272–279.
[147] N. Li, W. Li, X. Yang, Y. Xu, A. Vairis, Surf. Coat. Technol. 349 (2018) 1069–1076.
[148] Y. Wang, B. Normand, N. Mary, M. Yu, H. Liao, Surf. Coat. Technol. 315 (2017) 314–325.
[149] U. Ahmed, L. Yi, L.F. Fei, M. Yasir, C.J. Li, C.X. Li, J. Therm. Spray Technol. 30 (2021) 668–679.
[150] Y. Wang, B. Normand, H. Liao, G. Zhao, N. Mary, J. Tang, Coatings 10 (2020) 325.
[151] B. Morończyk, E. Ura-Bińczyk, S. Kuroda, J. Jaroszewicz, R.M. Molak, Surf. Coat. Technol. 363 (2019) 142–151.
[152] D. Zhang, B. Wei, Z. Wu, Z. Qi, Z. Wang, Surf. Coat. Technol. 303 (2016) 94–102.
[153] Y.K. Wei, X.T. Luo, X. Chu, Y. Ge, G.S. Huang, Y.C. Xie, R.Z. Huang, C.J. Li, Corros. Sci. 184 (2021) 109397.
[154] Y.K. Wei, X.T. Luo, C.X. Li, C.J. Li, J. Therm. Spray Technol. 26 (2017) 173–183.
[155] Z. Zhang, F. Liu, E.H. Han, L. Xu, Surf. Coat. Technol. 385 (2020) 125372.
[156] M.A. Amin, Corros. Sci. 52 (2010) 3243–3257.
[157] G.E. Kiourtsidis, S.M. Skolianos, E.G. Pavlidou, Corros. Sci. 41 (1999) 1185–1203.
[158] J. Ma, J. Wen, Q. Li, Q. Zhang, Int. J. Hydrog. Energy 38 (2013) 14896–14902.
[159] H. Ezuber, A. El-Houd, F. El-Shawesh, Mater. Des. 29 (2008) 801–805.
[160] R.P.S. Chakradhar, G. Chandra Mouli, H. Barshilia, M. Srivastava, J. Therm. Spray Technol. 30 (2021) 371–384.
[161] X.T. Luo, C.J. Li, Mater. Des. 83 (2015) 249–256.
[162] E. Irissou, J.G. Legoux, B. Arsenault, C. Moreau, J. Therm. Spray Technol. 16 (2007) 661–668.
[163] E. Sansoucy, P. Marcoux, L. Ajdelsztajn, B. Jodoin, Surf. Coat. Technol. 202 (2008) 3988–3996.
[164] Y. Wang, B. Normand, N. Mary, M. Yu, H. Liao, Surf. Coat. Technol. 251 (2014) 264–275.
[165] R. Huang, M. Sone, W. Ma, H. Fukanuma, Surf. Coat. Technol. 261 (2015) 278–288.
[166] F. Gartner, T. Stoltenhoff, J. Voyer, H. Kreye, S. Riekehr, M. Koçak, Surf. Coat. Technol. 200 (2006) 6770–6782.
[167] Z. Arabgol, H. Assadi, T. Schmidt, F. Gärtner, T. Klassen, J. Therm. Spray Technol. 23 (2014) 84–90.
[168] H. Bu, M. Yandouzi, C. Lu, B. Jodoin, J. Therm. Spray Technol. 21 (2012) 731–739.
[169] A.C. Hall, D.J. Cook, R.A. Neiser, T.J. Roemer, D.A. Hirschfeld, J. Therm. Spray Technol. 15 (2006) 233–238.
[170] H. Bu, M. Yandouzi, C. Lu, B. Jodoin, Surf. Coat. Technol. 205 (2011) 4665–4671.
[171] K. Spencer, M.X. Zhang, Scr. Mater. 61 (2009) 44–47.
[172] S. Siddique, A.A. Bernussi, S.W. Husain, M. Yasir, Surf. Coat. Technol. 394 (2020) 125882.
[173] F.F. Lu, K. Ma, C.X. Li, M. Yasir, X.T. Luo, C. Li, Surf. Coat. Technol. 394 (2020) 125865.
[174] F. Guo, W. Jiang, G. Tang, Z. Xie, H. Dai, E. Wang, Y. Chen, L. Liu, Vacuum 182 (2020) 109772.
[175] F.S. da Silva, N. Cinca, S. Dosta, I.G. Cano, J.M. Guilemany, A.V. Benedetti, J. Therm. Spray Technol. 29 (2020) 1040–1053.
[176] W. Li, C. Cao, S. Yin, Prog. Mater. Sci. 110 (2020) 100633.
[177] H.R. Wang, W.Y. Li, L. Ma, J. Wang, Q. Wang, Surf. Coat. Technol. 201 (2007) 5203–5206.
[178] M. Daroonparvar, M.A.M. Yajid, C.M. Kay, H. Bakhsheshi-Rad, R.K. Gupta, N.M. Yusof, H. Ghandvar, A. Arshad, I.S.M. Zulkifli, Corros. Sci. 144 (2018) 13–34.
[179] H.R. Bakhsheshi-Rad, M. Akbari, A.F. Ismail, M. Aziz, Z. Hadisi, E. Pagan, M. Daroonparvar, X. Chen, Surf. Coat. Technol. 377 (2019) 124898.
[180] M. Daroonparvar, J. Rare Earths 33 (2015) 983–994.

[181] J. Martin, K. Akoda, V. Ntomprougkidis, O. Ferry, A. Maizeray, A. Bastien, P. Brenot, G. Ezo'o, G. Henrion, Surf. Coat. Technol. 392 (2020) 125756.
[182] S. Luo, Q. Wang, R. Ye, C.S. Ramachandran, Surf. Coat. Technol. 375 (2019) 864–876.
[183] M. Daroonparvar, M.A.M. Yajid, R.K. Gupta, N.M. Yusof, H.R. Bakhsheshi-Rad, H. Ghandvar, Prot. Met. Phys. Chem. Surf. 54 (2018) 425–441.
[184] M. Treviño, N.F. Garza-Montes-de-Oca, A. Pérez, M.A.L. Hernández-Rodríguez, A. Juárez, R. Colás, Surf. Coat. Technol. 206 (2012) 2213–2219.
[185] Y. Rao, Q. Wang, J. Chen, C.S. Ramachandran, Mater. Today Commun. 26 (2021) 101978.
[186] Y. Rao, Q. Wang, D. Oka, C.S. Ramachandran, Surf. Coat. Technol. 383 (2020) 125271.
[187] F.F. Lu, K. Ma, C. Li, C. Li, J. Therm. Spray Technol. 30 (2021) 680–693.
[188] P.C. King, G. Bae, S.H. Zahiri, M. Jahedi, C. Lee, J. Therm. Spray Technol. 19 (2010) 620–634.
[189] Q. Wang, D. Qiu, Y. Xiong, N. Birbilis, M.X. Zhang, Appl. Surf. Sci. 289 (2014) 366–369.
[190] K.H. Ko, J.O. Choi, H. Lee, Y.K. Seo, S.P. Jung, S.S. Yu, Mater. Lett. 149 (2015) 40–42.
[191] Y.Y. Zhang, J.S. Zhang, Mater. Lett. 65 (2011) 1856–1858.
[192] M. Hassani-Gangaraj, D. Veysset, K.A. Nelson, C.A. Schuh, Scr. Mater. 145 (2018) 9–13.
[193] H. Assadi, F. Gartner, T. Stoltenhoff, H. Kreye, Acta Mater. 51 (2003) 4379–4394.
[194] S.K. Shaha, H. Jahed, Materials 12 (2019) 1317 (Basel).
[195] K. Kim, M. Watanabe, K. Mitsuishi, K. Iakoubovskii, S. Kuroda, J. Phys. D Appl. Phys. 42 (2009) 065304.
[196] C. Chen, Y. Xie, S. Yin, M.P. Planche, S. Deng, R. Lupoi, H. Liao, Mater. Lett. 173 (2016) 76–79.
[197] S. Kumar, M. Ramakrishna, N.M. Chavan, S.V. Joshi, Acta Mater. 130 (2017) 177–195.
[198] S. Yin, J. Cizek, J. Cupera, M. Hassani, X. Luo, R. Jenkins, Y. Xie, W. Li, R. Lupoi, Mater. Des. 200 (2021) 109444.
[199] A. Tan, J. Lek, W. Sun, A. Bhowmik, I. Marinescu, X. Song, W. Zhai, F. Li, Z. Dong, C. Boothroyd, E. Liu, Coatings 8 (2018) 327.
[200] S. Siddique, C.X. Li, A.A. Bernussi, S.W. Hussain, M. Yasir, J. Therm. Spray Technol. 28 (2019) 1739–1748.
[201] W. Sun, A.W.Y. Tan, I. Marinescu, W.Q. Toh, E. Liu, Surf. Coat. Technol. 326 (2017) 291–298.
[202] R. Nikbakht, S.H. Seyedein, S. Kheirandish, H. Assadi, B. Jodoin, Surf. Coat. Technol. 367 (2019) 75–85.
[203] Z. Liu, H. Wang, M. Haché, E. Irissou, Y. Zou, Scr. Mater. 177 (2020) 96–100.
[204] Y. Xie, S. Yin, J. Cizek, J. Cupera, E. Guo, R. Lupoi, Surf. Coat. Technol. 337 (2018) 447–452.
[205] S.B. Dayani, S.K. Shaha, R. Ghelichi, J.F. Wang, H. Jahed, Surf. Coat. Technol. 337 (2018) 150–158.
[206] S. Yin, P. Cavaliere, B. Aldwell, R. Jenkins, H. Liao, W. Li, R. Lupoi, Addit. Manuf. 21 (2018) 628–650.
[207] V. Champagne, D. Kaplowitz, V.K. Champagne, C. Howe, M.K. West, B. McNally, M. Rokni, Mater. Manuf. Process. 33 (2018) 130–139.
[208] V. Champagne, D. Helfritch, Mater. Sci. Technol. 31 (2015) 627–634.
[209] M. Rashad, F. Pan, M. Asif, Mater. Sci. Eng. A 649 (2016) 263–269.
[210] M. Rashad, F. Pan, A. Tang, M. Asif, M. Aamir, J. Alloys Compd. 603 (2014) 111–118.
[211] M. Rashad, F. Pan, M. Asif, X. Chen, J. Magnes. Alloy. 5 (2017) 271–276.
[212] M. Shahin, C. Wen, K. Munir, Y. Li, J. Magnes. Alloy. 10 (2022) 458–477.
[213] L. Liu, F. Peng, D. Zhang, M. Li, J. Huang, X. Liu, J. Magnes. Alloy. (2021), doi:10.1016/j.jma.2021.03.003.
[214] W. Gong, R. Zheng, S. Harjo, T. Kawasaki, K. Aizawa, N. Tsuji, J. Magnes. Alloy. (2022), doi:10.1016/j.jma.2022.02.002.
[215] Z. Yu, X. Xu, K. Shi, B. Du, X. Han, T. Xiao, S. Li, K. Liu, W. Du, J. Magnes. Alloy. (2022), doi:10.1016/j.jma.2022.01.005.
[216] S. Zhang, L. Hu, Y. Ruan, T. Zhou, Q. Chen, Y. Zhong, L. Shi, M. Li, M. Yang, S. Jiang, J. Magnes. Alloy. (2022), doi:10.1016/j.jma.2022.01.011.
[217] W. Yin, F. Briffod, T. Shiraiwa, M. Enoki, J. Magnes. Alloy. (2022), doi:10.1016/j.jma.2022.02.004.
[218] H.T. Jeong, W.J. Kim, J. Magnes. Alloy. 10 (2022) 1133–1153.
[219] Y. Wang, P. Fu, N. Wang, L. Peng, B. Kang, H. Zeng, G. Yuan, W. Ding, Engineering 6 (2020) 1267–1275.
[220] Y. Zhang, X. Feng, Q. Huang, Y. Li, Y. Yang, J. Magnes. Alloy. (2022), doi:10.1016/j.jma.2021.12.017.
[221] Y. Yang, C. Lu, L. Shen, Z. Zhao, S. Peng, C. Shuai, J. Magnes. Alloy. (2021), doi:10.1016/j.jma.2021.04.009.
[222] M. Shahin, K. Munir, C. Wen, Y. Li, J. Alloys Compd. 828 (2020) 154461.
[223] G. Jia, H. Huang, J. Niu, C. Chen, J. Weng, F. Yu, D. Wang, B. Kang, T. Wang, G. Yuan, H. Zeng, J. Magnes. Alloy. 9 (2021) 1954–1966.
[224] H. Zhou, B. Liang, H. Jiang, Z. Deng, K. Yu, J. Magnes. Alloy. 9 (2021) 779–804.
[225] R. Radha, D. Sreekanth, J. Magnes. Alloy. 5 (2017) 286–312.
[226] M. Haghshenas, J. Magnes. Alloy. 5 (2017) 189–201.
[227] S. Abazari, A. Shamsipur, H.R. Bakhsheshi-Rad, J. Magnes. Alloy. (2021) Dec 17, doi:10.1016/j.jma.2021.09.016.
[228] M. Rashad, F. Pan, D. Lin, M. Asif, Mater. Des. 89 (2016) 1242–1250.
[229] M. Daroonparvar, M.A.M. Yajid, N.M. Yusof, M.S. Hussain, J. Nanomater. 2013 (2013).
[230] M. Daroonparvar, M.A.M. Yajid, N.M. Yusof, H.R. Bakhsheshi-Rad, Z. Valefi, E. Hamzah, J. Rare Earths 32 (1) (2014) 57–77.
[231] H.R. Bakhsheshi-Rad, E. Hamzah, M.R. Abdul-Kadir, M. Daroonparvar, M. Medraj, Vacuum 119 (2015) 95–98.